THE SEDIMENTOLOGY AND GEOCHEMISTRY OF PHOSPHATIC AND ASSOCIATED STRATA IN JORDAN: IMPLICATIONS FOR PHOSPHOGENESIS AND THE FORMATION OF ECONOMIC PHOSPHORITE

by

PEIR KENNETH PUFAHL

H.B.Sc., M.Sc., Lakehead University, 1994, 1996

A THESIS SUBMITTED IN PARTIAL FULFILLMENT OF THE REQUIREMENTS FOR THE DEGREE OF

DOCTOR OF PHILOSOPHY

in

THE FACULTY OF GRADUATE STUDIES

(Department of Earth and Ocean Sciences)

We accept this thesis as conforming to the required standard

THE UNIVERSITY OF BRITISH COLUMBIA

December 2001

In presenting this thesis in partial fulfillment of the requirements for an advanced degree at the University of British Columbia, I agree that the Library shall make it freely available for reference and study. I further agree that permission for extensive copying of this thesis for scholarly purposes may be granted by the head of my department or by his or her representatives. It is understood that copying or publication of this thesis for financial gain shall not be allowed without my written permission.

Peir Pfahl

Department of Earth and Ocean Sciences

The University of British Columbia
Vancouver, Canada

December 19, 2001

ABSTRACT

Sedimentary, authigenic, and biological processes are preserved within the Upper Cretaceous (Campanian) Alhisa Phosphorite Formation (AP) in central and northern Jordan. The AP formed near the eastern extremity of the South Tethyan Phosphorite Province (STPP), a carbonate-dominated Upper Cretaceous to Eocene "phosphorite giant" that extends from Colombia, North Africa to the Middle East. Multidisciplinary research of the AP and associated cherts, chalks, and oyster buildups indicate that phosphatic strata formed on a highly productive, storm-dominated, east-west trending epeiric platform along the south Tethyan margin. The onset of phosphogenesis and the accumulation of economic phosphorite coincided with a rise in relative sea level that onlapped peritidal carbonates of the Ajlun Group. Authigenic precipitation of phosphate occurred in a broad array of sedimentary environments - herein termed a "phosphorite nursery" – that spanned the entire platform. Sedimentologic data indicate that pristine phosphates were concentrated into phosphatic grainstones through storm wave winnowing, and storm-generated, shelf-parallel geostrophic currents. Economic phosphorites formed through the amalgamation of storm-induced event beds. Stratigraphic packaging of phosphatic strata indicates that temporal variations in storm frequency were a prerequisite for the formation of economic phosphorite. Syndepositional phosphogenesis, reworking, and amalgamation to form phosphorites contrasts sharply with the concepts of "Baturin Cycling". A transgressive systems tract coupled with high surface productivity created detritally starved settings for the establishment of a "phosphorite nursery" and amalgamation of storm-generated event beds formed economic phosphorite within a single systems tract.

Coated phosphate grains were investigated to elucidate the processes governing phosphogenesis. Stable isotopic data ($\delta^{13}C_{carbonate\ fluorapatite}$) indicate that coated grains precipitated in association with the suboxic to anoxic microbial respiration of organic matter. The microstratigraphies of some grains suggest that phosphogenesis is commonly accompanied

by changes in pore water redox chemistry. These changes reflect fluctuations in the biological oxygen demand within suboxic pore water environments resulting from variations in the surface productivity and/or ecological dynamics in the overlying water column. Coated phosphate grains record low and/or net negative sediment accumulation rates and are the granular equivalent to condensed beds.

The trace element chemistry (Mg and Sr) of skeletal calcite from the Cretaceous oyster, *Oscillopha figari* was analyzed in sclerochronological profile in order to determine the temperature and salinity regime that prevailed over the Jordanian shelf. Although there is significant uncertainty in interpreting the data, the results provide clear objectives for future research, and support sedimentologic evidence that suggests oysters developed on a productive epeiric platform that experienced periods of intense upwelling.

TABLE OF CONTENTS

LIST OF TABLES

LIST OF FIGURES

FOREWORD

Chapters 2, 3, and 4 of this dissertation constitute stand-alone papers. Material presented in each chapter is the first author's own work arising from a collaborative research project between the University of Jordan (Dr. Abdulkader Abed), Jordan Phosphate Mining Company (Dr. Rushdi Sadaqah), and the University of British Columbia. Chapters 2 and 3 have been submitted for publication. Drs. Kurt Grimm, Steve Calvert, Abdulkader Abed, and Rushdi Sadaqah provided editorial guidance in Chapters 2 and 3. Chapter 4 benefited from the editorial comments of Drs. Tom Pedersen, Phil Fralick, and David Hastings.

The following papers, based on chapters 2 and 3 respectively, have been submitted:

Pufahl, P.K., Grimm, K.A., Abed, A.M., and Sadaqah, R.M.Y., 2001, submitted. Upper Cretaceous (Campanian) phosphorites in Jordan: Implications for the formation of a south Tethyan phosphorite giant. Sedimentary Geology, 90p., 15 figures, 4 tables

Pufahl, P.K., and Grimm, K.A., 2001, submitted. Coated phosphate grains: The granular equivalent of condensed beds. Geology, 26p., 3 figures, 1 table

I attest that both works listed above are predominately the work of P.K. Pufahl.

Lee A. Groat
Associate Professor

ACKNOWLEDGMENTS

I would like to thank my thesis advisor, Kurt Grimm, for introducing me to phosphorites, and for his direction and input throughout this study. I am grateful to my thesis committee, Paul Smith, Steve Calvert, and Marc Bustin for their patient guidance. My deepest appreciation goes to Abdulkader Abed and Rushdi Sadqah, two friends to whom I'm truly indebted, and without whose help this study could never have been undertaken. Special thanks go to Lee Groat, Stuart Sutherland, Jim Mortensen, Mary Lou Bevier, and Phil Fralick for their friendship and advice.

This thesis benefited greatly from interactions with Tom Pedersen, Kristen Orians, Mati Raudsepp, Bert Mueller, and Maureen Soon. I would also like to thank, Abu Amamdoo, Sharkil, Abu Ismael, and Abu Dayub for their assistance in the field; Jim Haggart, Ellen Thomas, and Katrina von Salis for their help in fossil identification, Ulf Sturesson, Bob Garrison, Bruce Wilkinson, John Compton, Andrew Knoll, and Rich Harris for generously providing samples of coated grains, Bonnie Pemberton for her expertise in making probe mounts, and Mike Inglet and James Manders for providing oyster specimens used in this study and educating me on the finer details of oyster farming.

This research was supported by an NSERC operating grant to Kurt Grimm. Field work was funded in part by a Geological Association of America Grant (6116-97) and the Society of Economic Geologists Foundation through a Hugh Exton McKinstry Grant. Chemical analysis of oyster shells was made possible by an NSERC operating grant to Phil Fralick. This research was also supported by Predoctoral Fellowships from the Killam Foundation and the University of British Columbia's Graduate Fellowship Program.

A very special thanks go to my mom and dad. They were always there for me with their never ending love and support. Their untimely deaths forced me to grow in ways I never new possible. They are deeply missed, but their ideals remain steadfast in my heart.

I am especially indebted to my wife, Christa, and our new son Callum. Callum is the best thing that happened to us. Christa's unwavering love, patience, support and encouragement gave me the strength to finish. She was always there for me and never asked for anything in return. I couldn't have done it without her. We did it!

To Mom and Dad,
for your love and support

CHAPTER 1

INTRODUCTION

1.1 GENERAL STATEMENT AND PROBLEMS

Phosphorites are poorly understood marine biochemical deposits commonly associated with coastal upwelling environments (Glenn et al., 1994; Grimm,1997). Apart from being the primary source of P for fertilizer manufacture, phosphorites are also of great scientific interest because they contain important information regarding the physical and chemical characteristics of ancient oceans, and they provide valuable insight into the feedback processes that govern Earth's environmental evolution. As an essential nutrient for life, P governs biologic productivity on Earth (Froelich et al., 1982; Filippelli and Delaney, 1994; Delaney, 1998) and thus controls the rate at which CO_2 is removed from the atmosphere and is converted into organic matter (Föllmi et al., 1993; 1994). Despite a great deal of research, the formation of phosphatic strata remains enigmatic because of the complex interactions amongst the biological, authigenic, and sedimentary processes that govern their formation. Although increased utilization of interdisciplinary studies (based on sedimentology, paleontology, taphonomy, and geochemistry; e.g. Föllmi et al., 1994) in recent years has yielded novel insights into the controls governing the stratal architecture and origin of phosphatic facies, a controversy surrounds the paleoenvironmental factors that led to the formation of the regionally developed "phosphorite giants" of Earth's past.

"Phosphorite giants" are large, areally extensive economic phosphorites that lack precise modern analogues. Their distribution in the Phanerozoic is episodic (Cook and McElhinny, 1979), and most accumulated beneath shallow waters of marginal seas and epeiric platforms. There is uncertainty whether the distribution of "phosphorite giants" in the geologic record results from global variations in P cycling related to changes in the ocean-climate state of the Earth (e.g. Cook and McElhinny, 1979; Föllmi et al., 1994), or local sedimentologic and tectonic controls on P burial and hydraulic concentration processes (Baturin, 1971; Filippelli and Delaney, 1992; Filippelli, and Delaney, 1994). Sedimentologic data suggest that the

development of "phosphorite giants" is linked to marine transgressions through a number of interrelated factors: (1) elevated sea levels increase the accommodation volume on shelves, expanding the potential for suitable sites for phosphorite accumulation and increased upwelling into shelf seas; (2) marine transgressions may favour phosphorite accumulation by restricting the locus of diluting siliciclastics to nearshore environments; and (3) wave-induced and other cross-shelf currents may develop along flooded margins contributing to the winnowing, reworking, and concentration of phosphatic sediments into large deposits (Glenn et al., 1994).

The goal of this dissertation is to resolve the paleoenvironmental factors governing the formation of a "phosphorite giant", with particular reference to the South Tethyan Phosphogenic Province (STPP) in Jordan. The STPP is a carbonate-dominated Upper Cretaceous to Eocene phosphorite giant that extends from Colombia, through Venezuela, North and Northwest Africa to the Middle East (e.g. Notholt, 1980, 1985; Notholt et al., 1989; Föllmi et al., 1992), and is host to over 65% of the world's phosphate reserve base (Jasinski, 2000). Phosphatic strata in Jordan are associated with laterally extensive oyster buildups, and form a mosaic of facies that were deposited in a broad range of depositional environments. Economic phosphorites consist of thick, laterally continuous granular phosphorite beds that are interbedded with intervals of pristine phosphate, representing the preserved loci of phosphogenesis (Abed, 1988, 1989; Abed and Al-Agha, 1989; Abed and Sadaqah, 1998).

Three conceptually unified areas of research are the focus of this dissertation: (1) the sedimentology and stratigraphy of Upper Cretaceous (Campanian) phosphatic and related strata in Jordan (Chapter 2); (2) the petrography of multiply coated sedimentary apatite grains (Chapter 3); and (3) the skeletal trace element chemistry (Mg and Sr) of fossil oysters associated with economic phosphorite in Jordan (Chapter 4). Together, these investigations provide novel insights into the sedimentary and authigenic processes affecting phosphogenesis and the reworking of phosphatic sediment into economic phosphorite.

Chapter 2 highlights the depositional and stratigraphic controls governing the formation of economic phosphorite. In Chapter 2, sedimentological, paleontological, and geochemical evidence are presented that collectively suggest that economic phosphorites in Jordan accumulated on a productive epeiric platform in response to storm-induced amalgamation of granular phosphorite beds derived from contemporaneous pristine phosphate facies. This chapter brings to light the critical role an increase in storm frequency and intensity has in forming thick amalgamated phosphorite beds. These findings challenge the principles of "Baturin Cycling" for the origin of economic phosphorite (Baturin, 1971), and suggest that the STPP was fundamentally different from modern environments where phosphogenesis is occurring.

Chapter 3 focuses upon the sedimentologic and authigenic conditions influencing phosphogenesis. In Chapter 3, I construct a model for the formation of coated phosphate grains using backscattered electron (BSE) imaging, energy dispersive spectrometry (EDS), and stable isotope data. This model emphasizes the importance that changes in pore water redox chemistry have on the formation of some types of coated phosphate grains. These changes are attributed to variations in the biological oxygen demand within suboxic pore water environments that result from fluctuations in the sedimentation rate of organic carbon. The circumgranular record of diverse shallow burial and seafloor processes suggests that coated grains are the granular equivalent of condensed beds (Grimm and Galway, 1995), and may assist in the identification of transgressive and highstand systems tracts in phosphogenic systems.

In Chapter 4, an attempt is made to determine the temperature and salinity regime that prevailed over the Jordanian shelf during the accumulation of economic phosphorite using the trace element (Mg and Sr) chemistry of skeletal calcite from the Cretaceous oyster, *Oscillopha figari*. *O. figari* form laterally extensive buildups in Jordan that developed in association with the economic phosphorite. I compare the trace metal chemistry of the modern oyster *Crassostrea gigas* to *O. figari*, and highlight the problems of using oysters in

paleoenvironmental analysis. Although there is significant uncertainty in interpreting the trace element data, the results provide clear objectives for future research, and are consistent with sedimentologic evidence suggesting that oyster development occurred on a productive epeiric platform that underwent periods of intense upwelling.

The results of my research are presented as three stand-alone papers, which have been divided into chapters. The overlap of subject material between chapters is regrettable, but unavoidable when adopting this dissertation format. Your patience is appreciated when encountering repetitious material that is necessary in each chapter.

1.2 REFERENCES CITED

Abed, A.M., 1988. Eleventh International Field Workshop and Symposium - Guidebook: Third Jordanian Geological Conference International Geological Correlation Program Project 156 - Phosphorites. 124p.

Abed, A.M., 1989. On the genesis of the phosphorite-chert association of the Amman Formation in the Tel e Sur Area, Ruseifa, Jordan. Sciences Geologiques Bulletin. 42, 141-153.

Abed, A.M., and Al-Agha, M.R., 1989. Petrography, geochemistry and origin of the NW Jordan phosphorites. Journal of the Geological Society of London. 146, 499 - 506.

Abed, A.M., and Sadaqah, R., 1998. Role of Upper Cretaceous oyster bioherms in the deposition and accumulation of high-grade phosphorites in Central Jordan. Journal of Sedimentary Research. 68, 1009-1020.

Baturin, G.N., 1971. Stages of phosphorite formation on the ocean floor. Nature. 232, 61-62.

Cook, P.J., and McElhinny, M.W., 1979. A re-evaluation of the spatial and temporal distribution of sedimentary phosphate deposits in light of plate tectonics. Economic Geology. 74, 315-330.

Delaney, M.L., 1998. P accumulation in marine sediments and the oceanic P cycle. Global Biogeochemical Cycles. 12, 563-572.

Delaney, M.L., and Filippelli, G.M., 1994. An apparent contradiction in the role of phosphorus cycling in Cenozoic mass balances for the world ocean. Paleoceanography. 9, 513-527.

Filippelli, G.M., and Delaney, M.L., 1992. Similar phosphorus fluxes in ancient phosphorite deposits and a modern phosphogenic environment. Geology, 20, 709-712.

Filippelli, G.M., and Delaney, M.L., 1994. The oceanic P cycle and continental weathering during the Neogene. Paleoceanography. 9, 643-652.

Föllmi, K.B, Garrison, R.B., Ramirez, P.C., Zambrano-Ortiz, F., Kennedy, W.J., and Lehner, B.L., 1992. Cyclic phosphate-rich successions in the upper Cretaceous of Colombia. Palaeogeography, Palaeoclimatology, Palaeoecology. 93, 151-182.

Föllmi, K.B., Weissert, H., and Lini, A., 1993. Nonlinearities in phosphogenesis and P -carbon coupling and their implications for global change. In: Wollast, R., Mackenzie, F.T., and Chou, L. (Eds.), Interactions of C, N, P, and S Biogeochemical Cycles and Global Change. NATO ASI Series. Springer-Verlag, Berlin, 447-474.

Föllmi, K.B., Weissert, H., Bisping, M., and Funk, H., 1994. Phosphogenesis, carbon-isotope stratigraphy, and carbonate-platform evolution along the Lower Cretaceous northern Tethyan margin. Geological Society of America Bulletin. 106, 729-746.

Froelich, P.N., Bender, M.L., Luedtke, N.A., Heath, G.R., and DeVries, T., 1982. The marine P cycle. American Journal of Science. 282, 474-511.

Glenn, C.R., Föllmi, K.B., Riggs, S.R., Baturin, G.N., Grimm, K.A., Trappe, J., Abed, A.M., Galli-Oliver, C., Garrison, R.E., Ilyin, A.V., Jehl, C., Rohrlich, V., Sadaqah, R.M.Y., Schidlowski, M., Sheldon, R.E., and Siegmund, H., 1994. P and phosphorites: sedimentology and environments of formation. Eclogae Geologicae Helveticae. 87, 747 -788.

Grimm, K.A., 1997, Phosphorites feed people, Farm Folk/City Folk's Newsletter. 13, 4-5.

Grimm, K.A., and Galway, S., 1995. Phosphorite grain stratigraphies from the Oligo-Miocene sediments, Baja California Sur, Mexico: Clues towards shelf-to-basin correlation. Peninsular Geological Society, Third International Conference on the Geology of Baja California (Mexico), Abstract Volume.

Jasinski, S.M., 2000, Phosphate Rock. U.S. Geological Survey Mineral Commodity Summaries, U.S. Geological Survey. (http://minerals.usgs.gov/minerals/pubs/mcs/)

Notholt, A.J.G., 1980. Economic phosphatic sediments: mode of occurrence and stratigraphical distribution. Journal of the Geological Society of London. 137, 793-805.

Notholt, A.J.G., 1985. Phosphate resources in the Mediterranean (Tethyan) phosphogenic province: A progress report. Sciences Geologiques. Memoire 77, 9-21.

Notholt, A.J.G., Sheldon, R.P., and Davidson, D.F., 1989, Phosphate deposits of the world, Volume 2, Phosphate Rock Resources. Cambridge University Press, Cambridge. 566p.

Sheldon, R.P., 1980. Episodicity of phosphate deposition and deep ocean circulation – a hypothesis. In: Bentor, Y.K. (Eds.), Marine Phosphorites - Geochemistry, Occurrence, Genesis. Society of Economic Paleontologists and Mineralogists, 239-247.

CHAPTER 2

UPPER CRETACEOUS (CAMPANIAN) PHOSPHORITES IN JORDAN: IMPLICATIONS FOR THE FORMATION OF A SOUTH TETHYAN PHOSPHORITE GIANT

2.1 ABSTRACT

A well-preserved record of phosphorite depositional processes is preserved within the Campanian (Upper Cretaceous) Alhisa Phosphorite Formation in central and northern Jordan. The Alhisa Phosphorite Formation (AP) is part of the South Tethyan Phosphogenic Province (STPP), and contains a suite of sedimentary features that record storm reworking, stratigraphic condensation and the amalgamation of granular phosphorite event beds to form thick economic phosphorite. The AP is conformably underlain by cherts of the Amman Silicified Limestone Formation (ASL), and is conformably overlain by chalks of the Muwaqqar (M) Formation. The stratal architecture and stacking patterns, as well as the character of individual lithofacies, indicate that this succession forms the upper portion of a transgressive systems tract (TST) that accumulated on a highly productive, storm-dominated, east-west trending epeiric platform along the south Tethyan margin.

Prominent rock types include pristine phosphate, granular phosphorite, chert, chalk, and oyster rudstones organized into banks and isolated bioherms. Pristine phosphates are associated with well-developed micritic concretionary horizons and contain abundant spiral planktic foraminifera and a low diversity benthic assemblage of Buliminacean foraminifera, suggesting that pristine phosphates are a condensed facies and phosphogenesis was stimulated by the effects of a highly productive surface ocean and the suboxic diagenesis of sedimentary organic matter. The bulk sediment composition and absence of glauconite and other iron-bearing authigenic phases, such as pyrite and siderite within pristine phosphates, suggest that deposition and authigenesis occurred under conditions of detrital starvation and that "iron redox pumping" played a minimal role in phosphogenesis. Phosphogenesis in Jordan occurred in sedimentary environments spanning the entire platform. This is a non-uniformitarian phenomenon reflecting precipitation of sedimentary apatite across a wide depositional spectrum in a variety of depositional settings wherever the conditions were suitable for the precipitation of sedimentary

apatite. Establishment of this "phosphorite nursery" may have resulted from the combined effects of coastal upwelling, lagoonal circulation and P regeneration, which acted in concert to cyclically pump and sequester P across the platform.

Granular phosphorites consist of sharply-based, tabular amalgamated beds of massive, normally graded, and indistinctly stratified phosphatic grainstone that form thick economic phosphorites. Sedimentologic and stable isotopic data suggest that amalgamated beds formed through the amalgamation of storm-induced event beds derived from the pristine phosphates, and that temporal variations in storm frequency and intensity may have been a prerequisite for the formation of economic phosphorite.

The interpreted processes of syndepositional phosphogenesis and amalgamation to form economic phosphorites within a TST contrast sharply with the principles of "Baturin Cycling", emphasize the interplay of both auto- and allocyclic sedimentary processes to produce economic phosphorite. A TST coupled with high surface productivity and lagoonal circulation creates detritally starved settings for the establishment of a "phosphorite nursery"; storm reworking of pristine phosphate facies produces granular phosphorite; and amalgamation of storm-generated granular event beds forms economic phosphorite in a single systems tract.

2.2 INTRODUCTION

Economic phosphorites in Jordan are part of the South Tethyan Phosphogenic Province (STPP), a carbonate-dominated Upper Cretaceous to Eocene phosphorite giant that extends from Colombia, through Venezuela, North and Northwest Africa to the Middle East (e.g. Notholt, 1980, 1985; Notholt et al., 1989; Föllmi et al., 1992). The STPP constitutes the greatest accumulation of sedimentary phosphorites known and is of considerable economic importance as it hosts 66% of the world's phosphate reserve base and accounts for approximately 30% of phosphate rock production globally (Grimm, 1997; Jasinski, 2000). These deposits accumulated

on a carbonate-dominated epeiric platform along the South Tethyan margin (e.g. Abed, 1989, 1998, 1999; Glenn, 1990; Glenn and Arthur, 1990; Kolodny and Garrison, 1994; Lüning et al., 1998; Pufahl et al., 1998; 2000a,b). Like many phosphatic successions, these occurrences are also associated with biogenic carbonates and cherts.

Fascination with the STPP stems from the enormous size of the phosphorite deposits and the array of biologic and sedimentary processes that govern their stratigraphic distribution. Phosphorites contain important information regarding the physical and chemical characteristics of the ancient oceans, and provide valuable insight into the feedback processes that modify the biosphere. As one of the essential nutrients for life, P together with N governs biological productivity on Earth and thus controls the rate at which CO_2 is removed from the atmosphere and is converted into organic matter (Froelich et al., 1982; Filippelli and Delaney, 1994; Delaney, 1998). This interaction links the P cycle to the biogeochemical cycling of C, and makes P an important regulator of the Earth's climate and ecological change over geologic time (Föllmi et al., 1994; Föllmi, 1996). Furthermore, the economic implications of phosphorites as a non-renewable fertilizer ore emphasize the importance of reconstructing their stratigraphic architecture, paleoenvironmental settings, and the sedimentary processes that govern their formation (Herring and Fantel, 1993; Grimm 1997).

The extraordinary exposures of phosphatic and associated strata in Jordan provide an excellent opportunity to examine the paleoenvironmental factors that governed the formation of economic phosphorite in Jordan and the STPP. The purpose of this paper is to integrate sedimentologic, petrographic, paleoecologic, and stable isotopic studies of Jordanian phosphorites to: (1) elucidate the sedimentologic and authigenic conditions that prevailed over the Jordanian shelf; and (2) construct a depositional model for the formation of economic phosphorite that may be applicable to phosphatic successions elsewhere in the world.

2.3 METHODS

The interpretations presented in this paper are based on detailed measurement and sampling of ten stratigraphic sections from Ruseifa and the northern portion of the Al Abiad/Alhisa mining districts (Fig. 2.1). Reconnaissance studies of phosphorite deposits in northwest Jordan and southern Al Abiad/Alhisa (Abed, 1988; Sadaqah, 2000) were also undertaken to assist with the stratigraphic correlation of phosphatic strata. Emphasis was placed on field relations, regional stratigraphic trends, collection of samples for fossil identification and geochemistry, and petrographic analysis of polished thin sections.

Paleocurrent analysis of selected lithofacies was done with GeoOrient v. 7, a software package for plotting stereographic projections and current rose diagrams, using vector statistics (Potter and Pettijohn, 1963). Local and mean transport directions, and differences in mean orientation and variance of measured paleocurrents, were used to augment paleoenvironmental interpretations.

The petrography of samples was studied using transmitted light microscopy complemented with back scattered electron (BSE) imaging. BSE photomicrographs and energy-dispersive X-ray spectra of specimens were acquired with a Philips XL-30 scanning electron microscope equipped with a Princeton Gamm-Tech thin-window detector.

Phosphatic samples intended for carbon and oxygen stable isotopic analysis of the carbonate anionic complex in francolite were first disaggregated by leaching specimens for 48 hours in tri-ammonium citrate solution at pH 8.1 (Silverman et al., 1952). This treatment removes calcite but does not alter the isotopic composition of carbonate fluorapatite (CFA) (Kolodny and Kaplan, 1970; McArthur et al., 1986). Phosphatic grains were handpicked using tweezers and a dissecting microscope. Grains were then re-introduced into a solution of tri-ammonium citrate for 10 hours to ensure that all calcium carbonate had been dissolved from grain surfaces. Stable isotopic analyses were performed at the University of Western Ontario in

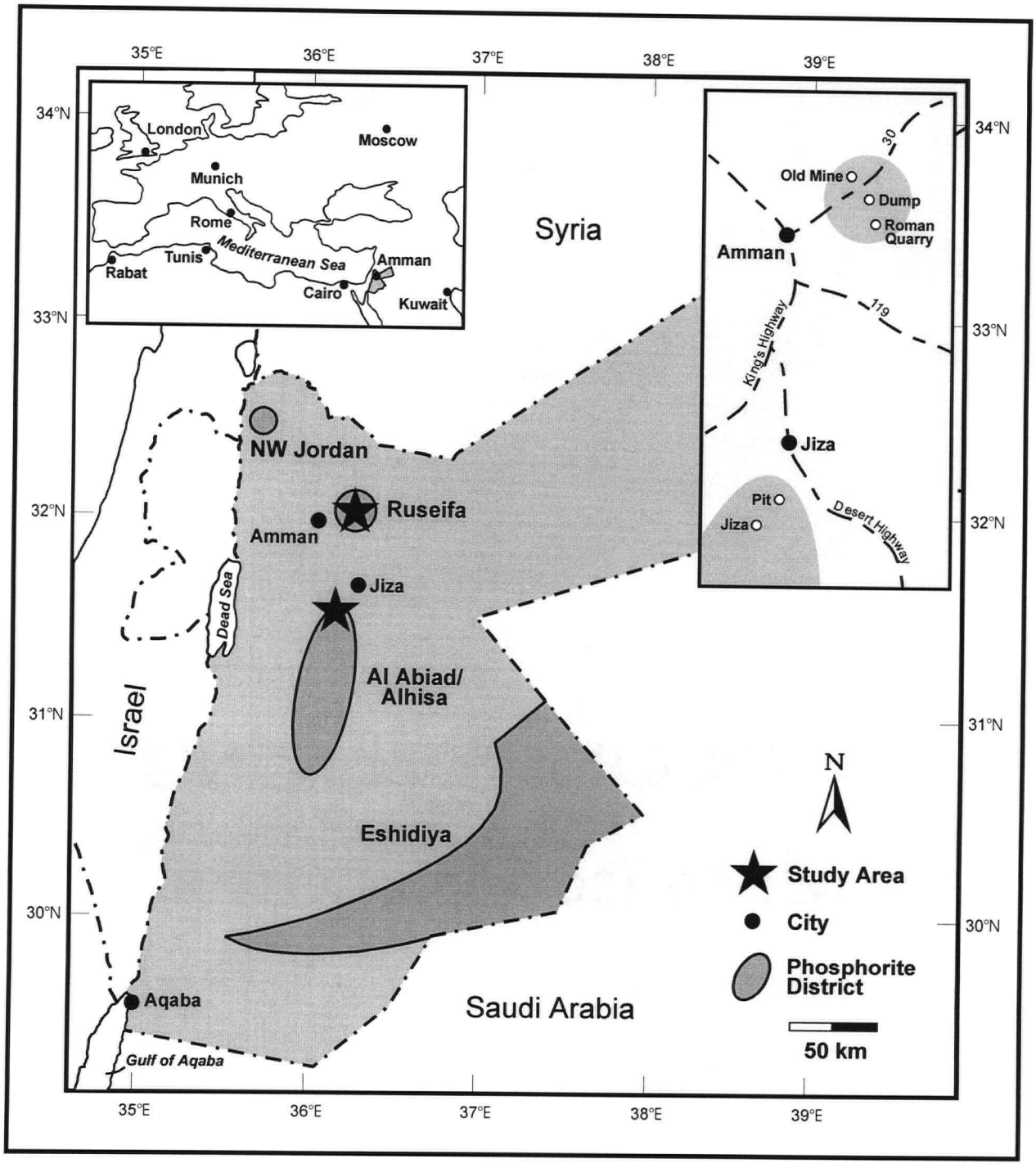

Figure 2.1 Map of Jordan showing phosphorite districts, location of project area, and position of stratigraphic sections.

the Laboratory for Stable Isotope Studies following the methods of McCrae (1950) using a fully automated Micromass Prism II mass spectrometer. Carbon and oxygen isotopic results are reported in per mil relative to the PDB standard using the delta notation.

2.4 GENERAL GEOLOGY

Phosphatic strata in Jordan underlie approximately 60% of the country (Abed, 1988), but economically exploitable deposits occur in only four regions; (1) NW Jordan; (2) Ruseifa; (3) Al Abiad/Alhisa; and (4) Eshidiya (Fig. 2.1). Together these deposits contain an estimated 5.5 billion tonnes of mineable phosphate (Abed and Amireh, 1999; Jasinski, 2000), nearly 15% of the global phosphate reserve base. Phosphorites in NW Jordan, Ruseifa, and Al Abiad/Alhisa reside within the Alhisa Phosphorite Formation (AP) (Abed, 1988, 1989; Abed and Al-Agha, 1989; Abed and Sadaqah, 1998) of the Belqa Group, a 1000 m thick conformable succession of Late Coniacian to Eocene, hemipelagic chalks, cherts, micrites, and phosphorite (Fig. 1) (Bender, 1974; Powell, 1989) (Fig. 2.2). At Eshidiya, the economic phosphorites have been interpreted by Abed and Amireh (1999) to belong to the Ajlun Group (Fig. 2.2) which consists of 600 m of Cenomanian to Turonian peritidal carbonates, cherts and chalks that disconformably underlie the Belqa Group.

The present report describes the sedimentary facies and facies associations of the AP in the Ruseifa and Al Abiad/Alhisa mining districts (Figs. 2.1 and 2.2). Consequently, only the formations within the Belqa Group are described below. Field investigations at Al Abiad/Alhisa were focused on the northern extremity of this mining district near the village of Jiza (Pufahl, 1998, 2000a,b). The Alhisa Phosphorite Formation crops out within the walls of open pit mines and wadis eroded through phosphatic successions. The stratigraphic nomenclature used in this report is that of Powell (1989).

The base of the Belqa Group is characterized by detrital chalks of the Ghudran Formation

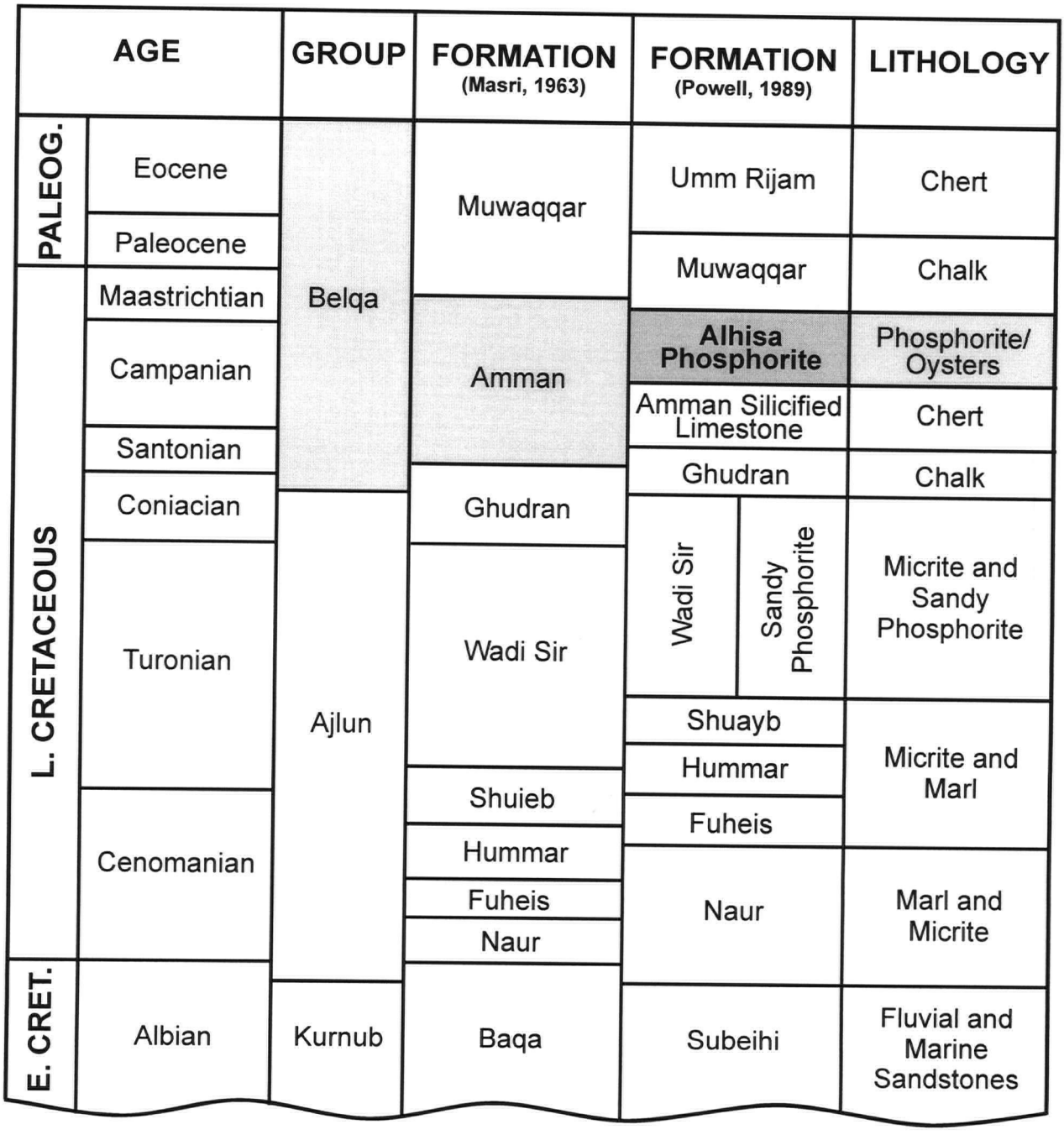

Figure 2.2 Age and general lithologies within the Kurnub, Ajlun, and Belqa groups showing the stratigraphic subdivisions used by previous workers (Masri, 1963) and those used in this study (Powell, 1989). Shading denotes portion of the section studied.

(G). This formation has been shown to thin from 80m in central Jordan to 50 m in the north, and has been determined to be Santonian in age based on ostracod-foraminifera assemblages (Bender, 1974; Powell, 1989).

The G is overlain by nearly 70m of cherts, chalks, and micrites of the Amman Silicified Limestone Formation (ASL) (Powell, 1989). The ASL thins from Al Abiad/Alhisa, where it attains a maximum thickness of 75 m, towards the north and east to 47 m and 13 m, respectively. The age of the ASL within the study area has been determined by Haggart (2000) to be upper Campanian, based on the occurrence of *Baculites* cf. *ovatus* within the formation. This age determination supports the assignment of the ASL to the Campanian (Wetzel and Morten, 1959), and correlates with the biozonation and range charts of macro- and micro fauna of equivalent strata west of the Dead Sea Rift (Reiss et al., 1985). The diachronous ASL has been shown by Powell (1989) and Bender (1974) to young towards the southeast; in northern Jordan this formation conformably overlies chalks of the Ghudran Formation (Bender, 1974; Powell, 1989) and the Ajlun Group in southern Jordan (Abed and Amireh, 1999).

The Alhisa Phosphorite Formation (AP) overlies the ASL and consists predominantly of interbedded phosphatic marls and granular phosphorites (Fig. 2.2). The AP also thins from central Jordan in a northward direction from a thickness of 65 m at Al Abiad/Alhisa to 10m in NW Jordan and Zakimat Al Hasah in the east of Jordan. At Al Abiad/Alhisa the AP is divisible into three stratigraphic members, from base to top these are: the Sultani Phosphorite (SP), Bahiya Oyster Coquina (BC), and Qatrana Phosphorite (QP) members. Foraminifera and coccoliths indicate an upper Campanian to lower Maastrichtian age (Powell, 1989; Huber, written comm., 1999; Von Salis, written comm., 1999; Sadaqah, 2000) for this formation. The presence of the ammonites *Libycoceras* sp. and *Anaklinoceras refluxum* at the top of the AP at Al Abiad/Alhisa (El-Hiyari, 1985; Khalil, 1986; Powell, 1989) suggests the upper formation boundary is coincident with or, very close to, the Campanian-Maastrichtian boundary. This is in agreement

with the Campanian age of similar deposits in Egypt, Israel, and Syria (e.g. Reiss et al., 1985; Notholt et al., 1989; Glenn and Arthur, 1990). Bender has shown (1974), based on regional mapping and field relations, that the AP is diachronous and onlaps successively younger strata towards the east and south-east.

The AP is conformably overlain by chalks of the Muwaqqar Formation (M). This formation ranges in age from the Maastrichtian to Paleocene based on planktic foraminifera and nannofossils (Bender, 1974; Powell, 1989). The M ranges in thickness from 20 to 780 m and exhibits large variations in thickness over short lateral distances (Powell, 1989).

The Umm Rijam Formation (UR) conformably overlies the M and is the uppermost unit of the Belqa Group. The UR consists predominantly of chalky limestone, chalk, and chert (Powell, 1989). Its thickness is difficult to reconstruct because its upper boundary forms the present-day erosion surface. There is, however, a general trend of decreasing thickness from ~200 m in northwest Jordan to ~130 m in southern Jordan (Powell, 1989). Foraminferal assemblages indicate a Paleocene to Eocene age for the UR. In the vicinity of the Dead Sea Rift the UR is unconformably overlain by conglomerates of the Oligocene to Neogene Dana Formation (Bender, 1974; Powell, 1989). The UR is not exposed within the study area.

2.5 PALEOGEOGRAPHY

Economic phosphorites within the STPP accumulated at paleolatitudes between 10° and 15° N (Sheldon, 1981; Al-Hunjul, 1995; Hay et al., 1999) on an east-west trending mixed carbonate-phosphorite epeiric platform along the south Tethyan margin. The common association of phosphatic strata with chert and organic-rich sediments in Israel and Egypt has been interpreted as an indication that phosphorite accumulation was associated with highly productive surface waters possibly caused by intense upwelling (Cook and McElhinny, 1979;

Reiss, 1988; Shemesh and Kolodny, 1988; Almogi-Labin et al., 1990, 1993; Kolodny and Garrison, 1994; Nathan et al., 1997;).

During the Late Cretaceous the South Tethyan margin underwent periodic episodes of tectonism associated with the northward movement of the African and Arabian plates into Eurasia (Garfunkel et al., 1981; Dercourt et al., 1986; Bowen and Jux, 1987; Ben-Avraham, 1989). These pulses resulted in widespread syndepositional folding of platform sediments producing an undulatory sea floor topography consisting of intrashelf sub-basins and swells (Kolodny, 1967; Bender, 1974; Steinitz, 1974; Avital et al., 1983; Bandel and Mikbel, 1985; Abed, 1998). In the eastern Mediterranean the most pronounced of these episodes produced the Syrian Arc, an S-shaped fold belt that extends from southern Turkey into the Sinai peninsula (Freund, 1965; Bowen and Jux, 1987). The Syrian Arc consists of a series of northeast to southwest trending asymmetric plunging anticlines with amplitudes of up to ~700 m and wavelengths on the order of ~20 km. Deformation along this tectonic front was contemporaneous with Upper Cretaceous phosphorite deposition, beginning in the Coniacian and continuing into the Miocene (Abed, 1988).

2.6 RESULTS

2.6.1 Lithofacies

Fifteen lithofacies are recognised within the study area that reflect the range of authigenic and sedimentary processes that operated on the Jordanian shelf. We first provide a detailed description and documentation of the lithofacies types, and then show how they are associated within the ASL, AP, and M formations. For descriptive purposes lithofacies have been arranged into three broad classes: (1) phosphatic; (2) carbonate; and (3) chert facies. The general attributes of each facies class are given in Table 2.1, and detailed descriptions follow.

Table 2.1 Characteristics and interpretation of lithofacies from the Ruseifa and Al Abiad/Alhisa mining districts.

Facies Category	Facies	Description	Trace fossils	Interpretation
Phosphate	Phosphatic marl	Parallel, thinly laminated chalk-rich marls interbedded with wavy, thickly laminated granular phosphatic grainstone; marly laminae contain *in situ* phosphatic peloids and a poorly preserved assemblage of non-keeled, biserial and trochospiral plankic foraminifera; granular laminae are sometimes graded and have sharp, erosive bases; micrite concretionary horizons are common	Unbioturbated except when overlain by parallel bedded grainstones; facies contact bioturbated with firmground *Thalassinoides* (*Glossi-fungites* ichnofacies)	Hemipelagic rainout in highly productive waters; phospho-genesis, and storm wave winnowing during periods of stratigraphic condensation under suboxic conditions
	Wavy laminated grainstone	Laminae are fine grained, non-graded, and range in thickness between 3-8mm; sharp lower and upper contacts; wavy laminated grainstones change laterally over several meters into poorly organised HCS grainstone sets	Unbioturbated	Deposition between fair- and storm-weather wave base under waning storm conditions
	Parallel bedded grainstones	Coarse-tail graded, massive, and indistinctly stratified beds that occur separately or in tabular, 100-150cm thick amalgamated beds; individual beds 1-50cm thick; moderately well sorted; coarsest and thickest layers contain transported micrite concretions and chalk rip ups along their bases	Firmground *Thalassinoides* (*Glossifungites ichnofacies*); micrite concretions contain simple cylindrical borings	Storm-induced amalgamation of granular beds to produce economic phosphorite; aerobic
Carbonate	Chalk	Parallel laminated, massive, and biotrubated varieties; laminae composing parallel laminated chalks are recrystallized and contain *in situ* phosphatic peloids and a poorly preserved assemblage of trochospiral planktic foraminifera	Bioturbated chalk contains well developed *Thalassinoides* burrow networks	Rainout of nannofossils; parallel laminated chalk, phosphogenesis, suboxic; bioturbated chalk, oxic
	Micritic Limestone	Parallel bedded and massive varieties; beds composing bedded micrites are recrystallized and contain a poorly preserved assemblage of biserial and trochospiral planktic and triserial benthic foraminifera; rare coquina- and grainstone filled scours	Unibioturbated	Suspension rain of fine grained carbonate in an open marine, suboxic environment; periodic storm scouring
Oyster buildups ↑	Highly fragmental oyster rudstone	Massive, 80-120cm thick beds composed of pebble-sized oyster shell fragments in clast support; forms bottomset beds to megacrossbedded oyster rudstone banks		Records bank progradation through offbank shedding into more distal shelfal areas
	Megacrossbedded oyster rudstone	Massive and normally graded, 40-150cm thick oyster coquina beds organized into megacrossbedded foresets aligned 25-30° to master bedding	Endolithic borings on shell surfaces	Cascading of shell material down bank from during progradation
	Oyster framestone	Forms cores of oyster buildups and composed of large, disarticulated valves and articulated *N. nicaisei* and *A. villei* in life position; mas-sive teardrop shaped mounds that taper in a down-current direction	Endolithic borings on shell surfaces	*In situ* growth of oysters within the photic zone
↓	Chalk-rich, highly fragmental oyster rudstone	Chalk-rich, massive, 30-60cm thick beds composed of oyster shell fragments in clast support; forms topset beds that overlie oyster framestones and truncates megacrossbedded oyster rudstone beds		Records eventual stranding and storm reworking of buildup top
	Graded oyster rudstone	Graded, 30-80cm thick beds composed of pebble-sized oyster shell fragments in clast support; intimately interbedded with chert facies	Endolithic borings on shell surfaces	Storm-induced calciclastic turbidites
	Medium bedded baculitid ammonite coquina	Consists of poorly sorted, massive and normally graded coquina beds containing abundant *Baculites* cf. *ovatus*, turretella-form gastropods, disarticulated *N. nicaisei* valves and crinoid fragments; orientated baculitid ammonite shells indicate offshore directed flow; beds are commonly silicified	Unbioturbated	Accumulation of storm-induced, calciclastic turbidites derived from unstressed shallower marine environments
	Thinly bedded bivalve coquina	Massive, sharp-based, poorly sorted beds containing thin-shelled bivalves and phosphatic peloids; facies blankets micrite concretion horizons within phosphatic marl facies	Unbioturbated	Storm wave winnowing of seafloor; suboxic environment
Chert	Bedded chert	Alternating beds of tan and dark-brown chert with sharp upper and lower contacts; dark-brown beds contain organic-rich blebs and form replacement seams in fractured tan cherts; pot scours common	In rare instances upper surfaces of beds contain simple cylindrical borings	Accumulation, storm sweeping and silicification of bedded micrites
	Chert breccia	Thin beds containing angular, pebble-sized fragments of tan chert floating in a matrix of dark-brown chert; chert fragments fit together like pieces of a jigsaw puzzle	Unbioturbated	Syneresis dessication/auto-brecciation associated with opal-to-chert transformations
	Chert conglomerate	Massive, poorly sorted, sharp-based beds that range in thickness from 10-30cm and contain subangular, pebble to cobble-sized clasts of tan chert in a matrix of dark-brown chert; clasts oriented long axis subparallel to bedding; intimately interbedded with bedded cherts	Pebble-sized chert clasts often contain simple cylindrical borings	Storm reworking, transport and redeposition of bedded chert and chert breccia; reworked hardgrounds

2.6.1.1 Phosphatic

Three lithofacies comprise this facies class: *phosphatic marl*, *wavy laminated grainstone*, and *parallel bedded grainstone*.

Phosphatic marl

The *phosphatic marl* facies is composed predominantly of parallel and wavy, thinly laminated (<3 mm thick), reddish-orange marls that are interbedded with wavy, thickly laminated, granular phosphatic grainstone (Fig. 2.3A). This facies has a friable texture resulting from intense chemical weathering. In thin section parallel laminated marly laminae contain abundant *in situ*, granule-sized phosphatic peloids, fish bone fragments, silt-sized detrital quartz grains, and a poorly preserved assemblage of non-keeled, biserial and trochospiral planktic foraminifera (Figs. 2.3B,C). The poor preservation of foramanifera precludes their exact identification. Phosphatic peloids are structureless, in matrix support and oriented long axes parallel to bedding. Laminae conform sympathetically above and below phosphatic grains. Organic carbon-rich blebs are also ubiquitous throughout marly layers suggesting that this facies was initially rich in sedimentary organic matter. The wavy laminated marls are characterized by a higher proportion of phosphatic peloids. Peloids within these layers are commonly abraded and are concentrated along laminae contacts.

Granular laminae consist of moderately to poorly sorted, structureless granule-sized phosphatic peloids in a chalk matrix (Fig. 2.3A). Slightly abraded planktic foraminifera tests, bone fragments, and pebble-sized subangular, *phosphatic marl* intraclasts are important accessory grains. Laminae have erosive bases and pinch and swell rhythmically over a lateral distance of 30 to 40 cm. The thickest laminae are graded and frequently contain thin, wispy, reddish-orange, marly partings throughout.

Figure 2.3 A) *Phosphatic marl* with discontinuous granular phosphatic laminae. This facies is a pristine phosphate facies and is composed predominantly of parallel, thinly laminated marl with abundant *in situ* granule-sized phosphatic peloids (white specs). B) Transmitted light photomicrograph of *phosphatic marl* facies. Laminae contain structureless phosphatic peloids (p), silt-sized detrital quartz grains and a poorly preserved assemblage of planktic foraminifera (f). Laminae conform sympathetically around *in situ* phosphatic peloids. C) Back-scatter electron image (BSE) of *phosphatic marl* facies showing abundant non-keeled, biserial, and trochospiral planktic foraminifera (light gray). Foraminifera tests are occluded with blocky calcite. The matrix is composed of chalk (dark gray) and organic carbon blebs (black). D) Discontinuous concretionary horizons associated with *phosphatic marl*. E) Bioturbated contact between *phosphatic marl* and *thickly bedded grainstone*. The contact is bioturbated with well developed *Thalassinoides* burrow networks excavated around micrites concretionary horizons, indicating firm ground formation and the development of the *Glossifungites* ichnofacies. Burrows within the *phosphatic marls* are infilled with granular phosphorite piped from the overlying amalgamated *parallel bedded grainstone* bed. F) Field shot of the *wavy laminated grainstone* facies. The inset highlights the hummocky cross stratification. G) Transmitted light photomicrograph of wavy laminae. Laminae are composed of well-rounded fine-grained phosphatic peloids in a chalk-rich micritic matrix. Both structureless and coated phosphatic peloids are common. Dark regions between grains are organic carbon-rich blebs (c). H) BSE image of coated phosphatic peloid nucleated around a phosphatized foraminifera test within the *wavy laminated grainstones*. Light gray clasts are structureless phosphatic peloids. Dark gray matrix material between clasts is a chalk-rich micrite.

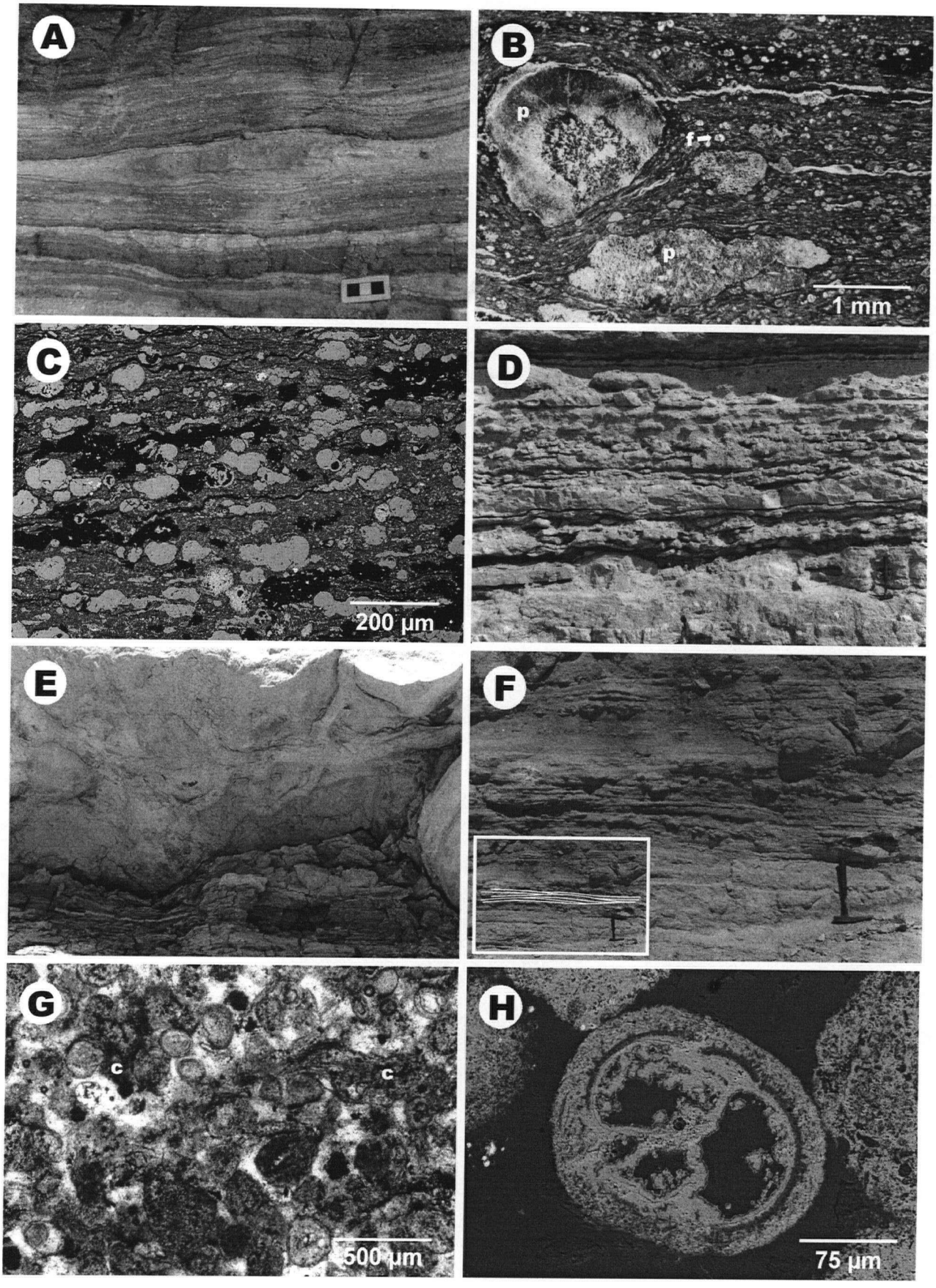
A
B
p
f
p
1 mm
C
200 µm
D
E
F
G
c
c
500 µm
H
75 µm

Discontinuous horizons of cobble-size, micrite concretions are also common within the *phosphatic marls* (Fig. 2.3D). Concretions are composed of calcite, and are massive oblate ellipsoids flattened in the plane of bedding that have commonly coalesced to form composite bodies 50 cm in length. Some concretions possess simple cylindrical, subvertical borings on their upper surfaces. Borings are 0.7 to 1.0 cm in width and penetrate to a maximum depth of 3cm.

This facies is unbioturbated except when directly overlain by amalgamated *parallel bedded phosphatic grainstones* (Fig. 2.3E). In these instances the facies contact is bioturbated with well-developed *Thalassinoides* burrow networks. This facies relation occurs seven times within the logged sections and is bioturbated in every case. Burrows are very sharp walled, have diameters of 2 to 3 cm and penetrate the *phosphatic marl* to a depth of 10 cm. Traces are passively infilled with granular phosphorite piped from overlying beds, reflecting the stable cohesive nature of the substrate at the time of colonization. *Thalassinoides* are also excavated to avoid micrite concretions, suggesting a preference of the trace-maker for firm, rather than hard substrates. These features are characteristic of the *Glossifungites* ichnofacies (redefined by Frey and Seilacher, 1980; Pemberton and Frey, 1985; MacEachern et al., 1991, 1992) and record trace fossil development within semilithified or firm substrates.

Interpretation: The *phosphatic marls* are a pristine phosphate facies (Föllmi et al., 1991) where apatite precipitated authigenically. The ubiquity of organic-rich blebs implies that this facies was once organic-rich and the abundance of non-keeled planktic foraminifera suggests that the *phosphatic marls* accumulated in a highly productive environment under suboxic conditions (Reiss, 1988; Almogi-Labin et al., 1993). Differential compaction around carbonate concretions and the presence of bored, reworked and transported concretions within *parallel bedded*

grainstones indicates an early diagenetic origin for concretionary development at very shallow burial levels prior to significant compaction.

Sadaqah (2000) reached similar conclusions from correlative *phosphatic marls* in northwestern and south-central Jordan. These marls are also unbioturbated and have yielded low diversity assemblages of planktic and benthic foraminifera. Planktic assemblages consist primarily of *Globigerinelloides volutus* with rare *Heterohelix globulosa*. Almogi-Labin et al. (1993) have compared similar Upper Cretaceous planktic foraminifera assemblages from correlative strata in Israel to modern upwelling-related foraminifera populations and have shown that high abundances of *Globigerinelloides* are indicative of a highly productive photic zone. Benthic assemblages are composed of abundant *Bulimina* cf. *aspera* and *Neobulimina fararensis*, sometimes accompanied by *Gavelinella* sp., *Anaomalinoides aegyptiacus,* and *Marginulina austina*. The abundance of Buliminacean foraminifera in a low diversity fauna is charactersitic of a relatively stable, dysaerobic ecosystem (Reiss, 1988; Almogi-Labin et al., 1993; Jorrisen et al., 1995; Widmark and Speijer, 1997; Jorrisen, 2000, written comm.). Highly productive surface waters and the export of organic matter to the sea floor presumably created quasi-anaerobic seafloor conditions through the microbial respiration of organic matter (Pedersen and Calvert, 1990). Only specialized benthic organisms, such as Buliminacean foraminifera, can thrive under these conditions. Buliminacean assemblages have been recorded in highly productive, modern and ancient low oxygen settings from around the world (Reiss, 1988). Their common occurrence in laminated, non-bioturbated sediments like porcelanites, cherts, organic-rich carbonates, and pristine phosphates from northern South America, Morocco, Egypt, Syria, and Iraq indicate that low diversity Beliminacean assemblages (Reiss, 1988) are characteristic of Upper Cretaceous high-productivity paleoenvironments and are indicative of suboxic bottom waters (Savrda and Bottjer, 1991; Tyson and Pearson, 1991).

The *phosphatic marl* facies reflects a continuum in the intensity of authigenesis and current reworking, and is similar to the wave-generated parallel and cross-laminated sand-streaked sand lithofacies described by de Raaf et al. (1977). The parallel laminated *phosphatic marls* are an unreworked pristine phosphate end-member formed from the hemipelagic rainout of phytoplankton and nannofossils. Wave-induced suspension and winnowing of the substrate produced the wavy laminated marly layers. During settling, wave oscillations apparently reached the sea floor, molding these layers into wavy laminae (de Raaf et al., 1977). As the intensity of wave reworking increased laminae became progressively more coarse-grained until granular laminae were formed from the concentration of *in situ* phosphatic peloids through winnowing.

Wavy laminated grainstone

This facies is composed predominantly of wavy laminated, fine-grained phosphatic grainstone. Laminae are non-graded and have sharp lower and upper contacts. Wavy laminated grainstones commonly change laterally over several meters into poorly organized hummocky cross-stratified grainstone sets (Fig. 2.3F). Sets are 10 to 20 cm thick and consist of thin, undulating and gently dipping fine-grained, phosphatic grainstone beds forming low amplitude (5 to 7 m), low relief (0.1 to 0.2 m) mounds and troughs. The dip orientation of beds within sets is highly variable, but is consistently less than 10º. Lower and upper set boundaries are nonerosive, passing gradationally into wavy bedded phosphatic grainstone over a vertical distance of 5 to 7 cm.

Laminae are composed of well-rounded, fine-grained phosphatic peloids in a chalky micritic matrix (Fig. 2.3G). Coated grains constitute approximately 5% of the grain population; foraminifera tests are the most common type of grain nuclei (Fig. 2.3H). Fragments of thin-shelled bivalves are also common constituents within some laminae.

Interpretation: The presence of hummocky cross-stratified phosphatic grainstone with the absence of wave-rippled reworked tops indicates that this facies accumulated between fair weather and storm wave base from suspension under waning storm conditions (Harms et al., 1975; Kreisa, 1981; Dott and Bourgeois, 1982; Arnott and Southard, 1990; Southard et al., 1990; Duke et al., 1991). The lack of bioturbation may be a result of high rates of sedimentation during storm deposition and/or the absence of benthic organisms related to suboxic/anoxic bottom conditions (Molina et al., 1997).

Parallel bedded grainstones

Parallel bedded grainstones consist of coarse-grained, granular phosphorite beds. Beds are tabular, sharp-based, generally with planar to subplanar basal contacts and occur separately or amalgamated (Fig. 2.4A). Beds are either coarse-tail graded, massive, or indistinctly stratified, and are demarcated within amalgamated beds by basal scour surfaces and discontinuous phosphatic and/or micritic concretionary horizons formed at bed tops.

Coarse-tail graded beds are 1 to 40 cm thick and grade from a granular/pebbly base to a coarse-grained top. The thinnest beds only occur within intervals of *phosphatic marl*, where they commonly blanket micrite concretionary horizons (Fig. 2.4B,C). The coarsest and thickest beds contain abundant transported, whole and broken micrite concretions along their bases (Fig. 2.4D). Concretions are commonly bored, and concentrated within the lower quarter of the bed (Fig. 2.4E).

Indistinctly stratified beds are 40 to 80 cm thick and contain laterally persistent, diffuse stratification bands (Fig. 2.4F). Bands range in thickness from 15 to 30 cm, and consist of (1) a basal zone of inverse-graded granular grainstone; (2) a pebbly core composed of pebble-sized

Figure 2.4 A) Amalgamated *parallel bedded grainstone* bed. This facies constitutes the economic phosphorite. Amalgamation surfaces between individual layers are demarcated by discontinuous micritic and phosphatic concretionary horizons. B) Thin *parallel bedded grainstone* beds interbedded with thin packages of *phosphatic marl* (recessive). C) Close-up of thin, coarse-tail graded *parallel bedded grainstone* beds. Beds are poorly sorted and grade from a granular base with angular chalk rip ups (white clast above scale) to a medium grained top. Beds are separated by wavy laminated *phosphatic marl* partings. White specs within beds are phosphatic peloids. D) Coarse-tail graded grainstone bed with broken micrite concretions (arrows). Concretions are in matrix support, sometimes bored, and concentrated in the lower quarter of the layer. E) Close-up of micrite concretion along the base of a coarse-tail graded grainstone layer showing cylindrical borings (arrows) on its surface. F) Indistinctly stratified grainstone bed. The dark band in the centre of the layer is composed of subangular, pebble-sized chert clasts and coarsens then fines upward through the thickness of the bed. G) Close-up showing the texture of a massive grainstone layer. White specs are granule- and pebble-sized phosphatic peloids. Grain orientation is highly variable with pebble-sized clasts exhibiting the strongest grain fabric, aligned long-axis sub-parallel to bedding. H) Well developed *Thalassinoides* burrow networks along the base of a *thickly bedded grainstone* layer. Networks consist of horizontal tiers of cylindrical, bifurcating burrows infilled with granular phosphorite. The white area beneath the hammer is a micrite concretion.

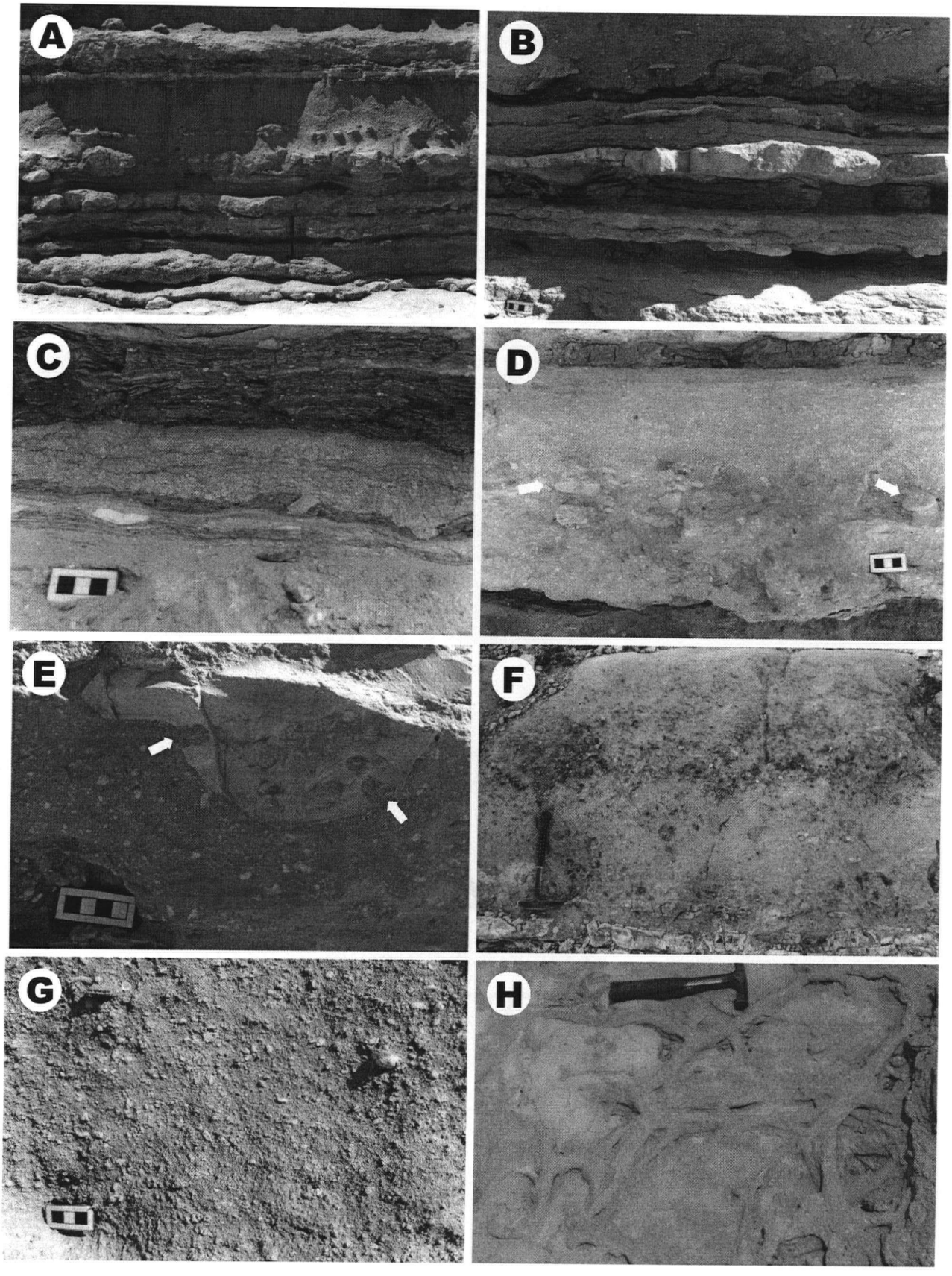
A
B
C
D
E
F
G
H

phosphatic intraclasts, shell fragments, vertebrate fossils, and rare angular chert clasts floating in a granular matrix; and (3) a normally graded granular top. Bands do not possess distinct boundaries, but coarsen- then fine-upward gradationally over the entire layer. The thickness of individual bands is directly proportional to overall layer thickness; the broadest bands occurring in the thickest beds. Grains within indistinctly stratified beds show no preferential orientation except in band centres, where in rare instances pebble-sized phosphatic intraclasts and shell fragments are aligned with their long axes subparallel to bedding.

Massive beds range in thickness from 30 to 50 cm, are moderately sorted and lack internal structure (Fig. 2.4G). Grain orientation is highly variable with pebble-sized clasts exhibiting the strongest grain fabric, aligned with their long axes sub-parallel to bedding.

Amalgamated *parallel bedded grainstones* are 100 to 150 cm thick and are commonly bioturbated with well developed *Thalassinoides* burrow networks (Fig. 2.4H). Networks consist of horizontal tiers of cylindrical, bifurcating burrows infilled with granular phosphatic grainstone. Galleries are common and are developed at irregular spacings along burrows and where traces split. As in the *phosphatic marls*, burrow networks are always excavated to avoid *in situ* phosphatic and micritic concretions developed at bed tops, reflecting the stable, cohesive nature of the substrate and the development of the *Glossifungites* ichnofacies.

Transmitted light and backscattered electron microscopy reveal that grainstone beds are predominantly composed of well rounded, very coarse sand and granule-sized phosphatic peloids and sub-rounded, phosphatic intraclasts in a chalk matrix (Fig. 2.5A). Bone fragments and pebble-size chalk intraclasts are also common constituents within beds. Phosphatic peloids are generally structureless, but in rare instances are coated (Fig. 2.5B). Coated peloids are concentrically laminated around nuclei of phosphatized foramanifera tests, bone fragments, and other phosphatic peloids (Fig. 2.5C, D). Phosphatic intraclasts are composed of phosphatized chalk and commonly contain fish bones, unaltered foraminifera tests, and phosphatic peloids.

Figure 2.5 A) Transmitted light photomicrograph of *parallel bedded grainstone*. Grainstone layers are composed of well rounded, very coarse sand and granule-sized phosphatic peloids (p), subrounded, phosphatic intraclasts (i), vertebrae bone fragments (b). Grains are in point or tangential contact and randomly oriented. B) Transmitted light photomicrograph of coated phosphate grains within *parallel bedded grainstone* beds. Grains are concentrically laminated around nuclei of granule-sized phosphatic peloids, and are cemented with blocky calcite (light gray) and carbonate fluorapatite (dark gray). C) BSE image of a coated phosphatic peloid showing concentric lamination around a granule-sized phosphatic peloid. D) BSE image of coated phosphatic peloid showing concentric lamination around a phosphatized foraminifera test that is partially occluded with francolite. E) BSE image of phosphatic intraclast with indurated grain margin (light gray rim). F) BSE image of microporosity showing submillimetre thick, intervoid coatings of francolite. G) Transmitted light photomicrograph of intraclasts with structured voids interpreted as endolithic borings. H) Cross polarized light photomicrograph of a well-cemented *parallel bedded grainstone*. Blocky calcite is the dominant cement type.

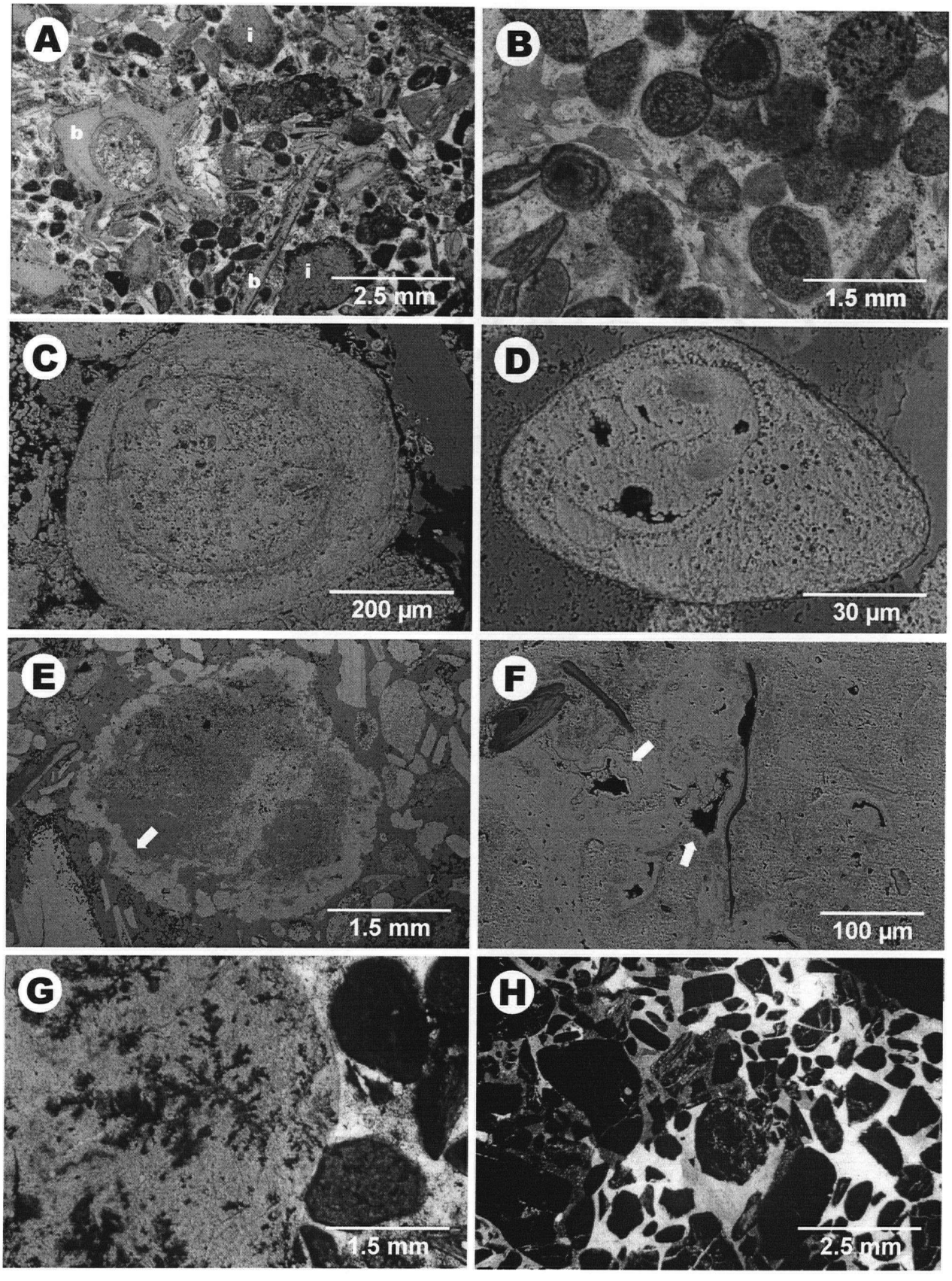
A
i
b
b
i
2.5 mm
B
1.5 mm
C
200 µm
D
30 µm
E
1.5 mm
F
100 µm
G
1.5 mm
H
2.5 mm

Backscattered electron microscopy reveals that some intraclast margins are indurated (Fig. 2.5E), and possess a well-developed microporosity that is partially occluded by submillimetre thick, coatings of phosphate (Fig. 2.5F). In rare instances intraclast surfaces contain structured voids interpreted as endolithic borings (Fig. 2.5G). Blocky calcite is the principal cement type (Fig. 2.5H).

Some layers are silicified and, in addition to the grain types outlined above, also contain angular, pebble-sized, chert rip ups, and rare silt-sized monocrystalline quartz grains. Chert rip ups are composed of microcrystalline quartz and are commonly coated with a thin isopachous calcite rim. Silicification of clasts took place selectively and incompletely, only occurring in bone fragments where the original material was replaced by microcrystalline quartz. The dominant cement types in silicified beds are equigranular microcrystalline and mosaic drusy quartz with subordinate amounts of blocky calcite. Silicification in grainstone layers occurs preferentially along layer tops, penetrating to a depth of 5 to 10 cm.

Interpretation: This facies represents phosphatic event beds. Normally graded beds are interpreted to have been deposited by rapid grain-by-grain deposition from suspension, with rapid burial and no significant traction transport on the bed from a single-surge, high density turbidity current (Walker, 1977, 1978; Lowe, 1982; Pickering et al., 1986).

Massive and indistinctly stratified grainstones are interpreted to record traction carpet deposition under a sustained, turbulent current (Lowe, 1982; Hiscott, 1994; Sohn, 1997). Sohn (1997) has shown that deposition from traction carpets occurs progressively from the bottom up in response to the deposition of grains at the base of the traction carpet, producing an aggraded bed whose cumulative thickness is a function of flow duration and deposition rate. Massive beds form if the grain size of the supplied sediment does not vary during deposition. However, if the grain size of the supplied sediment varies with time under sustained traction carpet

sedimentation, indistinctly stratified deposits with coarsening- then fining-upward intervals with diffuse boundaries are produced. The pebbly bands within indistinctly stratified grainstone layers are interpreted to have formed in this manner, and thus record incremental aggradation of the traction carpet together with variations in the grain size and lithology of the sediment being deposited.

2.6.1.2 Carbonate

This facies class consists of a *chalk* and *micrite* facies, and a subgroup that includes the bioclastic carbonates.

Chalk

This facies is formed of reddish-orange, parallel laminated, massive and bioturbated chalk. The parallel laminated chalks are the most common, and consist of non-erosive but sharply based laminae (Fig. 2.6A). In thin section laminae are recrystallized and consist of calcareous nannofossils and microcrystalline aggregates of medium silt-sized, subhedral calcite rhombs, organic carbon-rich blebs, *in situ* phosphatic peloids, and recrystallized trochospiral planktic and uniserial benthic foraminifera tests (Thomas, 1999, written comm.) in a nannofossil matrix. Calcareous nannofossils are generally poorly preserved and include *Micula decussata*, *Uniplanarius gothicus*, *Lithastrinus quaricuspis*, *Watznaueria barnesae*, *Zuegrahabdotus bicrescenticus*, *Kamptnerius magnificus*, *Reinhardtites levis*, *Eifellithus turriseiffelii*, and *Thoracosphaera* (Von Salis, 1999, written comm.).

The parallel laminated chalks are a pristine phosphate facies distinguished from the *phosphatic marls* by their higher chalk content, lower proportion of *in situ* phosphatic peloids, and the absence of associated micrite concretionary horizons. As in the *phosphatic marls* laminae conform sympathetically around peloids. In rare instances phosphatic peloids are

Figure 2.6 A) Parallel bedded chalk. Dashed line highlights the erosive base of a thin *parallel bedded grainstone* bed. B) Bioturbated chalk with well developed *Thalassinoides* boxworks. C) Field shot of the parallel bedded micritic limestone showing the monotonous nature of its bedding. D) (left) BSE image of a trochospiral planktic foraminifera that is common within the *micritic limestones*. (right) BSE image of a triserial benthic foraminifera within the *micritic limestones*. Foraminifera tests are partially occluded with blocky calcite and float within a matrix of recrystallized micrite. Black regions are intercrystalline voids. E) Field shot showing grainstone-filled scours within the *micritic limestone*. The inset highlights the base of the scours. F) Burrowed contact between a package of parallel bedded micritic limestone and an amalgamated *thickly bedded grainstone*. Burrows consist of subvertical cylindrical tubes (arrow) infilled with granular phosphorite piped from the overlying grainstone bed.

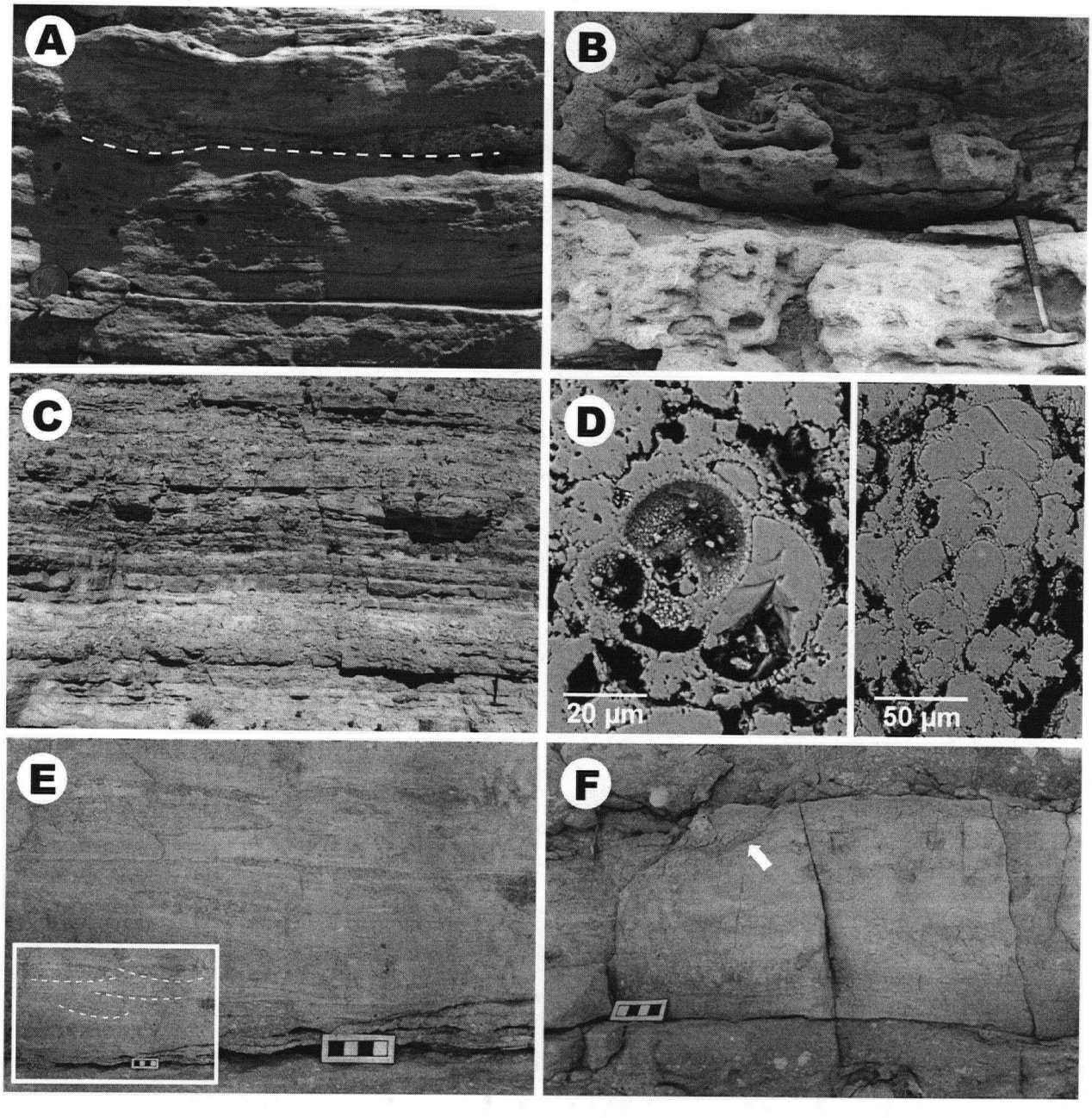
A
B
C
D
20 µm
50 µm
E
F

concentrated along the contacts between chalky laminae. Graded, thin *parallel bedded grainstones* also occur interbedded within this facies.

Massive chalks are similar in composition to the wavy layered chalks except for the conspicuous absence of *in situ* phosphatic peloids. Bioturbated chalks contain well developed *Thalassinoides* burrow networks identical to those within the *phosphatic marl* and *thickly bedded grainstone* facies (Fig. 2.6B).

Interpretation: The chalks were deposited by the rainout of nannofossils to the seafloor. The lack of bioturbation and the ubiquity of organic-rich blebs in the laminated chalks suggest that they were once organic-rich and may have been deposited under suboxic conditions. The presence of concentrated accumulations of phosphatic peloids along the contacts of some laminae records episodes of wave winnowing of *in situ* phosphatic peloids. The occurrence of graded, thin bedded grainstone beds indicates that high density turbidity currents also operated to concentrate phosphorite within with facies.

Micritic limestone

Parallel bedded micritic limestones characterize this facies (Fig. 2.6C). Laminae are formed of subhedral, fine silt-sized calcite rhombs with sutured grain boundaries. Most beds contain a poorly preserved assemblage of biserial and trochospiral planktic foraminifera and triserial benthic foraminifera (Thomas, 1999, written comm.). Foraminfera tests are recrystallized and partially or completely occluded with blocky calcite (Fig. 2.6D). Contacts between beds are sharp and non-erosive. Massive micritic limestones are completely recrystallized and consists of interlocking, silt-sized, microcrystalline aggregates of calcite.

Rare, thin *parallel bedded grainstones*, scour structures (Fig. 2.6E), and burrowed firm grounds are also present within this facies (Fig. 2.6F). Scours are infilled with either phosphatic

grainstone and/or *baculitid ammonite coquina*, and are preserved as 5 to 10cm long lenses with erosive soles. Baculitid ammonite shell fragments are in clast support and oriented long axis sub-parallel to the base of the scour. Oyster shell fragments are also in clast support and positioned concave-side down sub-parallel to the scour base. The three-dimensional geometry of the scours is difficult to discern, but exposures where the outcrop walls are irregular suggest that they are scoop-shaped.

Firmgrounds are sometimes reworked and best observed along facies contacts with *parallel bedded grainstones*. This facies relationship occurs twenty six times and shows evidence of burrowing along the facies contact five times. The burrows consist of branching, smooth-walled, cylindrical tubes, 1 to 2 cm in diameter, that penetrate the micrites to a depth of 10cm. These structures resemble *Thalassinoides*, and are infilled with granular phosphorite piped from the overlying grainstone bed, reflecting the cohesive nature of the substrate at the time of colonisation.

Interpretation: The parallel bedded nature and the presence of biserial and trochospiral planktic foraminifera suggests that the micrites accumulated from suspension rain of fine-grained carbonate in an open marine environment (Almogi-Labin et al., 1993; Widmark and Speijer, 1997) below fair-weather wave-base. The scours within this facies closely resemble pot scours and indicate that the seafloor was periodically swept by storms. Pot scours are relatively common features of ancient storm deposits, and result from erosion by storm-induced currents flowing along an irregular seafloor (Myrow, 1992; Leithold and Bourgeois, 1984; Tsujita, 1995). Scouring was initiated by vortical and/or turbulent flow developed within seafloor depressions. As storm energy increases, the depression deepens and sediment transported along the bottom is redeposited in the newly formed scour (Tsujita, 1995).

Bioclastic

The bioclastic carbonates consist of seven lithofacies, four of which comprise oyster buildups. Those facies that form oyster buildups will be described and interpreted collectively followed by interpretation and discussion of the remaining lithofacies.

Oyster buildups

Buildups are composed of four facies: (1) *highly fragmented oyster rudstone*; (2) *megacrossbedded oyster rudstone*; (3) *oyster framestone*; and (4) *chalk-rich, highly fragmented oyster rudstone*. These facies are organized into banks and isolated bioherms as defined by Wilson (1975) (Fig. 2.7A). Under Wilson's classification scheme a bank is formed of detrital biogenic sediment that accumulates by trapping, baffling, and/or mechanical piling through current action. Bioherms are buildups formed largely by the *in situ* production of carbonate by organisms or as framework or encrusting growth as opposed to hydrodynamic piling. Oyster banks in Jordan consist of a basal bed of *highly fragmented oyster rudstone* overlain by a set of *megascrossbedded oyster rudstone* that is truncated at its top by a bed of *chalk-rich highly fragmented oyster rudstone* (Fig. 2.7A, 2.8A). Composite banks containing stacked sets of *megacrossbedded oyster rudstone* are also present within the study area (Fig. 2.7B). These structures consist of a lower megacrossbedded set overlain by an upper set with very different dip orientations. Banks are 8 to 12 m thick and pinch out laterally over several kilometres. Isolated bioherms are tear-dropped shaped and formed of an *oyster framestone* core that is flanked on its sides by *megacrossbedded oyster rudstone* (Fig. 2.7C). They are 6 to 10 m thick and extend laterally for several hundred meters. Banks and bioherms are monospecific and composed of either *Nicaisolopha nicaisei* at Ruseifa or *Ambigostrea Villei* at Al Abiad/Alhisa.

Figure 2.7 A) Oyster bank from Al Abiad/Alhisa. Dashed lines in all figures marks the contact between the ASL and AP. Solid, slanted lines show the foreset dip orientation of *megacrossbedded oyster rudstones*. B) Composite oyster bank from Al Abiad/Alhisa. These structures consist of a lower east-directed megacrossbedded oyster rudstone set that is sharply overlain by an upper, south-directed set. C) Isolated oyster bioherm. Stratigraphic relations indicate that bioherms are tear-drop shaped and taper in a down current direction. They are sometimes overlain by south-directed *megacrossbedded oyster rudstone* sets.

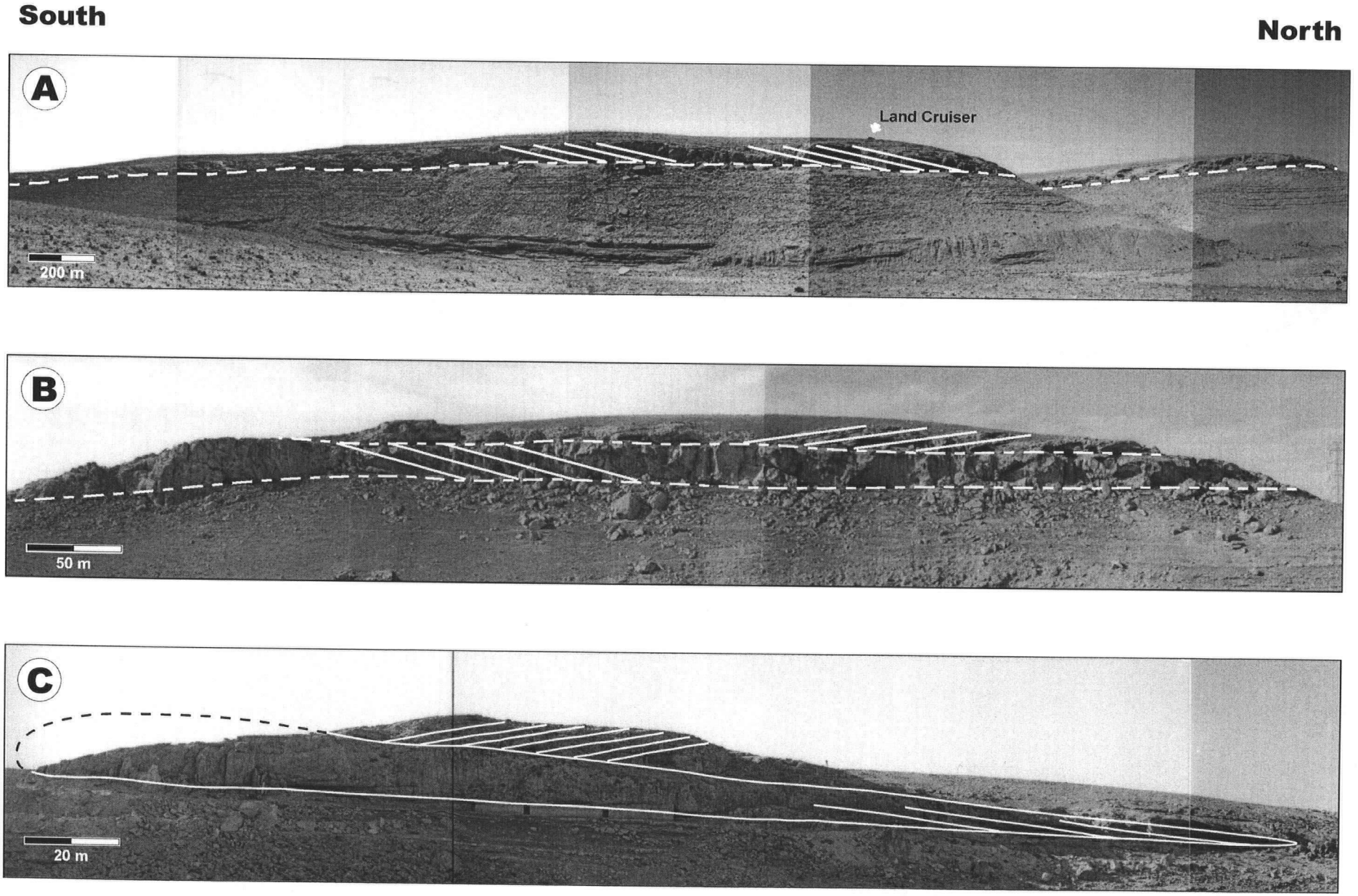
South
North
A
Land Cruiser
200 m
B
50 m
C
20 m

Figure 2.8 A) Cross section through an oyster bank at Al Abiad/Alhisa showing the different architectural elements: FO - *highly fragmental oyster rudstone* bottomset bed, MO - foreset beds consisting of *megacrossbedded oyster rudstone*, and CO - *chalk-rich, highly fragmental oyster rudstone* topset bed. Buildups at Al Abiad/Alhisa conformably overlie the Sultani Phosphorite (SP). Solid lines mark the contacts between elements. Dashed lines parallel the dip orientations of foreset beds within *megacrossbedded oyster rudstones*. Note how CO erosionally truncates MO. B) Photo showing the relationship between *highly fragmental* and *megacrossbedded oyster rudstones*. *Megacrossbedded oyster rudstone* beds thin and become finer grained down dip over several decimeters, eventually changing into *highly fragmental oyster rudstone* beds (dashed lines in inset) that drape the underlying strata. The solid line within the inset marks the facies contact. C) Field shot of *megacrossbedded oyster rudstone*. This facies consists of massive and normally graded thickly bedded oyster coquina beds. Beds have sharp bottom contacts aligned at 25-30° to master bedding. D) Transmitted light photomicrograph of a partially silicified oyster shell from a *megacrossbedded oyster rudstone*. Silicification within shells typically occurs preferentially along shell margins as chalcedonic replacement (c) of the oyster calcite. Silicified shells possess unrecrystallized centres. E) Basal contact of oyster bioherm. This contact is sharp with the *chalks* of the SP, and is characterized by an abundance of slightly abraded, disarticulated oyster valves oriented in a concave-up position. F) Field shot of *oyster framestone* that comprises the core of oyster bioherms. Articulated *A. villei* are firmly attached to each other by their left valve and in life position. G) Transmitted light photomicrograph of *oyster framestone* showing unrecrystallized and partially recrystallized *A. villei* valves. Shells are cemented with blocky calcite (b). Unrecrystallized regions in the matrix are chalk-rich micrite (m). H) *Chalk-rich, highly fragmental oyster rudstone* bed. This facies sharply overlies *oyster framestone* cores of oyster bioherms and erosively truncates *megacrossbedded oyster rudstone* sets within oyster banks.

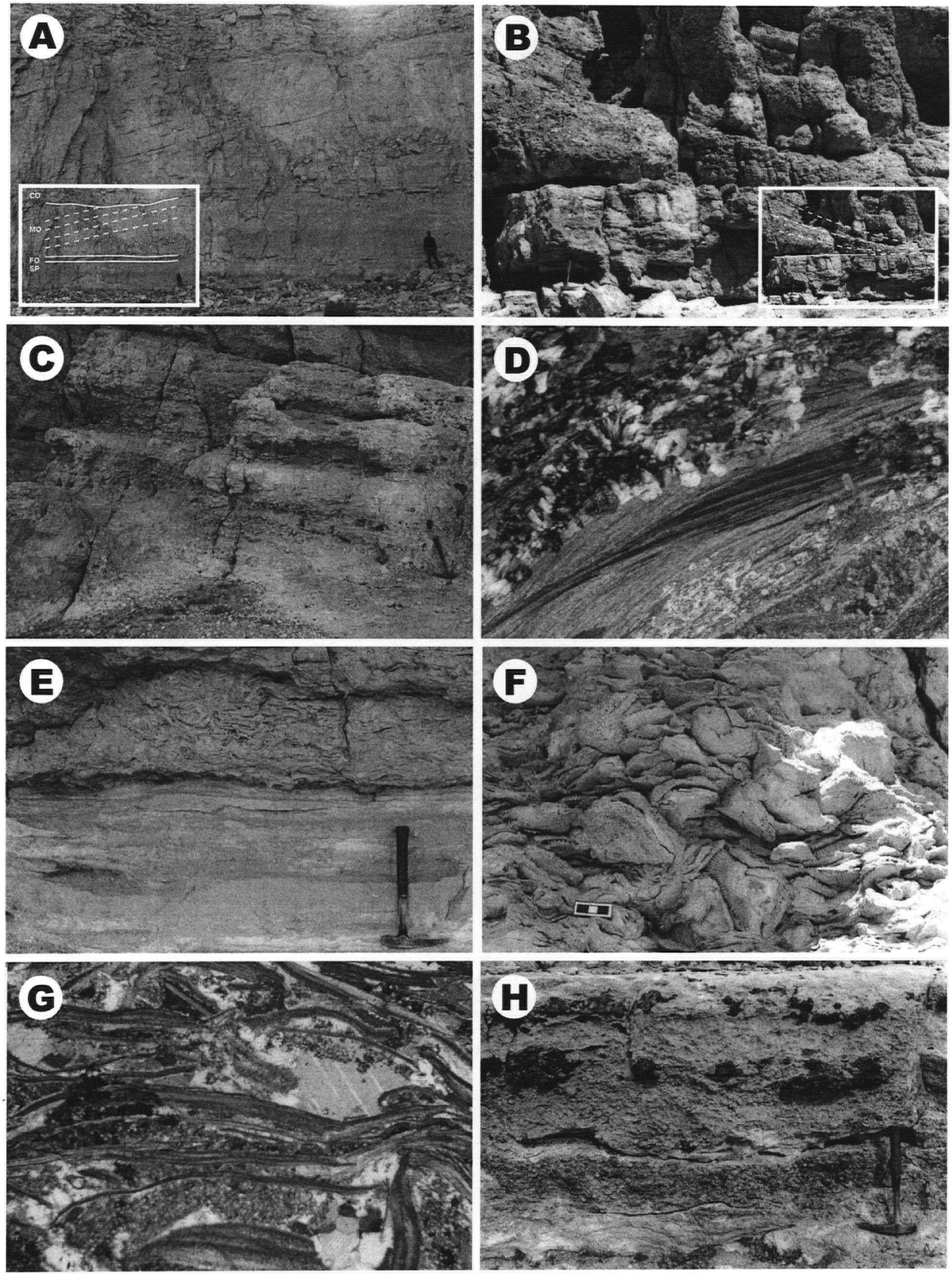
A
CO
MO
FO
SP
B
C
D
E
F
G
H

Highly fragmented oyster rudstone

This facies is restricted to Al Abiad/Alhisa where it forms the base of *megacrossbedded oyster rudstone* banks (Fig. 2.8B). Beds are massive, range in thickness from 80 to 120 cm, and are composed of pebble-sized shell fragments. Shells are in clast support and oriented parallel to bedding. Individual beds show a grain size diminution in an offbank direction. In thin section shells are completely recrystallized and cemented with blocky calcite.

Megacrossbedded oyster rudstone

Massive and normally graded, 40 to 150 cm thick oyster coquina beds organized into megacrossbedded foresets constitute this facies (Fig. 2.8A,C). Graded beds contain whole and slightly abraded, disarticulated oysters with rare micrite rip ups at their bases, and grade gradationally to a chalk-rich top consisting of pebble-sized oyster shell fragments. Massive beds are primarily composed of disarticulated and broken oyster shells in equal proportion. Shells are in clast support and oriented concave side up or down with long axis parallel to bedding. In north central Jordan megacrossbedded oyster rudstones are composed predominantly of *A. villei* valves. *A. villei* shells range in length from 7 to 15 cm and are typically 1.5 to 2 cm thick. At Ruseifa beds consist exclusively of disarticulated and broken *N. nicaisei* shells. *N. nicaisei* shells are slightly smaller than *A. villei*, ranging in length from 5 to 9 cm and 0.5 to 1 cm in thickness. Valve surfaces contain endolithic borings identical to those in the *oyster rudstones*. In northern Jordan graded and massive chert conglomerate beds are also interbedded with oyster rudstones. Chert conglomerates are composed of pebble- and small cobble-sized chert intraclasts in clast support. Both rudstone and chert beds have sharp, erosive bottom contacts aligned 25 to 30° to master bedding.

In some localities the graded and massive oyster coquina beds that comprise the *megacrossbedded oyster rudstone* facies are observed to thin and become finer grained down dip

over several decimetres along the base of the bank, changing over several decimetres into *highly fragmental oyster rudstones* that drape the underlying strata. Where several beds converge, a single thick, tabular, highly fragmented oyster rudstone bed is formed (Fig. 2.8B).

In thin section unrecrystallized oyster shells preserve a foliated structure consisting of lath-like calcite crystallites. Partially recrystallized shells have corroded margins and a patchy distribution of blocky calcite. Shells that have undergone complete recrystallization are totally replaced by blocky calcite. The matrix consists of microcrystalline calcite with rare, granule-sized phosphatic peloids, reptile and fish bone fragments, and subrounded silt-sized, microcrystalline chert intraclasts and detrital quartz grains disseminated throughout. Coated grains are extremely rare but when present have quartz grains and silt-sized phosphatic intraclasts at their centres. In pervasively recrystallized beds shelter and interparticle pore spaces are completely occluded with blocky calcite.

Silicification within rudstone beds is common and occurs preferentially within shells and shell fragments, forming siliceous nodules. Silicified shells are preferentially replaced along shell margins with either mosaic quartz or spherulitic chalcedony, preserving the primary calcitic fabric at the shell centre (Fig. 2.8D). Drusy quartz and spherulitic chalcedony are the dominant cement types within silicified beds. The distribution of these phases is patchy and the replacement of the carbonate matrix is incomplete in places, producing a mottled texture.

Crossbed dip orientations measured from *megacrossbedded oyster rudstones* indicate that paleoflow was predominantly towards the east and south (Fig. 2.9). Easterly paleoflows were obtained from *megacrossbedded oyster rudstone* sets at the base of composite banks. South directed paleocurrent directions were measured from isolated outcrops of crossbedded rudstones, and from crossbedded sets immediately above east directed oyster rudstone sets within composite banks. The transition from east-directed to south-directed paleoflows is sharp from one set to the next.

Figure 2.9 Geological map with mean paleocurrent directions for the Bahiya Coquina member of the Alhisa Phosphorite Formation. Crossbed dip orientations were measured on *megacrossbedded oyster rudstones* that form oyster banks, composite banks, and isolated bioherms. A total of 786 readings were recorded. Black arrows record east- and northeast-directed flow. White arrows indicate south-directed flow. Where white arrows overlie black arrows paleocurrent measurements were taken from composite banks in which south-directed *megacrossbedded oyster rudstone* sets stratigraphically overlie east- and north-east directed sets.

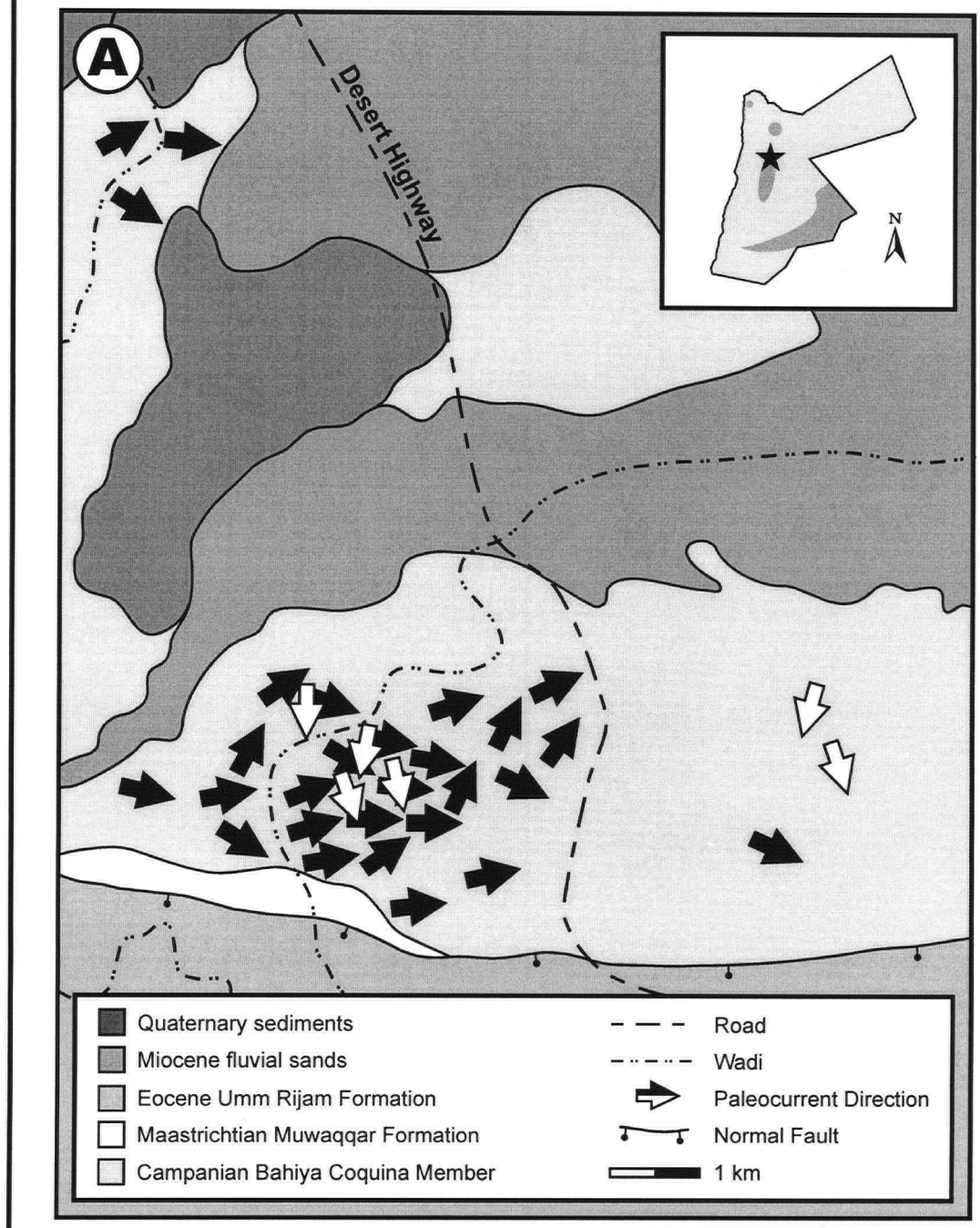
A
Desert Highway
N
Quaternary sediments
Miocene fluvial sands
Eocene Umm Rijam Formation
Maastrichtian Muwaqqar Formation
Campanian Bahiya Coquina Member
Road
Wadi
Paleocurrent Direction
Normal Fault
1 km

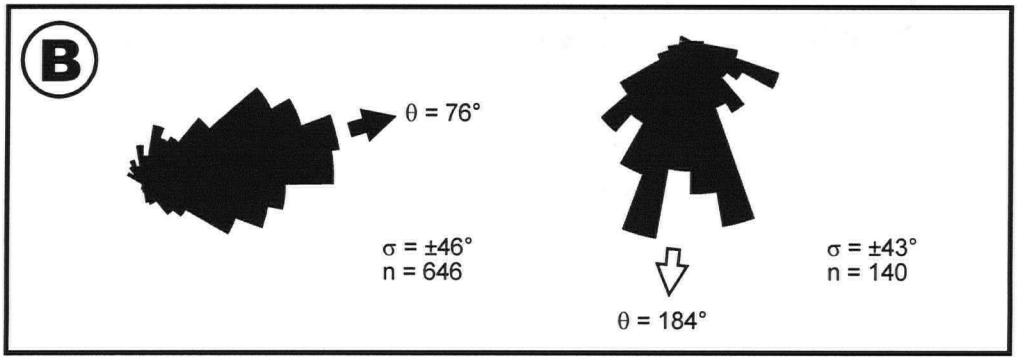
B
θ = 76°
σ = ±46°
n = 646
θ = 184°
σ = ±43°
n = 140

Oyster framestone

Oyster framestone comprises the centre of oyster buildups and consists of large, disarticulated valves and articulated oysters (up to 20 cm) in life position. This facies forms a mound in three dimensions. Mound bases are sharp and characterized by an abundance of slightly abraded, disarticulated oyster valves oriented in concave-up direction (Fig. 2.8E). Bases pass gradationally into a core predominantly consisting of articulated oysters in life position (Fig. 2.8F). This transition is marked by an increase in the relative proportion of whole to disarticulated oysters over the lower quarter of the mound. Articulated oysters are firmly attached to each other and show no evidence of reworking. Cores become progressively more chalk-rich stratigraphically upwards and commonly change laterally into poorly organized *megacrossbedded oyster rudstones* (Fig. 2.7C). Mound tops are chalk-rich and are marked by a gradational increase in the proportion of disarticulated oysters.

Articulated shells are partially filled with micrite and/or sparry calcite, forming geopetal structures. In thin section geopetal micrites are commonly replaced with microcrystalline quartz and contain abundant, silt-sized dolomite rhombs and organic-rich blebs. Valves are generally completely recrystallized to, and cemented with, blocky calcite. Partially recrystallized shells have margins, of blocky calcite and possess an unrecrystallized interior consisting of foliated calcite crystallites (Fig. 2.8G). Silicification is rare and occurs preferentially along valve margins producing rims of blocky quartz which are in turn coated with blocky calcite.

Shell surfaces are conspicuously microbored. Endolithic borings are cylindrical and range in diameter from 8 to 10 μm. In cross section, borings consist of lateral branches extending in all directions that penetrate perpendicular to the shell surface to a depth of 1 cm.

Chalk-rich, highly fragmented oyster rudstone

This facies forms beds that overlie mound centres and truncate megacrossbedded foresets (Fig. 2.8A,H). Beds range in thickness from 30 to 60 cm and are composed predominantly of pebble-sized shell fragments in a chalk matrix. Fragments are in clast support and oriented subparallel to bedding. Common accessory grains include structureless phosphatic peloids, angular chert-intraclasts and pebble-sized micrite. Some micrite rip ups are plastically deformed around impinging clasts indicating that these intraclasts were semilithified during transport and redeposition. At Ruseifa these beds are characterized by a significantly higher proportion of angular chert clasts than those in Al Abiad/Alhisa, producing beds composed almost entirely of chert conglomerate with an oyster rudstone matrix.

Recrystallization is commonly pervasive and is recorded in thin section by the complete alteration of carbonate phases to blocky calcite. When topset beds are silicified, shell fragments and the chalky matrix are preferentially replaced by spherulitic chalcedony and microcrystalline quartz. Siliceous phases do not replace blocky calcite, but are instead overprinted by blocky calcite producing a poikiloblastic texture.

Interpretation: The *megacrossbedded oyster rudstones* are interpreted to be large-scale foresets formed by the cascading of shell material in turbulent suspension down the front of oyster banks during progradation. The *highly fragmented oyster rudstone* beds are bottomset beds that record the off-bank shedding of oyster debris into distal areas. The *oyster framestones* that compose the core of bioherms developed through the *in situ* growth and accumulation of oysters. The *chalk-rich, highly fragmented oyster rudstones* are interpreted as topset beds formed by the reworking/winnowing of shell material at the top of oyster banks and isolated bioherms. This facies records the cessation of active bank progradation and bioherm growth. The tear-drop shape of the oyster bioherms is controlled hydrodynamically, and suggests that

unidirectional currents formed the poorly organized *megacrossbedded oyster rudstone* sets that flank the *oyster framestone core*. The vertical stacking of *megacrossbedded oyster rudstone sets* within composite banks indicates that progradation was dominantly towards the east and changed abruptly towards the south in the later stages of bank development.

The presence of organic-rich blebs within geopetal micrites indicates that micrites associated with oyster buildups were once organic-rich, and the silt-sized dolomite rhombs show that the interiors of oyster shells provided a favourable microenvironment for the precipitation of authigenic dolomite. Dolomite authigenesis in organic-rich sediments is fueled by the anaerobic, stepwise microbial degradation of organic matter (Froelich et al., 1979), which removes sulfate, a potential inhibitor to dolomite precipitation (Baker and Kastner 1981; Morrow and Rickets 1988), and increases pore water alkalinity (Baker and Kastner 1981; Kulm et al. 1984; Baker and Burns 1985; Compton 1988; Middelburg et al. 1990; Compton et al. 1994).

Graded oyster rudstone

This facies consists of graded oyster coquina beds that range in thickness from 30 and 80 cm. Like the *parallel bedded grainstones*, *graded oyster rudstone* beds are also tabular, sharp-based and occur individually or amalgamated. Beds grade from a bottom of slightly abraded disarticulated oysters to a top consisting of pebble-sized oyster shell fragments. Shells are in clast support and oriented concave side up or down with long axis parallel to bedding. In thin section shells are completely recrystallized and cemented with blocky calcite. This facies occurs only within intervals of *micrite*, *bedded chert*, *chert breccia*, and *chert conglomerate*.

Interpretation: The *graded oyster rudstones* are interpreted to be event beds deposited from single-surge, high density turbidity currents. The occurrence of this facies within micritic

and cherty intervals suggests that *graded oyster rudstone* beds record the shedding of oyster material from oyster buildups in more proximal settings to distal shelf environments.

Baculitid ammonite coquina

This facies is formed of poorly sorted, massive and normally graded coquina beds containing abundant *Baculites* cf. *ovatus*, turritelliform gastropods, disarticulated *N. nicaisei* valves, and crinoid fragments in a micrite matrix (Haggart, 2000) (Fig. 2.10A). Beds range in thickness from 10 to 20 cm and have sharp, erosive bases. Fossils within this facies are in clast support and in many instances consist of internal molds with no preserved shell material. This facies is commonly silicified and is intimately interbedded with *micrites*, *bedded cherts, chert breccias,* and *chert conglomerates*. Silicified shell fragments are partially or completely replaced with microcrystalline quartz and/or spherulitic chalcedony. Paleocurrent directions measured from the molds of oriented whole and incomplete baculite shells from four *baculitid ammonite coquina* beds range from 100 to 335°, indicating shore parallel to offshore directed flow.

Interpretation: The *baculitid ammonite coquinas* are also interpreted as event strata deposited from single-surge high-density turbidity currents (Walker, 1977, 1978; Lowe, 1982; Pickering et al., 1986). The assemblage of fossil types that comprise this facies is suggestive of a shallow-water marine environment. The occurrence of *baculitid ammonite coquinas* interbedded with cherts and micrites, and offshore directed paleocurrents suggest that this facies was derived from more proximal shelf settings and transported offshore during storms.

Bivalve coquina

This facies consists of poorly sorted massive beds containing numerous species of thin-

Figure 2.10 A) *Baculitid ammonite coquina.* Photo shows oriented *Baculites* cf. *ovatus* (b), turritelliform gastropods (t), disarticulated *N. nicaisei* valves (o), and crinoid fragments (c) in a micrite matrix. Beds have sharp erosive bases and fossils are in clast support. B) Crossed polarized photomicrograph of *bivalve coquina.* Thin-shelled bivalve fragments (b) are completely recrystallized to blocky calcite. The dark grains are phosphatic peloids with thin isopachous calcite rims. The matrix consists predominantly of micrite (m) with patches of blocky calcite (c). C) Photo of *bedded chert.* The photo shows alternation of tan (light gray beds) and dark brown (dark gray beds) chert beds. Tan beds are typically fractured perpendicular to bedding. Fractures are infilled with dark brown chert. D) Transmitted light photomicrograph of tan (gray) and dark brown (dark gray) chert beds. Both types of beds are formed of microcrystalline chert. Some beds contain rare bivalve shell fragments that have been completely replaced by mosaic chert (m). Dark brown chert beds contain abundant organic carbon-rich blebs (c) and flow sympathetically around tan beds. E) Photo of *chert breccia* bed (arrow) intercalated with *bedded chert.* Note how the tan chert clasts fit together like a jig-saw puzzle and how the dark brown chert has flowed between breccia fragments. F) Close-up of a typical *chert breccia* bed showing the "jig-saw" fit of tan chert clasts. G) Poorly sorted *Chert conglomerate* bed at the top of an oyster bioherm. H) Photo of *chert conglomerate bed.* Beds have sharp bases and consist of subangular pebble- to cobble-sized chert clasts in a matrix of dark brown chert. Some beds contain cobble-sized clasts that are bored (arrow).

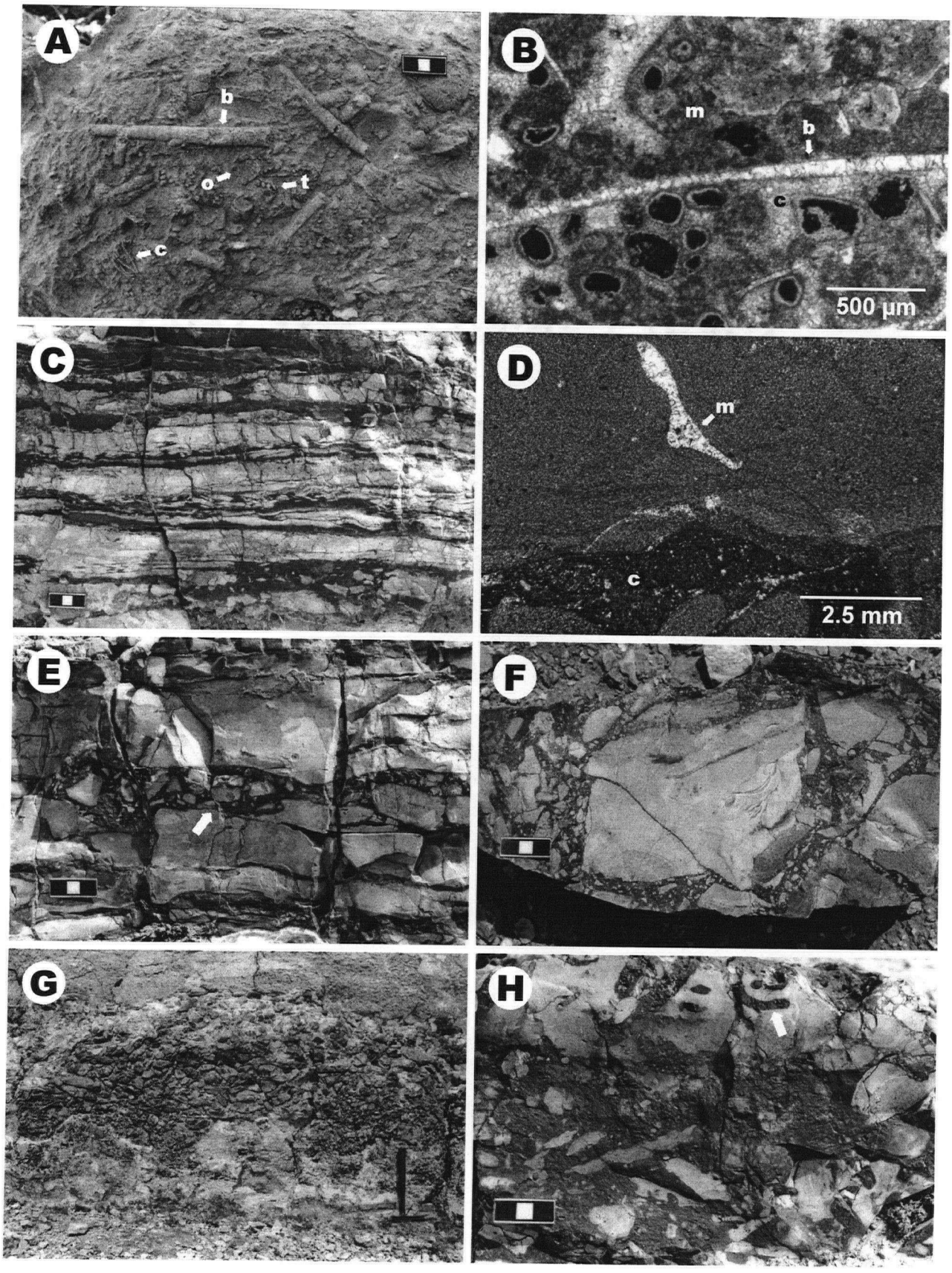
A
b
o
t
c
B
m
b
c
500 µm
C
D
m
c
2.5 mm
E
F
G
H

shelled bivalves (*Lucinidae*, *Tellinidae*, *Veneridae*), gastropods *(Actaeonellidae*), and baculitid ammonite shells (Haggart, 2001) (Fig. 2.10B). Oysters are conspicuously absent. Beds have sharp, erosive bases and range in thickness from 3 to 8 cm. Bivalve shells range in length from 0.75 to 1.5 cm. Single and broken valves are positioned both concave up and concave down. Baculitid ammonites are distributed both perpendicular and parallel to bed bases.

In thin section shells are completely recrystallized to blocky calcite. Phosphatic peloids contain a single concentric lamina around a nucleus consisting of a smaller phosphatic granule. Peloids are commonly coated with a thin isopachous rim of calcite and are disseminated throughout a matrix of recrystallized micrite. When recrystallization is pervasive shell fragments and phosphatic peloids are cemented with blocky calcite. Silicification within the *bivalve coquinas* is rare, but when present occurs preferentially as chalcedonic replacement of the microcrsytalline calcite matrix. This facies is rare and only occurs within intervals of *phosphatic marl*, blanketing micrite concretionary horizons.

Interpretation: The uniform size of shells and shell fragments and the random orientation of elongate baculitid ammonite shells suggest that wave winnowing of an *in situ* bivalve community produced the *bivalve coquinas*.

2.6.1.3 Chert

Three kinds of chert are recognised within the study area: bedded chert, chert breccia, and chert conglomerate. There is a complete progression of these facies types from bedded chert to chert conglomerate that reflects the diagenetic maturation of siliceous phases, and the relative intensity of hydraulic reworking.

Bedded chert

This facies is composed of alternating beds of tan and dark-brown chert (Fig. 2.10C). Beds range in thickness from 1 to 3 cm and have sharp lower and upper contacts. The tan beds predominate and are the thicker of the two. Both bed types consist of microcrystalline chert (Fig. 2.10D), and contain veins and rare trochospiral planktic foraminifera tests filled with mosaic quartz. Tan beds are typically fractured perpendicular to bedding and pinch and swell over several decimetres. Dark-brown beds contain organic-rich blebs and flow sympathetically around, and into fractured tan beds, forming replacement seams. Silicification of an originally carbonate matrix in dark-brown beds is indicated by the presence of isolated patches of unsilicified micrite. Silicified, bored hardgrounds and *baculitid ammonite coquina*-filled scours, identical to those in the *micrite* facies, are also present within the *bedded cherts*.

Interpretation: We interpret this facies to have been originally parallel bedded, diatom-rich micritic limestones. Although siliceous microfossils are conspicuously absent within this facies, Soudry et al. (1981) have shown in correlative cherts from Israel that the origin of silica is biogenic, derived mainly from a low diversity assemblage of diatoms consisting of abundant *Coscindiscus* (sp.), *Triceratium* (sp.), *Hemiaulus* (sp.), and *Stephanopyxis* (sp.). The low species diversity and high abundance of diatoms within this assemblage suggests that silicification occurred in a highly productive marine setting. The absence of structures typical of subaerial exposure such as teepees, raindrop imprints, foam impressions, bubble tracks, flat-topped ripple marks, and vertebrate fossils is also internally consistent with a subaqueous origin for the chert, and indicates this facies accumulated from the rainout of fine-grained carbonate below fair-weather wave-base in an open marine environment and was later silicified with remobilized biogenic silica.

Chert breccia

This facies consists of thin beds of angular fragments of tan chert floating in a matrix of dark-brown chert (Fig. 2.10E,F). Beds are 5 to 10 cm thick and are confined between intervals of *bedded chert*. Contacts between brecciated horizons and *bedded cherts* are sharp, and conform sympathetically to the pinches and swells of tan chert beds above and below. Breccia fragments are 2 to 8cm in length, have sharp boundaries and fit together like pieces of a jigsaw puzzle, indicating that beds were highly competent during brecciation and underwent little or no hydraulic reworking. As in the *bedded cherts* the dark-brown chert is richer in organic carbon and is often incompletely silicified.

Interpretation: The *chert breccias* are the product of *in situ* autobrecciation of the *bedded chert* facies. The splintered "jig saw puzzle" fabric that characterizes this facies indicates that the volume loss associated with the early diagenetic opal-chert transformations was apparently greater in this facies than in the *bedded cherts*. The precise origin of the breccia fabric is problematic; *in situ* subaqueous volume loss associated with syneresis is a likely explanation and is suggested by the fitted fabric (Burst, 1965; Donovan and Foster, 1972; Pratt, 1998).

Chert conglomerate

This facies consists of poorly sorted, massive chert conglomerate beds that are intimately interbedded with intervals of *bedded chert.* Beds are sharp based, range from 10 to 45 cm in thickness, and consist of sub-angular to rounded, pebble to cobble-sized clasts of tan chert in a matrix of dark-brown chert (Fig. 2.10G). Clasts are in matrix support and generally oriented long axis subparallel to bedding. Thicker beds often contain cobble-sized clasts that are conspicuously bored (Fig. 2.10H). Borings are identical to those on the upper surfaces of

concretions from the *phosphatic marl* facies, and consist of cylindrical, subvertical excavations that vary in width from 0.7 to 1.0 cm. As in the *bedded* and *brecciated* cherts the matrix is incompletely silicified in places, indicating an originally carbonate matrix. Blocky calcite is the dominant porefiller cementing clasts within incompletely silicified regions.

Interpretation: The *chert conglomerate* facies is an intraformational conglomerate formed through the erosional reworking of *bedded chert* and *chert breccia* horizons. The large average grain size of chert clasts within this facies indicates that highly competent currents reworked the seafloor. Considering the abundant evidence for storm-generated currents in other facies, we propose that the *chert conglomerates* record episodes of intense storm reworking/winnowing of the substrate during the largest and most powerful storms.

2.6.2 Postdepositional Processes

The ASL, AP, and M formations underwent extensive meteoric diagenesis as documented by the widespread development of blocky calcite cement, the pervasive recrystallization of shell fragments, and the poor preservation of microfossils within lithofacies. Shallow marine carbonate cements are completely absent and primary carbonate textures are best preserved within oyster shell fragments rimmed by mosaic quartz and/or spherulitic chalcedony. The common presence of intraformational chert conglomerates, the preferential silicification of the tops of grainstone beds, the development of siliceous rims on oyster shell fragments, and blocky calcite overprints on chert cements indicate that silicification occurred early, very soon after deposition near the sediment-water interface, and before the meteoric alteration of primary calcitic fabrics and cementation by blocky calcite.

Kolodny et al. (1980) have demonstrated, based on the $\delta^{18}O$ signature and B content of remarkably similar cherts in Israel, that the fractured and brecciated textures of the cherts are the

product of remobilization of biogenic silica in a two-stage silicification process. Assuming that the temperature of sea water is relatively constant, the $\delta^{18}O$ of the chert will reflect the isotopic composition of the water from which it precipitated; upon evaporation water becomes enriched in ^{18}O, whereas rainwater is depleted in ^{18}O (Hoefs, 1997). B is a conservative element in sea water and retains a constant ratio to chlorinity, and thus salinity, during evaporation (Kolodny et al., 1980). In the Israeli cherts, the first phase of silicification occurred soon after deposition in a normal marine environment, and resulted in the selective silicification and autobrecciation of organic-poor micrites that produced chert breccias enriched in both ^{18}O and B. The second stage occurred after initial brecciation and records the silicification of organic-rich micrites within meteoric waters that were depleted in ^{18}O and B. This phase of diagenesis was evidently driven by the equilibration of the tan cherts with fresh water at shallow burial levels.

The selective silicification observed within the Jordanian cherts is thought to reflect the compositional differences between organic-rich and organic-poor micrite beds. The presence of organic matter and clay has been shown to inhibit the rate of silicification (Isaacs, 1982; Behl and Garrison, 1994; Kastner et al., 1977; Hinman, 1990), whereas calcium carbonate accelerates chert formation by increasing the rate of diagenetic opal nucleation (Greenwood, 1973; Kastner et al., 1977; Isaacs, 1982; Behl and Garrison, 1994). These findings are in keeping with what is observed within chert facies, that silicification first occurred during early diagenesis within micrites barren of organic matter. We postulate that only when the sediments were exposed to, and equilibrated with, meteoric waters did the organic-rich micrites begin to silicify.

2.6.3 Phosphogenesis, stable isotopes and stratigraphic condensation

Primary phosphogenesis is the process of apatite precipitation (generally $Ca_{10-a-b}Na_aMg_b(PO_4)_{6-x}(CO_3)_{x-y-z}(CO_3{\cdot}F)_{x-y-z}(SO_4)_zF_2$; carbonate fluorapatite (CFA); Jarvis et al., 1994) within the upper few centimetres of sediment (Jahnke, 1983; Froelich et al., 1988; Glenn et al.,

1994; Jarvis et al., 1994; Schuffert et al., 1998). Phosphogenesis is a biogeochemical process governed by microbially mediated Eh and pH of bottom and pore waters, dissolved chemical species, and sedimentation rates (Föllmi et al., 1991; Glenn et al., 1994). It is distinct from the hydraulic and biological reworking and/or winnowing processes that concentrate phosphatic sediments into economic phosphorites (Baturin, 1971; Glenn et al., 1994).

In many modern environments phosphogenesis frequently occurs beneath the sites of active upwelling along the west coasts of South America, Baja California, southern Africa, and India (Sheldon, 1980; Glenn and Arthur, 1988; Glenn et al., 1994). In these regions intense coastal upwelling provides a supply of nutrients to surface waters, resulting in high primary productivities, and high organic carbon fluxes to the seafloor. The precipitation of CFA within these settings is stimulated by the production of pore water phosphate generated through the microbial degradation of organic matter (Table 2.2) (Burnett, 1977; Froelich et al., 1983; Jahnke et al., 1983; Glenn and Arthur, 1988; Glenn, 1990; Föllmi et al., 1991; Glenn et al., 1994; Jarvis et al., 1994), and the dissolution of fish bones (Suess, 1981). CFA precipitated within these environments has very distinctive $\delta^{13}C$ signatures, and is distinguished by having a significant portion of their carbon derived from microbially degraded organic carbon (Irwin et al., 1977).

The range of $\delta^{13}C$ (CO_3-CFA) values shown in Table 2.3 in comparison with modern pore water total dissolved $\delta^{13}C$ values from anoxic sediments and from other ancient deposits (McArthur et. al., 1980, 1986; Benmore et. al., 1983; Shemesh et al., 1983; Glenn and Arthur, 1990; McArthur and Herczeg, 1990; Compton et al., 1993) suggests that phosphatic grains from the *phosphatic marls, chalks*, and *parallel bedded grainstones* precipitated under conditions of sulfate reduction (Table 2.3). The diagenesis of organic matter progresses through a sequence of microbially-mediated redox reactions that include oxic respiration, denitrification, metal oxide reduction, sulfate reduction, and methanogenesis (Table 2.2) (Froelich et al., 1979). These reactions define distinct diagenetic zones within the sediment column and produce distinctive

Table 2.2 Stepwise microbial respiration of organic matter (CH_2O) and change in the $-\delta^{13}C$ signature of marine pore water with downward decreasing metabolic energy yields (after Glenn and Arthur, 1988; Curtis, 1977; Froelich et al, 1979).

TDC $-\delta^{13}C$	Reodx state	Oxygen ml/l	Diagenetic zone	Reaction
From:				
±0.5‰ (bottom water)	oxic	8.0-2.0	aerobic oxidation	$CH_2O + O_2 \rightarrow CO_2 + H_2O \rightarrow HCO_3^- + H^+$
	suboxic	2.0-0.0	manganese reduction	$CH_2O + 3CO_2 + H_2O + 2MnO_2 \rightarrow 2Mn^{2+} + 4HCO_3^-$
			nitrate reduction	$5CH_2O + 4NO_3^- \rightarrow 2N_2 + 4HCO_3^- + CO_2 + 3H_2O$
			ferric iron reduction	$CH_2O + 7CO_2 + 4Fe(OH)_3 \rightarrow 4Fe^{2+} + 8HCO_3^- + 3H_2O$
	anoxic	0.0	sulphate reduction	$2CH_2O + SO_4^{2-} \rightarrow H_2S + 2HCO_3^-$
To: -25‰				
			methanogenesis	$2CH_2O \rightarrow CH_4 + CO_2$
To: +25‰				

Table 2.3 Isotopic data.

Phosphorite District	Sample Number	Lithofacies	$\partial^{18}O$ (PDB)	$\partial^{13}C$ (PDB)	Reference
NW Jordan	T-1	*Phosphatic marl*	-6.86	-7.50	[2]
	T-3d	*Phosphatic marl*	-4.84	-6.55	[2]
	T-9	*Phosphatic marl*	-4.19	-7.31	[2]
	T-21	*Phosphatic marl*	-6.43	-9.37	[2]
	T-23	*Phosphatic marl*	-6.04	-11.18	[2]
	T-33	*Phosphatic marl*	-6.39	-8.65	[2]
	Z-3	*Phosphatic marl*	-5.18	-3.02	[2]
	J-7	*Phosphatic marl*	-6.20	-8.38	[2]
	J-21	*Phosphatic marl*	-3.90	-3.49	[2]
	K-1	*Phosphatic marl*	-5.85	-6.18	[2]
	K-3	*Phosphatic marl*	-3.78	-2.42	[2]
	K-9	*Phosphatic marl*	-8.26	-7.79	[2]
	K-11	*Phosphatic marl*	-7.20	-5.45	[2]
	K-15	*Phosphatic marl*	-5.99	-4.72	[2]
	K-21	*Phosphatic marl*	-6.92	-4.29	[2]
Ruseifa	OM-5	*Parallel bedded grainstone*	-5.51	-9.03	[1]
	OM-18	*Wavy laminated chalk*	-7.01	-8.19	[1]
	OM-16A	*Phosphatic marl*	-6.67	-11.59	[1]
	OM-27	*Phosphatic marl*	-7.28	-11.21	[1]
	RQ-1	*Parallel bedded grainstone*	-5.37	-7.95	[1]
	DJ-35	*Parallel bedded grainstone*	-6.23	-8.96	[3]
	DJ-40	*Parallel bedded grainstone*	-6.39	-9.36	[3]
	DJ-47	*Parallel bedded grainstone*	-5.93	-7.97	[3]
	DJ-51	*Parallel bedded grainstone*	-5.85	-6.21	[3]
	DJ-52B	*Parallel bedded grainstone*	-6.66	-5.67	[3]
	ASP-8	*Parallel bedded grainstone*	-9.2	-9.9	[4]
	ASP-9	*Parallel bedded grainstone*	-8.3	-8.9	[4]
Northern Al Abiad/Alhisa	Q-4	*Parallel bedded grainstone*	-8.40	-7.53	[1]
	Q-20	*Phosphatic marl*	-7.08	-6.24	[1]
Southern Al Abiad/Alhisa	W-30	*Phosphatic marl*	-7.31	-5.45	[2]
	W-43	*Phosphatic marl*	-7.22	-2.36	[2]
	W-46	*Phosphatic marl*	-6.37	-8.42	[2]
	W-49	*Phosphatic marl*	-9.74	-6.19	[2]
	S-9	*Phosphatic marl*	-8.80	-5.82	[2]
	S-15	*Phosphatic marl*	-8.65	-8.00	[2]
	S-17	*Phosphatic marl*	-6.86	-6.74	[2]
	S-22	*Phosphatic marl*	-7.50	-7.19	[2]
	S-23	*Phosphatic marl*	-7.35	-7.26	[2]
	F-13	*Phosphatic marl*	-5.49	-3.63	[2]
	F-15	*Phosphatic marl*	-4.67	-2.20	[2]
	F-16	*Phosphatic marl*	-2.83	-6.89	[2]
	F-18	*Phosphatic marl*	-3.28	-3.21	[2]
	F-20	*Phosphatic marl*	-6.54	-5.66	[2]
	DJ-61B	*Parallel bedded grainstone*	-10.88	-5.91	[3]
	DJ-64	*Parallel bedded grainstone*	-10.47	-10.44	[3]

Notes: 1- This study; 2 - Sadaqah (2000); 3 - McArthur et al. (1986); 4 - Shemesh et al. (1983)

pore water $\delta^{13}C$ values that reflect the degree of organic matter oxidation. Marine organic matter is highly depleted in ^{13}C, typically ranging between -20 and -28‰, and when oxidized produces dissolved inorganic carbon of the same isotopic composition (Jarvis et. al., 1994). In the oxic and suboxic upper layers of the sediment, where oxygen and then nitrate, and metal oxide reduction are used sequentially as an oxygen source, there is an increase in the dissolved organic carbon with depth, causing decreasing pore water inorganic $\delta^{13}C$ values to a minimum of ~ -6‰ (Jarvis et al., 1994). Below this sulfate reduction leads to an increase in bicarbonate production and a pronounced decrease in $\delta^{13}C$ to ~-25‰ (Irwin et al., 1977). These data also indicate that the *parallel bedded grainstones* were derived through the hydraulic concentration of phosphatic peloids from the *phosphatic marls* and wavy laminated chalks, and further supports the sedimentologic and microfossil data suggesting that pristine phosphates are a dysaerobic facies.

The intimate association of the *phosphatic marls* with well developed micrite concretionary horizons (Compton and Siever, 1986; Raiswell, 1987; Compton, 1988; Grimm, 2000; Wetzel and Allia, 2000) and firmground *Thalassinoides* (Pemberton et al., 1985, 1992; MacEachern et al., 1991, 1992) suggests that precipitation of carbonate fluorapatite was associated with periods of stratigraphic condensation. Sedimentologic and stable isotopic studies of similar concretionary horizons in the Miocene Monterey Formation, California (Garrison and Graham, 1984; Baker and Burns, 1985; Compton and Siever, 1986), the Oligo-Miocene Timbabichi Formation, Baja California Sur (Grimm, 2000), the Lower Jurassic Jet Rock, England, and the Middle Jurassic Opalinus mudstone, Switzerland (Wetzel and Allia, 2000) show that concretions form at shallow burial levels during periods of low net sedimentation. These "hiatal" concretions typically record a multiphase history that includes; (1) concretion formation, (2) concretion exhumation, (3) boring and/or encrustation, (4) transport/redeposition and (5) precipitation of additional cement (Wetzel and Allia, 2000). They precipitate at or near the sediment-water interface within a zone of high alkalinity generated by the microbial

respiration of sedimentary organic matter. The fixing of this zone at shallow burial levels during periods of arrested sedimentation thus favours carbonate precipitation by preconditioning pore waters with the necessary solution and surface chemistries for extended periods of time (Baker and Kastner 1981; Baker and Burns 1985; Compton and Siever 1986; Compton 1988; Middleburg et al., 1990; Slaughter and Hill 1990; Compton et al. 1994). In terms of sequence stratigraphy, these concretionary horizons are genetically linked to sediment starvation associated with a rise or highstand in relative sea level (Grimm, 2000; Wetzel and Allia, 2000).

Low net sedimentation rates also promote phosphogenesis by allowing high concentrations of porewater phosphate and fluoride (Föllmi et al., 1991). The precipitation of CFA is favoured by a high pH and is restricted to shallow burial levels by the diffusion of F from seawater (Burnett, 1977; Burnett and Veeh, 1977; Jahnke et. al., 1983; Glenn and Arthur, 1988). In Jordan, changes in this relationship between sedimentation rate and phosphogenesis are manifested as a continuum in the proportion of *in situ* phosphatic peloids within pristine phosphate facies, and in the stratigraphic density of associated micrite concretionary horizons; the higher the degree of stratigraphic condensation the greater the level of authigenesis. The *phosphatic marls* have the highest concentration of *in situ* peloids and density of micrite concretionary horizons, and are thus interpreted to record the lowest net sedimentation rates. The relatively low concentration of phosphatic peloids and the absence of micrite concretionary horizons within the parallel laminated chalk reflect the relatively high rates of sedimentation associated with chalk deposition (Zijlstra, 1995).

2.6.4 Depositional evolution of the Alhisa Phosphorite Formation

The sedimentary facies described above occur in three natural associations that reflect the range of sedimentary processes that operated on the Jordanian shelf. These groupings correspond to the ASL, AP, and M formations and form a fining upward succession that suggests

continuous, conformable depositional evolution during the accumulation of economic phosphorite. Figure 2.11 shows the stratigraphic relations of the ASL, AP, and M on a regional scale in a north-south transect through the NW Jordan, Ruseifa, and Al Abiad/Alhisa mining districts. Figure 2.12 illustrates local variations in the ASL, AP, and M within the study area.

Where the ASL crops out within the study area it is distinguished by the ubiquitous presence of chert, and consists of an 8 to 20 m thick succession of *bedded chert*, *micrite* interbedded with *chert breccia, chert conglomerate, baculitid ammonite coquinas, graded oyster rudstone beds*, and *thickly bedded phosphorite* beds (Fig. 2.12). The alternation of lithofacies is the most striking feature of this formation.

The AP is a condensed unit that becomes progressively more chalk-rich laterally to the north and stratigraphically upward throughout its entire thickness. This formation represents a shift from predominantly siliceous deposition to phosphate accumulation. The AP thins within the study area from approximately 35 m at Al Abiad Alhisa to 10 m in NW Jordan. In the Old Mine section the AP consists of alternating intervals of amalgamated beds of *parallel bedded grainstone* (P1 to P3 in Figure 2.12) and *phosphatic marl* (m in Figure 2.12) and is characterized by the ubiquitous presence of micrite concretionary horizons. Amalgamated phosphorite beds constitute the economic phosphorites at Ruseifa and occur at regular spacings of approximately 7 m. Correlation between mine sites suggests that amalgamated beds are tabular and extend laterally for several hundred meters (Fig. 2.13). *Phosphatic marl* intervals consist primarily of packages of *phosphatic marl* and *chalk* that are interbedded with thin *parallel bedded grainstones*, *wavy laminated grainstones*, *micrite*, and *bivalve coquinas* (Fig. 2.12). In the Dump section this rhythmic alternation of lithofacies is not recognized; this section contains a higher proportion of granular phosphorite and consists predominantly of amalgamated *thickly bedded grainstones* intercalated with intervals of thin *parallel bedded grainstones*, *wavy laminated grainstone*, and very thin packages of *phosphatic marl* (Fig. 2.12). In the Roman Quarry, Pit,

Figure 2.11 Generalized fence diagram showing the regional stratigraphic framework of the Alhisa Phosphorite Formation. Sections from Tubna, Hafira, Sultani, and Wadi Alhisa have been compiled from Sadaqah (2000). Inset shows the location of the sections used to construct the fence diagram. The section is hung on the top of the Amman Silicified Limestone Formation.

North — NW Jordan — Tubna — Ruseifa — Old Mine — Roman Quarry — Al Abiad/Alhisa — Pit — Hafira — Sultani — Wadi Alhisa — South

10 m

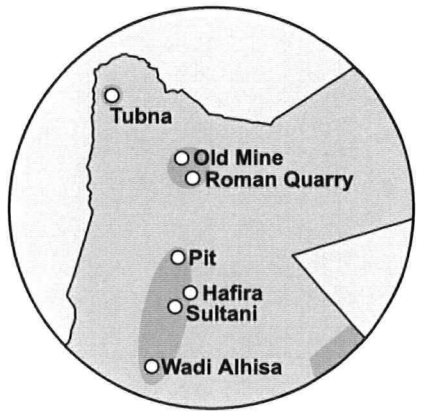

M
AP
ASL
BC
QP
SP
G
?

Legend

Phosphatic facies
- Parallel bedded grainstone
- Phosphatic marl

Carbonate facies
- Wavy laminated/massive chalk
- Wavy laminated/massive micrite
- Megacrossbedded oyster rudstone
- Oyster rudstone
- Highly fragmented oyster rudstone
- Oyster framestone

Chert facies
- Bedded chert/chert breccia

Symbols
- Micrite concretion/condensed interval

Units
- **M** Muwaqqar Chalk Formation
- **AP** Alhisa Phosphorite Formation
  - **QP** Qatrana Phosphorite Member
  - **BC** Bahiya Coquina Member
  - **SP** Sultani Phosphorite Member
- **ASL** Amman Silicified Limestone Formation
- **G** Ghudran Formation

Figure 2.12 Generalized fence diagram showing the detailed lithostratigraphy of the Alhisa Phosphorite Formation in the study area. Inset shows the location of the sections used to construct the fence diagram. Refer to the text for detailed descriptions and discussion of C1, P1, P2, P3, and m within the Old Mine section. The section is hung on the top of the Amman Silicified Limestone Formation.

North — Ruseifa — Al Abiad/Alhisa — South

Old Mine — Dump — Roman Quarry — Pit — Jiza

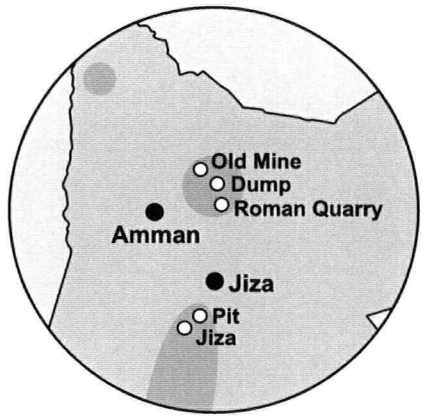

10 m

P3
m
P2
m
P1
C1
clay
cobble
G
AP
ASL
?
M
BC
QP
SP
SP
BC
ASL

Legend

Phosphatic facies
- Thick parallel bedded grainstone
- Thin parallel bedded grainstone
- Silicified grainstone
- Wavy laminated grainstone
- Phosphatic marl

Carbonate facies
- Chalk
- Wavy laminated micritic limestone
- Massive micritic limestone
- Megacrossbedded oyster rudstone
- Graded oyster rudstone
- Highly fragmented oyster rudstone
- Oyster framestone
- Silicified oyster rudstone

Chert facies
- Bedded chert
- Chert breccia/chert conglomerate

Symbols
- Micrite concretion
- Phosphate concretion
- Bored micrite concretion
- Vertebrate fossil
- Fish remains
- Baculitid ammonite
- Gastropod
- Bioturbation
- Bored hardground
- **G** Firmground *Thalassinoides*

Units
- **M** Muwaqqar Chalk Formation
- **AP** Alhisa Phosphorite Formation
- **QP** Qatrana Phosphorite Member
- **BC** Bahiya Coquina Member
- **SP** Sultani Phosphorite Member
- **ASL** Amman Silicified Limestone Formation

Figure 2.13 Composite photo of Alhisa Phosphorite Formation from the Old Mine section. Photo shows the intimate interbedding of an amalgamated *parallel bedded grainstones* (P2) and *phosphatic marl* intervals (m). *Parallel bedded grainstone* beds form tabular, laterally extensive bodies that are gently folded. Dark rectangles within the grainstone bed are abandoned stopes that were excavated to mine phosphate in the mid 1950's.

m
P2
m
5 m

and Jiza sections the AP is divisible into the SP, BC, and QP. The SP is approximately 10m thick in the Roman Quarry section and is composed almost entirely of amalgamated *thickly bedded grainstone* beds interbedded with thin packages of *bedded chert*, *chert breccia*, *chert conglomerate*, and *micrite*. The SP fines and thins towards the south to a minimum thickness of 5 m in the Jiza section, where it is composed of intercalated *parallel bedded grainstones* and *graded oyster rudstone* beds with packages of *phosphatic marl*, *micrite*, and *chalk*. The BC is the most striking lithologic unit in central Jordan and consists of mega-crossbedded oyster banks and isolated bioherms. Where buildups are vertically stacked they are separated by intervals of *phosphatic marl* and *chalk*. The QP crops out only at Al Abiad/Alhisa and is composed of *phosphatic marl* and *chalk* interbedded with *thinly bedded grainstone*.

Where the M is exposed within the study area it consists of *chalk* with thin packages of *phosphatic marl* and thin *parallel bedded grainstone* beds. Vertical and lateral facies transitions within the M cannot be deduced because its upper boundary forms the present-day erosion surface.

Synthesis: The regional stacking pattern of peritidal carbonates of the Ajlun Group overlain by hemipelagic cherts, phosphorites, and chalks of the Belqa Group indicate that the ASL, AP, and M form the upper portion of a detritally starved transgressive systems tract. The characteristics of individual lithofacies and their associations indicate that deposition occurred conformably on a highly productive, east-west trending epeiric platform (Fig. 2.14). The ubiquitous presence of chert and the abundance of non-keeled, trochospiral planktic foraminifera is suggestive of high levels of primary productivity (Soudry et al., 1981; Reiss, 1988; Amolgi-Labin et al., 1993; Thomas, 1999, written comm.). The ASL, AP, and M are analogous to the facies belts that develop in several modern upwelling environments (Fig. 2.14) (Bremner, 1983;

Figure 2.14 Paleogeography and current regime during the deposition of the Belqa Group. Refer to text for discussion. The reconstruction of nearshore environments is based on Glenn and Arthur (1990) and Abed and Amireh (1999).

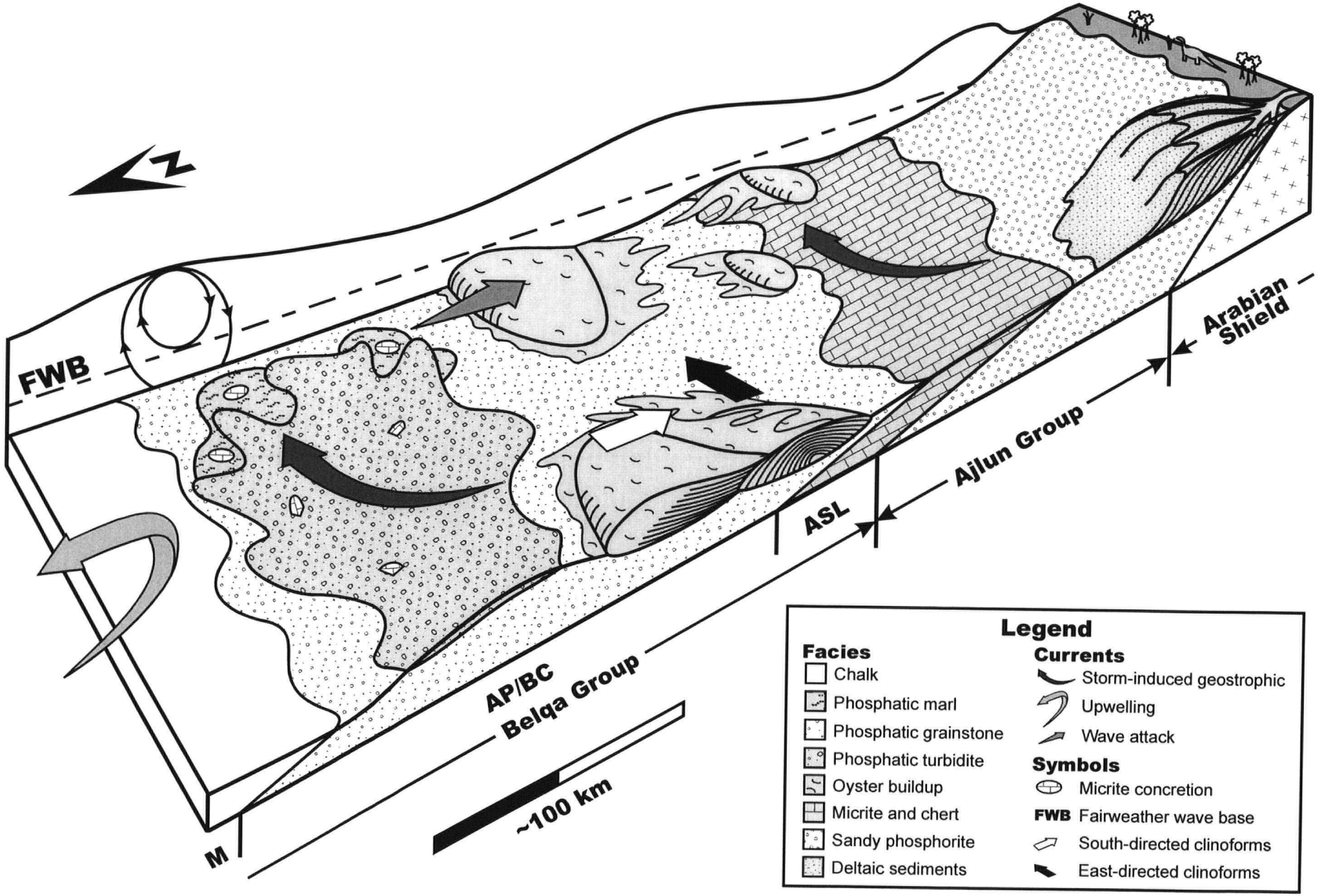
N
FWB
Arabian Shield
Ajlun Group
ASL
AP/BC
Belqa Group
M
~100 km
Legend
Facies
Chalk
Phosphatic marl
Phosphatic grainstone
Phosphatic turbidite
Oyster buildup
Micrite and chert
Sandy phosphorite
Deltaic sediments
Currents
Storm-induced geostrophic
Upwelling
Wave attack
Symbols
Micrite concretion
FWB Fairweather wave base
South-directed clinoforms
East-directed clinoforms

Suess et al., 1990; Wefer et al., 1998). Here, diatomaceous muds are confined to the middle and inner shelf, whereas organic-rich hemipelagic sediments accumulate farther offshore. These facies belts are diachronous and reflect lateral differences in the planktic ecosystems; the centre and most active parts of the upwelling systems are dominated by diatoms, whereas the margins are dominated by calcareous nannoplankton and autotrophic dinoflagellates (Raymont, 1980). By analogy, the ASL corresponds to the diatom-rich belt, the M corresponds to the lower nutrient nannofossil-rich belt, and the AP records stratigraphic condensation and phosphorite formation in the transitional area between these regions during a rise in relative sea level.

We concur with Glenn and Mansour (1979), Reiss (1988), and Kolodny and Garrison (1994) that the source of P for the STPP was from upwelled waters derived from the Tethyan trough to the north. The paleolatitude of this region was at 10° to 15° N during the Upper Cretaceous (Sheldon, 1981; Hay et al., 1999; Al-Hunjul, 1995) and northeast trade winds may have caused the northwest-directed Ekman transport of surface waters that drove coastal upwelling. Paleobotanical data from the Kurnub Group in Egypt indicating dry conditions (Wolfe and Upchurch, 1987), the presence of gypsum within Campanian cherts from Israel (Steinitz, 1977) and the peritidal carbonates of the Ajlun Group (Bender, 1974; Powell, 1989), and climate models suggest that this region was characterized by highly seasonal rainfall (Poulsen et al., 1999), and situated at the transition between the tropical and semidesert climatic belts during the Cretaceous (Upchurch et al., 1999). These data indicate that unlike correlative phosphorites from the Duwi Group in Egypt (Glenn and Arthur, 1990), riverine input was not an important source of P for the formation of economic phosphorites on the Jordan shelf. Glenn and Arthur (1990) have interpreted the Egyptian phosphorites to have formed in shallow water settings in association with prograding deltas, and have postulated that fluvially derived P was important for their formation.

The lack of tidally generated sedimentary structures (Bender, 1974; Bandel and Mikbel, 1985; Abed, 1988; Abed and Al-Agha, 1989; Powell, 1989; Abed and Kraishan, 1991; Abed and Sadaqah, 1998; Abed and Amireh, 1999) indicates that the Jordanian shelf had a low tidal range, suggesting that tidal currents played a minimal role in transporting and redistributing sediment. The presence of hummocky cross-stratified grainstones and grainstone/coquina-filled scours, the occurrence of coquinas containing shallow water faunas in hemipelagic environments, and the presence of reworked hardgrounds within the ASL and AP indicate episodes of intense storm activity (Aigner, 1985; Einsele and Seilacher, 1991). Considering the abundant evidence for storms we also interpret the *parallel bedded grainstones* and graded coquina beds to be storm-generated event beds. These observations are in keeping with those from other investigations of epeiric systems that have concluded tidal currents were damped in epeiric seas by friction effects operating over the very extensive shallow seafloor, and that the dominant processes affecting epeiric platform sedimentation are the frequency, direction, duration, and magnitude of storms (e.g., Tucker and Wright, 1990 and references therein).

Phosphogenesis on the Jordanian shelf was stimulated by the production of pore water phosphate within the upper few centimetres of sediment generated through the microbial respiration of sedimentary organic matter derived from a highly productive surface ocean. The general lack of bioturbation and the presence of benthic foraminifera tolerant of low oxygen conditions within *phosphatic marl* intervals, and $\delta^{13}C$ values from phosphatic peloids indicative of precipitation within the zone of sulfate reduction, all suggest that bottom waters were oxygen deficient, possibly due to the impingement of an oxygen minimum zone (OMZ) on the platform during the accumulation of pristine phosphate (Fig. 2.15). Phosphatic grainstones formed through the successive winnowing, transport and redeposition of phosphatic grains and intraclasts derived from pristine phosphate facies via storm-generated currents (Fig. 2.15). Economic phosphorites were produced through the event-driven amalgamation of the *parallel*

Figure 2.15 Depositional model for the formation of economic phosphorite. A) Pristine phosphate forms during "fairweather" periods under a stratified water column with a well developed oxygen minimum (OMZ) and a shallow storm-weather wave base (SWB). Phosphogenesis is stimulated by high surface productivity and relative stratigraphic condensation. These conditions are suggested by the absence of bioturbation, the abundance of non-keeled planktic foraminifera, and $\delta^{13}C$ values from phosphatic peloids indicative of precipitation within the zone of sulfate reduction. B) With an increase in storm frequency and intensity with time, the SWB deepens and destratifies the water column. Economic phosphorites form through the amalgamation of storm-induced event beds derived from pristine phosphate facies. Both pristine phosphate facies and the tops of economic phosphorite beds may undergo storm wave winnowing during storm events.

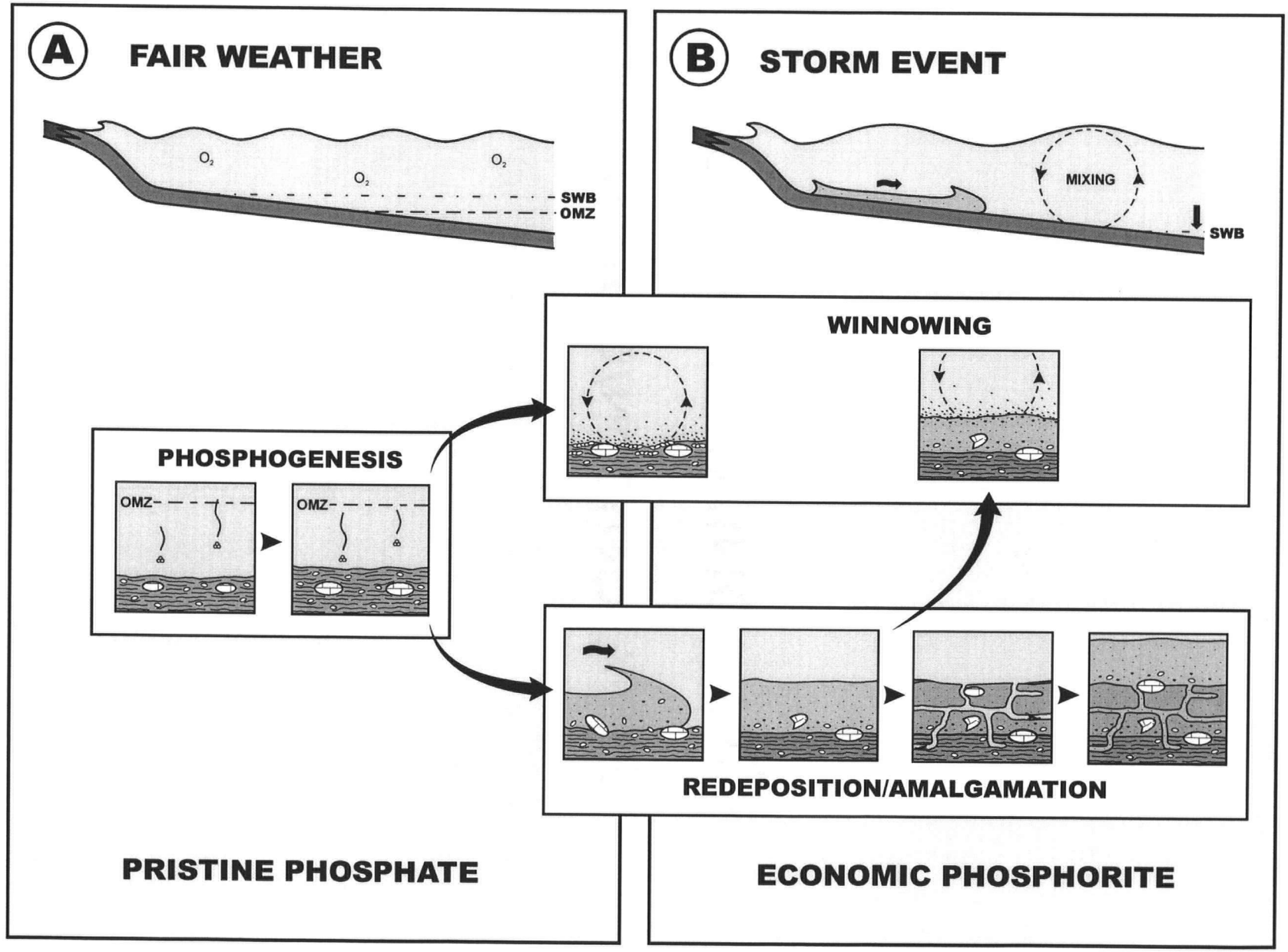
A
FAIR WEATHER
O2
O2
O2
SWB
OMZ
B
STORM EVENT
MIXING
SWB
WINNOWING
PHOSPHOGENESIS
OMZ
OMZ
REDEPOSITION/AMALGAMATION
PRISTINE PHOSPHATE
ECONOMIC PHOSPHORITE

bedded grainstones during periods of heightened storm activity. We interpret the increase in granular phosphorite and the degree of amalgamation of *parallel bedded grainstones* from the Old Mine to the Roman Quarry section (Fig. 2.12) to record storm wave winnowing and reworking of phosphatic strata along the flank of a seafloor topographic high that rose gradually in elevation towards the south.

The oyster buildups are similar to other Upper Cretaceous and Cenozoic oyster buildups that dominate (brackish/hypersaline) highly productive tropical marine environments. The enormous size, limited species diversity, and rapid community growth observed within banks and bioherms is attributable to reduced competition for space and nutrients (Glenn and Arthur, 1990). The east to south shift in paleocurrent directions within composite oyster banks is thought to record the onlapping of southerly prograding oyster banks over easterly prograding buildups that formed in more proximal shelf positions (Fig. 2.9). South-directed banks developed in the most distal environments suitable for oyster growth, and prograded landward during continued sea level rise through the attack of storm and fair-weather waves. We postulate that the dissipation of wave energy within this zone was sufficient to preclude wave-induced progradation of oyster buildups developing behind these distal banks, and suggest that progradation of east-directed buildups was driven by storm-generated currents. Buildup development ceased when the rate of sea level rise outpaced that of carbonate production and aggradation, effectively stranding oyster buildups on the shelf and eventually blanketing them with chalk.

We suggest, based on sedimentologic evidence that indicates the majority of *parallel bedded phosphatic grainstones* were deposited from sustained, turbulent currents as an aggrading traction carpet, the presence of HCS, pot scours, erosive bases to beds, redeposited and broken carbonate concretions, and the preponderance of east-directed oyster buildups, that sustained, storm-generated, geostrophic currents that flowed parallel to the platform margin were important

in redistributing sediment along the south Tethyan margin. The conspicuous absence of oyster shells within granular phosphorite beds also supports this interpretation and indicates that phosphogenesis and storm transport/amalgamation of phosphatic grainstones occurred contemporaneously in closely adjacent settings, and that sediment bypassing across facies belts was not an important mechanism for forming economic phosphorites in Jordan.

Geostrophic currents form in response to strong storm winds that drive surface waters onshore producing an ocean surface that is higher at the coast than offshore (Snedden et al., 1988; Duke, 1990; Walker and Plint, 1992; Johnson and Baldwin, 1996). This coastal set-up can be augmented by very low atmospheric pressures and results in a horizontal pressure gradient that acts to drive bottom water offshore that in time equilibrates to form a downwelling cell that circulates water through an elevated coastal water prism. Were it not for the effects of the Earth's rotation the bottom return flow would head straight out to sea. The Coriolis force acts to substantially change the pattern of flow within this cell by deflecting the trajectory of bottom water to the right in the northern hemisphere and to the left in the southern hemisphere. Ultimately, a balance between the pressure gradient force and the Coriolis force is achieved when the trajectory of the bottom return flow parallels the shoreline and ceases to accelerate. Direct measurements in the Gulf of Mexico during the passage of hurricanes and tropical storms indicate that geostrophic currents are powerful, and can achieve velocities of 100 to 200 cm/s (Murray, 1976; Forristall et al., 1977; Morton, 1981; Snedden et al., 1988). The flow of geostrophic currents is a continuous response to the pressure gradient, and is not a sudden surge of water related to the end of the storm. We hypothesize that powerful geostrophic currents could have developed along the south Tethyan margin in response to strong south-directed storm winds and coastal set-up. The resultant bottom return flow would be deflected to the east generating a shelf-parallel current competent enough to transport shell material, and produce a

highly competent, sustained current capable of winnowing/reworking pristine phosphates into granular phosphorite beds.

2.7 DISCUSSION

The temporal and spatial distribution of phosphorite giants such as the STPP in the Phanerozoic is associated with marine transgressions and has been attributed to extremes in the climatic states of the Earth, causing an accelerated P withdrawal from the ocean into marginal seas and epeiric platforms (Cook and McElhinny, 1979; Arthur and Jenkins, 1980; Sheldon, 1980; 1981; Föllmi et al., 1994; Glenn et al., 1994), and/or local sedimentologic and tectonic controls on P burial and hydraulic concentration processes (Baturin, 1971; Filipelli and Delaney, 1992; Filippelli and Delaney, 1994). Föllmi et al. (1993, 1994) have demonstrated, based on the correlation of global positive excursions in the pelagic $\delta^{13}C$ record with the deposition of Valanginian, Aptian-Albian, and Miocene phosphorites, that times of increased P deposition are linked to episodes of substantially increased atmospheric carbon dioxide and enhanced carbon burial. As an essential nutrient for life, P governs the biologic productivity on Earth and thus controls the rate at which carbon dioxide is removed from the atmosphere and is converted into organic matter (Föllmi et al., 1993, 1996; Delaney, 1998; Compton et al., 2000). During an accelerated carbon cycle, atmospheric carbon dioxide levels rise, propelling the Earth into a greenhouse state, in which an evolving warm and humid global climate causes precipitation, runoff, and weathering rates to increase. This, in turn, induces an increase in continental weathering rates and P input into the oceans that may initiate the following chain of negative feedback to cool the Earth's climate: increase in atmospheric carbon dioxide, global warming, enhanced greenhouse conditions → sea level rise, accelerated hydrologic cycle, and increased continental weathering → increase in primary production → increased burial of organic matter and increased phosphogenesis → lowering of atmospheric carbon dioxide, weakened greenhouse

conditions, global cooling (Fig. 2.16). These periods are associated with increased rates of input of primordial carbon dioxide to the atmosphere from persistent volcanic activity associated with rifting and/or short periods of flood-basalt volcanism [See Föllmi et al., (1993, 1994) for a more complete discussion of this topic]. It appears that when the P cycle becomes accelerated during these times, paleoceanographic and sedimentary conditions may favour phosphorite formation; cells of coastal upwelling may increase in size and number due to the intensification of continental low pressure systems that drive surface waters offshore (Bakun, 1990; Frakes, 1999), and sea level rises in response to an increase in the volume of mid-oceanic ridges, which increases the accommodation volume on continental shelves, expanding the number of suitable sites for phosphorite accumulation (Glenn et al., 1994).

Föllmi et al. (1993) has proposed that the Upper Cretaceous STPP records phosphorite deposition during an accelerated P cycle. General Circulation Models show that the Campanian had a warm climate (Frakes, 1999) characterized by significantly higher atmospheric carbon dioxide levels (about 4.4 times greater than today) (Hay and DeConto, 1999). Rampino and Stothers (1988) identified the Late Cretaceous as a period of increased flood-basalt activity, and Föllmi et al. (1993) have recognized significant positive $\delta^{13}C$ excursions in carbonates that correspond to major episodes of phosphorite accumulation along the south Tethyan margin, the southeastern United States, and Mexico. This interpretation is supported by stable oxygen isotopic data from foraminifera, ammonites, belemnites, nautiloids, and mollusks that indicate the Maastrichtian was appreciably cooler than the Campanian (possibly by as much as 3 to 4ºC) (Frakes, 1999; Barrera and Savin, 1999), suggesting that the Maastrichtian may record the onset of weakened greenhouse conditions associated with the draw down of atmospheric carbon dioxide into the ocean. This interpretation is further substantiated by stratigraphic data from this study that indicate phosphatic strata in Jordan were deposited during a major rise in sea level. This transgression is recognized throughout the eastern Mediterranean and is thought to be

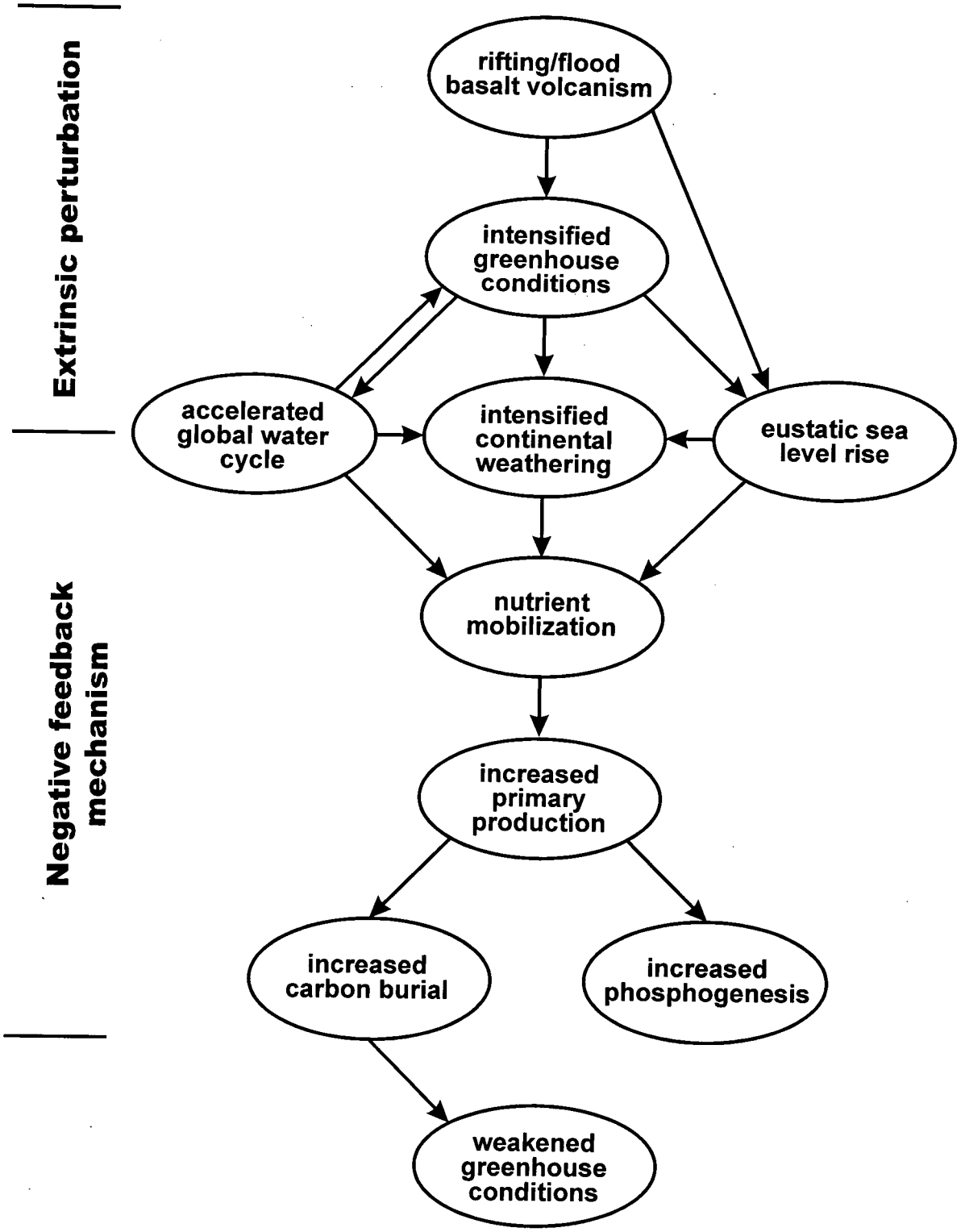

Figure 2.16 Flow chart showing possible feedback mechanism during an accelerated carbon cycle (from Föllmi et al., 1994).

associated with the reconfiguration of mid-oceanic ridges during the break-up of Pangea (Flexer et al., 1986; Abed, 1988; Powell, 1989; Compton, 2000). In Jordan this ocean-wide transgression began with the deposition of peritidal carbonates and cherts of the Ajlun Group in the late Albian and continued into the Eocene with the accumulation of hemipelagic carbonates, cherts, and phosphorites of the Belqa Group (Bender, 1974; Abed, 1988; Powell, 1989). Numerous short-term transgressive-regressive pulses superimposed on this long-term trend are also recognized throughout the eastern Mediterranean (Abed, 1988; Powell, 1989; Glenn, 1990; Lewy, 1990; Lüning et al., 1998). However, regional stratigraphic correlation of these events is difficult because they record the combined effects of an increase in ridge volume, and a change in the local subsidence/uplift rate along the south Tethyan margin associated with the compressive closure of the eastern Tethys during the Late Cretaceous (Dercourt et al., 1986; Abed, 1988; Powell, 1989).

The idea that phosphorite genesis is linked to marine transgressions is well established (McKelvey et al., 1959; Sheldon, 1980; Arthur and Jenkyns, 1981; Riggs and Sheldon, 1990; Föllmi et al., 1993, 1994; Glenn et al., 1994; Riggs et al., 2000; Taylor and MacQuaker, 2000). Aside from the role elevated sea level plays in expanding the accommodation volume on shelves, a rise in relative sea level also favours phosphogenesis by trapping diluting siliciclastics in nearshore environments, and by lowering sediment accumulation rates on shelves (Föllmi, 1990,1996; Glenn et al., 1994). This relationship between relative sea level rise and stratigraphic condensation also controlled phosphogenesis across the Jordanian shelf. The association of phosphorite with glauconite that is common in some phosphogenic systems, including correlative phosphatic sediments from the Duwi Group phosphorites in Egypt (Glenn, 1990), is not recognized in Jordan. The conspicuous absence of mudrocks and shales within Jordanian phosphorites is a defining feature and sets them apart from their Egyptian counterparts. In addition, other iron-bearing minerals such as pyrite (including pyrite molds) and siderite are also

absent. The phosphorite-glauconite association is dependent upon the availability of iron within the sediments and may exist only in siliciclastic-dominated phosphogenic systems. Iron has been shown to play an important role in "pumping" phosphate to pore water in depositional settings not associated with prominent upwelling and high levels of primary productivity (Froelich et al., 1988; Heggie et al., 1990). Iron redox pumping is a cyclic mechanism that enriches phosphate in pore waters by the release of phosphate sorbed onto iron oxyhydroxides in organic-lean sediments. In epeiric systems such as the Jordanian shelf, siliciclastics were trapped in nearshore environments, thereby starving the shelf of a source of iron. Consequently, glauconite did not form nor did other iron-bearing authigenic phases such as pyrite. Thus, iron pumping of pore water phosphate likely played a minimal role. Phosphogenesis is therefore inferred to have been stimulated solely by the microbial respiration of sedimentary organic matter derived from a highly productive surface ocean, and the role iron pumping plays in phosphogenesis is limited to phosphorites that formed in more proximal environments, such as those in Egypt.

Unlike many modern environments where upwelling-related phosphogenesis is restricted to the upper slope-outer shelf within biosiliceous and organic-rich muds along the west coasts of South America, southwest Africa, Baja California and India (Sheldon, 1980; Glenn and Arthur, 1988; Glenn et al., 1994), the precipitation of CFA along the south Tethyan margin occurred across a wide depositional spectrum in a variety of environments that spanned the entire platform, wherever conditions were suitable for phosphogenesis. This non-uniformitarian phenomenon may reflect the combined effects of nutrient transport away from the locus of upwelling, and the cyclic regeneration of P across the platform through the microbial respiration of sedimentary organic matter. In modern upwelling systems, surface waters are rapidly depleted in nutrients and productivity is greatly diminished within relatively short distances from the upwelling centre (Barber and Smith, 1981). However, in epeiric seas with highly seasonal or low net precipitation rates, such as the south Tethyan margin in Jordan, this may not have been

the case. According to recent climate models for the Campanian, the greatest deficit of precipitation minus evaporation would lie over the subtropical areas of the southern Tethys south of the subtropical highs between 10 and 30°N paleolatitude (Voigt et al., 1999 and references therein). The north Tethyan margin lay north of 30°N latitude and was influenced by enhanced continental weathering rates caused by the humid climatic conditions that characterized the Upper Cretaceous (Föllmi et al., 1993, 1994, 1996). We propose that within epeiric systems with low net precipitation and high evaporation rates, such as the Jordanian shelf, dissolved P may have been drawn to near-shore environments from the locus of upwelling through lagoonal circulation. Lagoonal circulation is characterized by the shoreward inflow of surface water and the outflow of saline water at depth, and is common within shallow basins with low and/or seasonal precipitation, high evaporation rates, and low riverine input (Rusnak, 1960). High evaporation rates cause an increase in the density of surface water in nearshore environments by increasing its salinity. This water sinks and flows below the surface in a seaward direction, resulting in an accompanying onshore-directed surface current. In epeiric systems associated with intense upwelling this cyclic circulation may result in the shoreward flow of P-rich surface water from the upwelling centre, thus stimulating primary production and phosphogenesis over the entire platform. The regeneration of P back into solution at depth, either in the water column via excretion by heterotrophs or by the microbial degradation of settled planktic detritus at the sediment-water interface, may also maintain the high levels of primary productivity that stimulated phosphogenesis across the Jordanian shelf. Some regenerated P would also be entrained in the saline, seaward-directed bottom flow and advected upwards back to the surface upon interaction with the upwelling centre, where landward directed surface flow would once again draw phosphate-rich surface waters across the platform. The combined effects of upwelling, lagoonal circulation and P regeneration is to support continual primary production and phosphogenesis in an array of sedimentary environments by cyclically pumping and

sequestering P across the platform. Admittingly, invoking a model that relies on both upwelling-related offshore directed surface flow and onshore directed surface currents operating concomitantly is problematic, and may reflect oceanographic circulation patterns operating on different timescales; i.e. lagoonal circulation with seasonal upwelling pulses.

Marine transgressions also permit wave-induced and other currents to develop along the flooded margin that winnow and rework phosphatic sediments into economic phosphorite (Glenn et al., 1994). In Jordan, storm currents were the most important agent in reworking and concentrating phosphatic sediment into economic phosphorite. The shallow water depths (100 - 200 m) and large fetches that characterize epeiric seas dramatically increases the area over which storm waves may build and interact with the sea floor (Tucker an Wright, 1990), thus permitting the winnowing and reworking of phosphatic strata across large portions of the platform. This differs significantly from modern shelves whose steeper slopes restrict the zone of wave abrasion (to ~70 m water depth) to nearshore environments (James et al., 1992; Boreen and James, 1995).

Sedimentologic evidence from this study also elucidates the importance of storm-induced currents in forming economic phosphorites. Economic phosphorites formed through the event driven amalgamation of granular phosphorite beds derived by the successive winnowing, transport and redeposition of phosphatic grains from pristine facies during storms. Unlike previous studies that outline the importance of event-driven amalgamation of single surge high density phosphatic turbidites to produce thick economic phosphorites (Föllmi and Grimm, 1990; Grimm and Föllmi, 1994), we suggest that sustained turbulent currents generated under storm-induced geostrophic flow are also important in forming laterally persistent economic phosphorite deposits. Geostrophic currents operate for the entire duration of a storm and are capable of reworking, winnowing, and transporting sediment over large areas on modern shelves. We propose that the high current velocities and the long duration over which these shore parallel

currents operate make them very effective agents in reworking and concentrating pristine phosphate facies into economic deposits on storm dominated epeiric platforms.

The data indicate that an increase in storm frequency and intensity with time is a prerequisite for the formation of economic phosphorite. Amalgamated *parallel bedded grainstone* beds with packages of *phosphatic marl* occur at regularly spaced intervals of approximately 6.5 m (P1-P3 in Fig. 2.12). This rhythmic alternation of amalgamated phosphorite beds is also recognized in correlative deposits in south-central Jordan (Abed, 1988; Abed and Fakhouri, 1996; Abed and Sadaqah, 1998), Iraq (Al-Bassam et al., 1983), Israel (Nathan et al., 1979; Avital et al., 1983; Soudry and Champtier, 1983), and Egypt (El-Kamar et al., 1979; Glenn, 1990). Using Almogi-Labin et. al.'s (1993) sedimentation rates based on planktic foraminifera from the Mishash Formation in central Israel, amalgamated beds in Jordan formed with a recurrence interval between 295 000 and 520 000 years (Table 2.4). Due to the lack of biostratigraphic data from the AP and correlative strata a finer resolution is not possible. However, it can be noted that the recurrence interval calculated brackets the 413 000 year eccentricity cycle of the Earth's orbit (Imbrie and Imbrie, 1979). This may suggest that Milankovitch forcing played a role in generating the closely spaced large storms that drove the formation amalgamated phosphorite beds across the south Tethyan margin.

Using resource estimates and past production data for granular phosphorite, calculations show that approximately 12 billion tonnes of pristine phosphate were reworked to produce nearly 1.7 billion tonnes of economic phosphorite in Jordan (Table 2.5). These calculations demonstrate how effective storm-generated currents are in concentrating phosphatic strata; however, phosphogenesis and event redeposition are insufficient by themselves to form economic phosphorite. Large storms must also be closely spaced in time to produce thick amalgamated deposits.

Table 2.4 Recurrence interval of amalgamated *parallel bedded grainstones*.

A. Mean sedimentation rates in correlative Mishash Formation in central Israel

Planktonic Foraminifera Zones	Sedimentation Rate (cm/Ky)
Globotruncanita calcarata	1.25
Globotruncana rosetta	2.2

(from Almogi-Labin et al., 1993)

B. Amalgamated *parallel bedded grainstones* occur at regularly spaced intervals of ~650cm within the Alhisa Phosphorite Formation

C. Recurrence interval of amalgamated *parallel bedded grainstones*

Lower Limit	Upper Limit
$\cong \frac{650\text{cm}}{2.2\text{cm/Ky}}$	$\cong \frac{650\text{cm}}{1.25\text{cm/Ky}}$
$\cong 295\text{Ky}$	$\cong 520\text{Ky}$

Therefore, the estimated recurrence interval for amalgamated *parallel bedded grainstones* ranges from 295 and 520Ky.

Table 2.5 Amount of pristine phosphate reworked to produce economic phosphorite.

A. Average volume % of phosphatic peloids in pristine phosphate and economic phosphorite facies

pristine phosphate	≅ 10 volume %	(*phosphatic marl* facies)
economic phosphorite	≅ 70 volume %	(*parallel bedded grainstone* facies)

Therefore economic phosphorites contain ~7 X the amount of phosphatic peloids as pristine phosphate.

* Percentages are based on estimates of the relative proportion of phosphatic peloids in thin section. The following calculations assume that all economic phosphorite is granular.

B. Economic phosphorite production in Jordan from 1953 to 2000

1953 - 1973	~ 1.30×10^7 tonnes	(JPMC website: www.jpmc-jordan.com)
1974 - present	~ 1.56×10^8 tonnes	(Abed, 1988; JPMC website: www.jpmc-jordan.com)

Total = ~ 1.69×10^8 tonnes

* Phosphorite production in Jordan began in 1953.

C. Economic phosphorite reserve base in Jordan

2001 and beyond	~ 1.54×10^9 tonnes	(Jasinski, 2000)

D. Total amount of economic phosphorite in Jordan

≅ B + C
≅ 1.69×10^8 tonnes + 1.54×10^9 tonnes
≅ 1.71×10^9 tonnes

E. Quantity of pristine phosphate reworked to produce economic phosphorite

Since granular economic phosphorite contains ~7 X the amount of phosphatic peloids as pristine phosphate the amount of pristine phosphate reworked to yield ~ 1.71×10^9 tonnes of economic phosphorite is

≅ D x 7
≅ 1.71×10^9 tonnes x 7
≅ 1.20×10^{10} tonnes

Syndepositional phosphogenesis, reworking and amalgamation to form economic phosphorite contrasts sharply with the principles of "Baturin Cycling" for the origin of phosphorites (Baturin, 1971). In "Baturin Cycling" major changes in sea level are invoked to drive the formation of economic phosphorite. "Baturin Cycling" is widely cited as a mechanism for forming economic phosphorites. Highstands in relative sea level are thought to promote phosphogenesis by increasing the accommodation volume on the shelf, expanding the potential for suitable sites for phosphogenesis and increased upwelling into midshelf and nearshore areas. Whereas, a lowering of wave base during a fall or low stand in relative sea level is suggested to aid in the reworking and concentration of phosphatic strata into economic phosphorite.

Our model does not necessitate major rises and falls in relative sea level to produce economic phosphorite, but emphasizes the interplay of both auto- and allocyclic sedimentary processes to form phosphatic strata within a single systems tract. Two lines of evidence support our interpretation over "Baturin Cycling". First, the vertical stacking pattern of the ASL, AP, and M formations indicates that phosphatic and associated strata in Jordan form a conformable sedimentary succession deposited during a rise in relative sea level. If the economic phosphorite formed through "Baturin Cycling", laterally continuous bounding discontinuities reflecting changes in relative sea level would punctuate the stratigraphy. Second, lithofacies associations indicate that pristine phosphate and reworked/event redeposited economic phosphorites are contemporaneous facies. In "Baturin Cycling" syndepositional phosphogenesis and reworking of phosphatic strata into economic phosphorites are discrete phenomena separated by a drop in relative sea level. Thus, we reject "Baturin Cycling" as a plausible model for the formation of economic phosphorite in Jordan because there is no sedimentologic evidence indicating that episodes of phosphogenesis and the subsequent reworking of pristine phosphate into economic phosphorite are discretely separated in time, and there are no detectable breaks in sedimentation within the stratigraphy. In our model a transgressive systems tract coupled with high surface

productivity created detritally starved settings for the establishment of a "phosphorite nursery", storm reworking of pristine phosphate facies produced granular phosphorite, and amalgamation of storm-generated granular event beds that were closely spaced in time formed economic phosphorite within a transgressive systems tract.

2.8 SUMMARY AND CONCLUSIONS

Economic phosphorites from the AP, associated cherts from the ASL, and chalks from the M in the Ruseifa and Al Abiad/Alhisa mining districts, Jordan, were described from field investigations, hand sample observations, transmitted light microscopy, and back-scatter electron images. These techniques were complemented with stable isotopic studies of phosphatic facies focused on constraining the authigenic conditions that prevailed over the Jordanian shelf. The stratigraphic architecture of the AP was deduced and a depositional model was developed to describe the formation of phosphatic strata in Jordan.

Fifteen lithofacies are recognised within the study area that reflect the range of authigenic conditions that prevailed over the Jordanian shelf. These facies occur in three natural groupings that correspond to the ASL, AP, and M. The ASL, AP, and M show close genetic relations with each other in the form of lateral and vertical transitional contacts, suggesting continuous, conformable depositional evolution during the accumulation of economic phosphorite. The ASL is characterized by the ubiquitous presence of chert and consists of *bedded chert*, *chert breccia*, *chert conglomerate*, *baculitid ammonite coquinas*, *graded oyster rudstone* beds, and *thickly bedded phosphorite* beds. The AP hosts the economic phosphorite and consists of *phosphatic marl*, *thinly bedded*, *thickly bedded*, and *wavy laminated and locally hummocky cross stratified grainstones*, *wavy laminated* and *massive micrite*, *wavy laminated* and *massive chalk*, and *oyster framestones and rudstones* organized into banks and patch reefs. The AP represents a change from predominantly siliceous to phosphatic sedimentation. The M is formed exclusively of *wavy*

laminated and *massive chalk* within the study area. We attribute these deposits to mixed phosphorite-carbonate deposition on a highly productive, storm-dominated epeiric platform during a marine transgression. The major findings and interpretations are summarized below:

(1) The Alhisa Phosphorite Formation forms the upper portion of a TST that was deposited over the peritidal carbonates of the Ajlun Group. These phosphatic sediments are a condensed stratigraphy associated with a rise in relative sea level that culminated with the widespread deposition of pelagic chalk.

(2) Economic phosphorites in Jordan were deposited on a storm-dominated, mixed carbonate-phosphorite epeiric platform along the south Tethyan margin. Sharply-based tabular amalgamated beds of massive, normally graded, and indistinctly stratified layers of intraclastic phosphorite are interpreted as granular event deposits. The preponderance of redeposited bored concretions, the presence of offshore directed paleocurrents, coquinas containing shallow water faunas in hemipelgaic environments, and hummocky cross stratified phosphatic grainstones indicates episodes of intense storm activity. Chalks record background sedimentation over the platform.

(3) The south Tethyan margin in Jordan was characterized by phosphogenesis in sedimentary environments spanning near-shore, mid-shelf, and distal shelf settings. This "phosphorite nursery" is a non-uniformitarian phenomenon reflecting phosphate precipitation across a broad paleoenvironmental spectrum.

(4) The presence of spiral planktic foramanifera and a low diversity benthic assemblage of Buliminacean foraminifera in laminated pristine phosphate facies is suggestive of a highly productive photic zone and a relatively stable dysaerobic benthic ecosystem.

(5) Pristine phosphate in Jordan is not associated with iron-bearing minerals such as glauconite, pyrite, and siderite, a common association in many phosphogenic systems, including correlative sediments in Egypt. This association is dependent upon the availability Fe within

diagenetic environments and may exist only in siliciclastic dominated phosphogenic systems. In epeiric systems such as the Jordanian shelf, siliciclastics were trapped in nearshore environments, thereby starving the shelf of an Fe source sufficient for the precipitation of Fe-bearing minerals. Consequently, glauconite and other Fe-bearing authigenic phases did not form, and Fe-pumping of pore water phosphate likely played a minimal role in phosphogenesis.

We therefore infer that phosphogenesis on the Jordanian shelf was stimulated primarily by the microbial respiration of sedimentary organic matter. Productive surface waters and the export of organic matter to the sediment-water interface created a suboxic seafloor and the necessary solution and surface chemistries for phosphogenesis, probably through the microbial degradation of organic carbon and dissolution of fish bones and teeth. Stable carbon isotopic data from phosphatic peloids within pristine facies support this interpretation and indicate that phosphogenesis occurred within the zone of sulfate reduction.

(6) Event-driven amalgamation of phosphatic grainstones derived from pristine phosphate facies produced the economic phosphorites. The intimate association of a spectrum of pristine facies with granular phosphorite facies indicates that these facies were contemporaneous. Amalgamated beds formed by the successive winnowing, transport and redeposition of phosphatic grains from pristine facies via storm-generated single-surge high density turbidity currents, and sustained, highly competent geostrophic currents. Using resource estimates and past production data for granular phosphorite, calculations show that approximately 12 billion tonnes of pristine phosphate were reworked to produce nearly 1.7 billion tonnes of economic phosphorite in Jordan.

(7) Pristine phosphates, phosphatic event strata, and thick amalgamated economic phosphorites are intimately interbedded in a conformable succession indicating that they were deposited as a mosaic of contemporaneous facies. Syndepositional phosphogenesis and amalgamation to form economic phosphorites contrasts sharply with the principles of "Baturin

Cycling" for the origin of phosphorites. Our model does not necessitate major rises and falls in relative sea level to produce economic phosphorites, but emphasizes the interplay of both autocyclic and allocyclic sedimentary processes to form phosphatic strata. A TST coupled with high surface productivity creates detritally starved settings for the establishment of a "phosphorite nursery"; storm reworking of pristine phosphate facies produces granular phosphorite; and amalgamation of storm-generated granular event beds forms economic phosphorite within a single systems tract. Our data is consistent with an interpretation that an increase in storm frequency and intensity with time may have been a prerequisite for the formation of economic phosphorite.

The paleoenvironmental reconstructions of the phosphatic and associated facies in Jordan provide a stratigraphic and genetic foundation for other studies in the STPP. Future studies that correlate phosphatic and associated strata from regions surrounding Jordan would further refine interpretations of paleoenvironment and depositional settings. Such a comprehensive study is a prerequisite to fully understanding the allocyclic and autocyclic processes that governed the environmental evolution, phosphogenesis and the formation of economic phosphorite along the south Tethyan margin.

2.9 REFERENCES CITED

Abed, A.M., 1988. Eleventh International Field Workshop and Symposium - Guidebook: Third Jordanian Geological Conference International Geological Correlation Program Project 156 - Phosphorites. 124p.

Abed, A.M., 1989. On the genesis of the phosphorite-chert association of the Amman Formation in the Tel es Sur Area, Ruseifa, Jordan. Sciences Geologiques Bulletin. 42, 141-153.

Abed, A.M., and Al-Agha, M.R., 1989. Petrography, geochemistry and origin of the NW Jordan phosphorites. Journal of the Geological Society of London. 146, 499 - 506.

Abed, A.M., and Kraishan, G.M., 1991. Evidence for shallow-marine origin of a 'Monterey -Formation Type' chert-phosphorite-dolomite sequence: Amman Formation (Late Cretaceous), Central Jordan. Facies. 24, 25-38.

Abed, A.M., and Fakhouri, K., 1996. On the chemical variability of phosphatic particles from Jordanian phosphorite deposits. Chemical Geology. 131, 1-13.

Abed, A.M., and Sadaqah, R., 1998. Role of Upper Cretaceous oyster bioherms in the deposition and accumulation of high-grade phosphorites in Central Jordan. Journal of Sedimentary Research. 68, 1009-1020.

Abed, A.M., and Amireh, B.S., 1999. Sedimentology , geochemistry, economic potential and palaeogeography of an Upper Cretaceous phosphorite belt in the southeastern desert of Jordan. Cretaceous Research. 20, 119-133.

Aigner, T., 1985. Storm Depositional System. Springer-Verlag, Berlin. 124p.

Al-Bassam, K.S., Al-Dahan, A.A., and Jamil, A.K., 1983. Campanian-Maastrichtian phosphorite of Iraq - petrology, geochemistry, and genesis. Mineralium Deposita. 18, 215-233.

Al-Hunjul, N.G., 1995, The Geology of Madaba Area , Bulletin 31 (Map Sheet 3153). Ministry of Energy and Mineral Resources of Jordan, Geological Mapping Division, Amman.

Almogi-Labin, A., and Sass, E., 1990. Agglutinated foraminifera in organic-rich neritic carbonate (Upper Cretaceous, Israel) and their use in identifying oxygen levels in oxygen-poor environments. In: Hemleben, C., et al. (Eds.), Paleoecology, Biostratigraphy, Paleoceanography and Taxonomy of Agglutinated Foraminifera. Kluwer Academic Publishers, Amsterdam, 565-585.

Almogi-Labin, A., Bein, A, and Sass, E., 1993. Late Cretaceous upwelling system along the southern Tethys margin (Israel): interrelationship between productivity, bottom water environments, and organic matter preservation. Paleoceanography. 8, 671-690.

Arnott, R.W., and Southard, J.B., 1990. Exploratory flow-duct experiments on combined-flow bed configurations, and some implications for interpreting storm-event stratification. Journal of Sedimentary Petrology. 60, 211-219.

Arthur, M.A., and Jenkyns, 1980. Phosphorites and paleoceanography. 26th International Geological Congress, Geology of Oceans Symposium. pp. 83-96.

Avital, Y., Starinsky, A., and Kolodny, Y., 1983. Uranium Geochemistry and Fission-Track Mapping of Phosphorites, Zefa Field, Israel. Economic Geology. 78, 121-131.

Baker, P.A., and Kastner, M., 1981. Constraints on the formation of sedimentary dolomite. Science. 213, 214-216.

Baker, P.A., and Burns, S.J., 1985. Occurrence and formation of dolomite in organic-rich continental margin sediments. AAPG Bulletin. 69, 1917-1930.

Bakun, A., 1990. Global climate change and intensification of coastal upwelling. Science. 247, 198-201.

Bandel, K., and Mikbel, S., 1985. Origin and deposition of phosphate ores from the Upper Cretaceous at Ruseifa (Amman, Jordan). Geologisch-Palaontologishe Institut, Mitteilungen. 59, 167-188.

Barber, R.T., and Smith, R.L., 1981. Coastal upwelling ecosystems. In: Longhurst, A.R. (Ed.), Analysis of Marine Ecosystems. Academic Press, New York, 31-68.

Barrera, E., and Savin S.M., 1999. Evolution of the Late Campanian-Maastrichtian marine climates and oceans. In: Barrera, E., and Johnson, C.C. (Eds.), Evolution of the Cretaceous ocean-climate system. Geological Society of America, Boulder, pp. 245-282.

Baturin, G.N., 1971. Stages of phosphorite formation on the ocean floor. Nature. 232, 61-62.

Behl, R.J., and Garrison, R.E., 1994. The origin of chert in the Monterey Formation of California (USA): In Iijima, A., Abed, and Garrison, R.E. (Eds.), Siliceous phosphatic and glauconitic sediments of the Tertiary and Mesozoic. Proceedings of the 29th International Geological Congress. VSP, Utrecht, 101-132.

Ben-Avraham, Z., 1989. Multiple opening and closing of the eastern Mediterranean and South China Basins. Tectonics. 8, 351-362.

Bender, F., 1974. Geology of Jordan. Gebrueder Borntraeger, Berlin. 196p.

Benmore, R.A., Coleman, M.L., and McArthur, J.M., 1983. Origin of sedimentary francolite from its sulphur and carbon isotope composition. Nature. 302, 516-518.

Boreen, T.D., and James, N.P., 1995. Stratigraphic sedimentology of Tertiary cool-water limestones, SE Australia. Journal of Sedimentary Research. 65, 142-159.

Bowen, R., and Jux, U., 1987. Afro-Arabian geology. Chapman and Hall, London. 295p.

Bremner, J.M., 1983. Biogenic sediments on the South West African (Namibian) Continental margin. In: Thiede, J., and Suess, E. (Eds.), Coastal Upwelling, Its sediment record, Part B. Plenum Press, New York, 73-104.

Burnett, W.C., 1977. Geochemistry and origin of phosphorite deposits from off Peru and Chile. Geological Society of America Bulletin. 88, 813-823.

Burnett, W.C., and Veeh, H.H., 1977. Uranium series disequilibrium series in phosphorite nodules from the west coast of South America. Geochimica et Cosmochimica Acta. 41, 755-764.

Burst, J.F., 1965. Subaqueous formed shrinkage cracks in clay. Journal of Sedimentary Petrology. 35, 348-353.

Calvert, S.E., 1974. Deposition and diagenesis of silica in marine sediments. Special Publication of the International Association of Sedimentologists Volume 1, Blackwell Scientific, Oxford, 273-299.

Calvert, S.E., and Price, N.B., 1983. Geochemistry of Nambian shelf sediments. In: Suess, E., and Thiede, J. (Eds.), Coastal Upwelling, Its sediment record, Part A. Plenum Press, New York, 337-376.

Compton, J.S., and Siever, R., 1986. Diffusion and mass balance of Mg during early dolomite formation, Monterey Formation. Geochimica et Cosmochimica Acta. 50, 125-135.

Compton, J.S., 1988. Degree of supersaturation and precipitation of organogenic dolomite. Geology. 16, 318-321.

Compton, J.S., Hodell, D.A., Garrido, J.R., and Mallinson, D.J., 1993. Origin and age of phosphorite from the south-central Florida Platform; relation of phosphogenesis to sea level fluctuations and delta ^{13}C excursions. Geochimica et Cosmochimica Acta. 57, 131-146.

Compton, J.S., Donald, H.L., Mallinson, D.J., and Hodell, D.A., 1994. Origin of dolomite in the phosphatic Miocene Hawthorn Group of Florida. Journal of Sedimentary Research. 64, 638-649.

Compton, J., Mallinson, D., Glenn, C.R., Filippelli, G., Follmi, K., Shields, G., and Zanin, Y., 2000. Variations in the global P cycle. In: Glenn, C.R., Prevot-Lucas, L., and Lucas, J. (Eds.), Marine Authigenesis: from Global to Microbial. SEPM Special Publication 66. SEPM, Tulsa, 21-33.

Cook, P.J., and McElhinny, M.W., 1979. A re-evaluation of the spatial and temporal distribution of sedimentary phosphate deposits in light of plate tectonics. Economic Geology. 74, 315-330.

Delaney, M.L., 1998. P accumulation in marine sediments and the oceanic P cycle. Global Biogeochemical Cycles. 12, 563-572.

De Raaf, J.F.M.,Boersma, J.R., and van Gelder, A., 1977. Wave-generated structures and sequences from a shallow marine succession, Lower Carboniferous, County Cork, Ireland. Sedimentology, 24, 451-483.

Dercourt, J., Zonenshain, L.P., Ricou, L-E., Kazmin, V.G., Le Pichon, X., Knipper, A.L., Grandjacquet, C., Sbortshikov, I.M., Geyssant, J., Lepvrier, C., Pechersky, D.H., Boulin, J., Sibuet, J-C., Savostin, L.A., Sorokhtin, O., Westphal, M., Bazhenov, M.L., and Lauer, J.P., 1986. Geological evolution of the Tethys Belt from the Atlantic to the Pamirs since the Lias. Tectonophysics. 123, 241-315.

Donovan, R.N., and Foster, R.J., 1972. Subaqueous shrinkage cracks from the Caithness Flagstone Series (Middle Devonian) of northeast Scotland. Journal of Sedimentary Petrology. 42, 309-317.

Dott, R.H., and Bourgeois, J., 1982. Hummocky stratification: significance of its variable bedding sequences. Geological Society of America Bulletin. 93, 663-680.

Duke, W.L., 1990. Geostrophic currents or shallow marine turbidity currents? The dilemma of paleoflow patterns in storm-influenced prograding shoreline systems. Journal of Sedimentary Petrology. 60, 870-883.

Duke, W.L., Arnott, R.W.C., and Cheel, R.J., 1991. Shelf sandstones and hummocky cross -stratification: new insights on a stormy debate. Geology. 19, 625-628.

Einsele, G., and Seilacher, A., 1991. Distinction of Tempestites and Turbidites. In: Einsele, G., Ricken, W., and Seilacher, A. (Eds.), Cycles and Events in Stratigraphy. Springer-Verlag, Berlin, 377-382.

El-Hiyari, M., 1985, The geology of Jabal Al-Mutarammil, Bulletin 1 (Map 3252). Ministry of Energy and Mineral Resources, Geology Mapping Division, Amman.

El-Kammar, A.M., Zayed, M.A., and Amer, S.A., 1979. Rare earths of the Nile Valley phosphorites, Upper Egypt. Chemical Geology. 24, 69-81.

Filippelli, G.M., and Delaney, M.L., 1994. The oceanic P cycle and continental weathering during the Neogene. Paleoceanography. 9, 643-652.

Flexer, A., Rosenfeld, A., Lipson, B., and Honigstein, A., 1986. Relative sea level changes during the Cretaceous in Israel. AAPG Bulletin. 70, 1685-1699.

Föllmi, K.B., 1990. Condensation and phosphogenesis: examples of the Helvetic mid-Cretaceous (northern Tethyan margin). In: Notholt, A.J.G., and Jarvis, I. (Eds.), Phosphorite Research and Development. The Geological Society, Oxford, 237-252.

Föllmi, K.B., and Grimm, K.A., 1990. Doomed pioneers: gravity-flow deposition and bioturbation in marine oxygen-deficient environments. Geology. 18, 1069-1072.

Föllmi, K.B., Garrison, R.E., and Grimm, K.A., 1991. Stratification in phosphatic sediments: illustrations from the Neogene of California. In: Einsele, G., Ricken, W., and Seilacher, A. (Eds.), Cycles and Events in Stratigraphy. Springer-Verlag, Berlin, Heidelberg, 492 -507.

Föllmi, K.B, Garrison, R.B., Ramirez, P.C., Zambrano-Ortiz, F., Kennedy, W.J., and Lehner, B.L., 1992. Cyclic phosphate-rich successions in the upper Cretaceous of Colombia. Palaeogeography, Palaeoclimatology, Palaeoecology. 93, 151-182.

Föllmi, K.B., Weissert, H., and Lini, A., 1993. Nonlinearities in phosphogenesis and P -carbon coupling and their implications for global change. In: Wollast, R., Mackenzie, F.T., and Chou, L. (Eds.), Interactions of C, N, P, and S Biogeochemical Cycles and Global Change. NATO ASI Series. Springer-Verlag, Berlin, 447-474.

Föllmi, K.B., Weissert, H., Bisping, M., and Funk, H., 1994. Phosphogenesis, carbon-isotope stratigraphy, and carbonate-platform evolution along the Lower Cretaceous northern Tethyan margin. Geological Society of America Bulletin. 106, 729-746.

Föllmi, K.B., 1996. The P cycle, phosphogenesis and marine phosphate-rich deposits. Earth-Science Reviews. 40, 55-124.

Forristall, G.Z., Hamilton, R.C., and Cardone, V.J., 1977. Continental shelf currents in Tropical Storm Delia: Observations and theory. Journal of Physical Oceanography. 87, 532-546.

Frakes, L.A., 1999. Estimating the global thermal state from Cretaceous sea surface and continental temperature data. In: Barrera, E., and Johnson, C.C. (Eds.), Evolution of the Cretaceous ocean-climate system. Geological Society of America, Boulder, 49-57.

Freund, R., 1965. A model of the structural development of Israel and adjacent areas since Upper Cretaceous times. Geological Magazine. 102, 189-205.

Frey, R.W., and Seilacher, A., 1980. Uniformity in marine invertebrate ichnology. Lethaia. 13, 183-207.

Froelich, P.N., Klinkhammer, G.P., Bender, M.L., Luedtke, N.A., Heath, G.R., Cullen, D., Dauphin, P., Hammond, D., Hartman, B., and Maynard, V., 1979. Early oxidation of organic matter in pelagic sediments of the eastern equatorial Atlantic: suboxic diagenesis. Geochimica et Cosmochimica Acta. 43, 1075-1090.

Froelich, P.N., Bender, M.L., Luedtke, N.A., Heath, G.R., and DeVries, T., 1982. The marine P cycle. American Journal of Science. 282, 474-511.

Froelich, P.N., Kim, K.H., Jahnke, R., Burnett, W.C., Soutar, A., and Deakin, M, 1983. Pore water fluoride in Peru continental margin sediments: Uptake from seawater. Geochimica et Cosmochimica Acta. 47, 1605-1612.

Froelich, P.N., Arthur, M.A., Burnett, W.C., Deakin, M., Hensley, V., Jahnke, R., Kaul, L., Kim, K.H., Roe, K., Soutar, A., and Vathakanon, C., 1988. Early diagenesis of organic matter in Peru continental margin sediments: phosphorite precipitation. Marine Geology. 80, 308-343.

Garfunkel, Z., Zak, I., and Freund, R., 1981. Active faulting in the Dead Sea rift. Tectonophysics. 80, 1-26.

Garrison, R.E., and Graham, S.A., 1984. Early diagenetic dolomites and the origin of dolomite -bearing breccias, lower Monterey Formation, Arroyo Seco, Monterey County, California. In: Garrison, R.E., Kastner, M., and Ziegler, D.H. (Eds.), Dolomites of the Monterey Formation and other organic-rich units. SEPM, Pacific Section, Los Angeles, 87-101.

Glenn, C.R., and Mansour, S.E.A., 1979. Reconstruction of the depositional and diagenetic history of phosphorites and associated rocks of the Duwi Formation (Late Cretaceous) Eastern Desert, Egypt. Annals of the Geological Survey of Egypt. IX, 388-407.

Glenn, C.R., and Arthur, M.A., 1988. Petrology and major element geochemistry of Peru margin phosphorites and associated diagenetic minerals: authigenesis in modern organic rich sediments. Marine Geology. 80, 231-268.

Glenn, C.R., and Arthur, M.A., 1990. Anatomy and origin of a Cretaceous phosphorite -greensand giant, Egypt. Sedimentology. 37, 123-154.

Glenn, C.R., 1990. Depositional sequences of the Duwi, Sibaiya and Phosphate Formations, Egypt; phosphogenesis and glauconization in a Late Cretaceous epeiric sea. In: Notholt, A.J.G., and Jarvis, I. (Eds.), Phosphorite Research and Development: Geological Society of London Special Publication 52. The Geological Society of London, Oxford, pp. 205 -222.

Glenn, C.R., Föllmi, K.B., Riggs, S.R., Baturin, G.N., Grimm, K.A., Trappe, J., Abed, A.M., Galli-Oliver, C., Garrison, R.E., Ilyin, A.V., Jehl, C., Rohrlich, V., Sadaqah, R.M.Y., Schidlowski, M., Sheldon, R.E., amd Siegmund, H., 1994. P and phosphorites: sedimentology and environments of formation. Eclogae Geologicae Helvetiae. 87, 747 -788.

Greenwood, R., 1973. Cristabolite: its relationship to chert formation in selected samples from the Deep Sea Drilling Project. Journal of Sedimentary Petrology. 43, 700-708.

Grimm, K.A., 1997, Phosphorites feed people, Farm Folk/City Folk's Newsletter. 13, 4-5.

Grimm, K.A., 2000. Stratigraphic condensation and the redeposition of economic phosphorite: allostratigraphy of Oligo-Miocene shelfal sediments, Baja California Sur, Mexico. In: Glenn, C.R., Prevot-Lucas, L., and Lucas, J. (Eds.), Marine authigenesis: from global to microbial: SEPM Special Publications. Society for Sedimentary Geology, Tulsa, 325 -347.

Grimm, K.A., and Föllmi, K.B., 1994. Doomed pioneers: allochthonous crustacean tracemakers in anaerobic basinal strata, Oligo-Miocene San Gregorio Formation, Baja California Sur, Mexico. Palaios. 9, 313-334.

Haggart, J.W., 2000, Report on Upper Cretaceous fossils from the Amman Formation, Jordan. Paleontological Report JWH-2000-06, Geological Survey of Canada, Vancouver.

Haggart, J.W., 2001, Report on Cretaceous fossils from the Amman Formation, Jordan, preserved in thin-section and lithological samples. Paleontological Report JWH2001-02, Geological Survey of Canada, Vancouver.

Harms, J.C., Southard, J.B., Spearing, D.R., and Walker, and R.G., 1975. Depositional environments as interpreted from primary sedimentary structures and stratification sequences, Short Course 2. Society of Economic Paleontologists and Mineralogists.161p.

Hay, W.W, DeConto, R.M., Wold, C.N., Wilson, K.M., Voigt, S., Schulz, M., Wold-Rossby, A., Dullo, W.C., Ronov, A.B., Balukhovsky, A.N., and Soding, E., 1999. Alternative global Cretaceous paleogeography. In: Barrera, E., and Johnson, C.C. (Eds.), Evolution of the Cretaceous Ocean-Climate System. Geological Society of America, Boulder, Colorado, 1-47.

Hay, W.W., and DeConto, R.M., 1999. Comparison of modern and Late Cretaceous meridianal energy transport and oceanology. In: Barrera, E., and Johnson, C.C. (Eds.), Evolution of the Cretaceous ocean-climate system. Geological Society of America, Boulder, 283-300.

Heggie, D.T., Skyring, G.W., O'Brien, G.W., Reimers, C., Herczeg, A., Moriarty, D.J.W., Burnett, W.C., and Milnes, A.R., 1990. Organic carbon cycling and modern phosphorite formation on the East Australia continental margin: an overview. In: Notholt, A.J.G., and Jarvis, I. (Eds.), Phosphorite research and development. The Geological Society of London, Oxford, 87-117.

Herring, J.R., and Fantel, R.J., 1993. Phosphate rock demand into the next century: Impact on World Food Supply. Nonrenewable Resources. 3, 226-246.

Hinman, N.W., 1990. Chemical factors influencing the rates and sequences of silica phase transitions: Effects of organic constituents. Geochimica et Cosmochimica Acta. 54, 1563 -1574.

Hiscott, R.N., 1994. Traction-carpet stratification in turbidites - fact or fiction? Journal of Sedimentary Research. A64, 204-208.

Hoefs, J., 1997. Stable isotope geochemistry. Springer-Verlag, Berlin. 201p.

Imbrie, J., and Imbrie, K.P., 1979. Ice ages: solving the mystery. Enslow, Hillside. 224p.

Irwin, H., Curtis, C. and Coleman, M., 1977. Isotopic evidence for source of diagenetic carbonates formed during burial of organic-rich sediments. Nature. 269, 209-213.

Isaacs, C.M., 1982. Influence on rock composition on kinetics of silica phase changes in the Monterey Formation, Santa Barbara area, California. Geology. 10, 304-308.

Jahnke, R.A., Emerson, S.R., Roe, K.K., and Burnett, W.C., 1983. The present day formation of apatite in Mexican continental margin sediments. Geochimica et Cosmochimica Acta. 47, 259-266.

James, N.P., Bone, Y., van der Borch, C.C., and Gostin, V.A., 1992. Modern carbonate and terrigenous clastic sediments on a cool water, high energy, mid-latitude shelf: Lacepe, southern Australia. Sedimentology. 39, 877-903.

Jarvis, I., Burnett, W.C., Nathan, Y., Almbaydin, F.S.M., Attia, A.K.M., Castro, L.N., Flicoteaux, R., Hilmy, M.E., Husain, V., Quatawnah, A.A., Serjani, A., and Zanin, Y.N., 1994. Phosphorite geochemistry: Stateof-the-art and environmental concerns. Eclogae Geologicae Helveticae. 87, 643-700.

Jasinski, S.M., 2000, Phosphate Rock. U.S. Geological Survey Mineral Commodity Summaries, U.S. Geological Survey. (http://minerals.usgs.gov/minerals/pubs/mcs)

Johnson, A.D., and Baldwin, C.T., 1996. Shallow siliciclastic seas. In: Reading, H.G. (Ed.), Sedimentary Environments: Processes, Facies and Stratigraphy. Blackwell Science, Cornwall, 232-280.

Kastner, M., Keene, J.B., and Gieskes, J.M., 1977. Diagenesis of siliceous oozes: I. Chemical controls on the rate of opal-A diagenesis - an experimental study. Geochimica et Cosmochimica Acta. 40, 1041-1059.

Khalil, B.M., 1986, The geology of Wadi El Buwayija, Bulletin 5 (Map 3251). Ministry of Energy and Mineral Resources of Jordan, Geological Mapping Division, Amman.

Kolodny, Y., 1967. Lithostratigraphy of the Mishash Formation, Northern Negev. Israel Journal of Earth Sciences. 16, 57-73.

Kolodny, Y., and Kaplan, I.R., 1970. Carbon and oxygen isotopes in apatite CO_2 and co-existing calcite from sedimentary phosphorite. Journal of Sedimentary Petrology. 40, 954-959.

Kolodny, Y., Taraboulos, A., and Frieslander, U., 1980. Participation of fresh water in chert diagenesis: evidence from oxygen isotopes and boron track mapping. Sedimentology. 27, 305-316.

Kolodny, Y., and Garrison, R.E., 1994. Sedimentation and diagenesis in paleoupwelling zones of epeiric sea and basinal settings: A comparison of the Cretaceous Mishash Formation of Israel and the Miocene Monterey Formation of California: In Iijima, A., Abed, and Garrison, R.E. (Eds.), Siliceous phosphatic and glauconitic sediments of the Tertiary and Mesozoic. Proceedings of the 29th International Geological Congress. VSP, Utrecht, 133 -158.

Kreisa, R.D., 1981. Storm-generated sedimentary structures in subtidal marine faces with examples from the Middle and Upper Ordovician of southwestern Virginia. Journal of Sedimentary Petrology. 51, 823-848.

Kulm, L.D., Suess, E., and Thornburg, T.M., 1984. Dolomites in the organic-rich muds of the Peru forearc basins. In: Garrison, R.E., Kastner, M., and Zenger, D.H. (Eds.), Dolomites of the Monterey Formation and Other Organic-rich Units. SEPM Pacific Section Special Publication, 29-48.

Leithold, E.L., and Bourgeois, J, 1984. Characteristics of coarse-grained sequences deposited in nearshore, wave-dominated environments - examples from the Miocene of south-west Oregon. Sedimentology. 31, 749-775.

Lewy, Z., 1990. Transgressions, regressions and relative sea level changes on the Cretaceous shelf of Israel and adjacent countries. A critical evaluation of Cretaceous global sea level correlations. Paleoceanography. 5, 619-637.

Lowe, D.R., 1982. Sediment gravity flows: II. Depositional models with special reference to the deposits of high-density turbidity currents. Journal of Sedimentary Petrology. 52, 279 -297.

Lüning, S., Marzouk, A.M., Morsi, A.M., and Kuss, J., 1998. Sequence stratigraphy of the Upper Cretaceous of central-east Sinai, Egypt. Cretaceous Research. 19, 153-196.

MacEachern, J.A., Pemberton, S.G., and Raychaudhuri, L., 1991. The substrate controlled *Glossifungites* ichnofacies and its application to the recognition of sequence stratigraphic surfaces: Subsurface examples from the Cretaceous of the Western Canada Sedimentary Basin, Alberta Canada: Proceedings of the 1991 NUNA Conference on High-Resolution Sequence Stratigraphy. Geological Association of Canada, 32-36.

MacEachern, J.A., Pemberton, S.G., and Raychaudhuri, L., 1992. Stratigraphic applications of the *Glossifungites* ichnofacies: delineating discontinuities in the stratigraphic record. In: Pemberton, S.G. (Ed.), Applications of ichnology to petroleum exploration. SEPM Core Workshop 17, SEPM, Tulsa, 169-198.

McArthur, J.A., and Herczeg, A., 1990. Diagenetic stability of the isotopic composition of phosphate oxygen: paleoenvironmental implications. In: Notholt, A.J.G., and Jarvis, I. (Eds.), Phosphorite Research and Development. The Geological Society Publishing House, Avon, 119-124.

McArthur, J.M., Coleman, M.L., and Bremner, J.M., 1980. Carbon and oxygen isotopic composition of structural carbonate in sedimentary francolite. Journal of the Geological Society of London. 137, 669-673.

McArthur, J.M., Benmore, R.A., Coleman, M.L., Soldi, C., Yeh, H.W., and O'Brien, G.W., 1986. Stable isotopes characterisation of francolite formation. Earth and Planetary Science Letters. 77, 20-34.

McCrea, J.M., 1950. On the isotopic chemistry of carbonates and a plaeotemperature scale. The Journal of Chemical Physics. 18, 849-857.

McKelvey, V.E., Williams, J.S., Sheldon, R.P., Cressman, E.R., Cheney, T.M., and Swanson, R.W., 1959. The Phosphoria, Park City and Shedhorn Formations in the Western Phosphate Field. United States Geological Survey Professional Paper 313-A. 47p.

Middleburg, J.J., De Lange, G.J., and Kreulen, R., 1990. Dolomite formation in anoxic sediments of Kau Bay, Indonesia. Geology. 18, 399-402.

Molina, J.M., Ruiz-Ortiz, P.A., and Vera, J.A., 1997. Calcareous tempestites in pelagic facies, Jurassic Betic Cordilleras, southern Spain. Sedimentary Geology. 109, 95-109.

Morrow, D.W., and Rickets, B.D., 1988. Experimental investigation of sulfate inhibition of dolomite and its mineral analogues. In: Shukla, V., and Baker, P.A. (Eds.), Sedimentology and Geochemistry of Dolostones. SEPM, Tulsa, 27-38.

Morton, R.A., 1981. Formation of storm deposits by wind-forced currents in the Gulf of Mexico and the North Sea. In: Nio, S.D., Shuttenhelm, R.T.E., van Weering, T.C.E. (Eds.), Holocene marine sedimentation in the North Sea basin. International Association of Sedimentologists, 385-396.

Murray, J.W., 1976. A method of determining proximity of marginal seas to an ocean. Marine Geology. 22, 103-119.

Myrow, P.M., 1992. Pot and gutter casts from the Chapel Island Formation, southeast Newfoundland. Journal of Sedimentary Petrology. 62, 992-1007.

Nathan, Y., Shiloni, Y., Roded, R., Gal, I., and Deutsch, Y., 1979. The geochemistry of the northern and central Negev phosphorites (southern Israel). Bulletin of the Israel Geological Survey. 34, 1-23.

Nathan, Y., Soudry, D., Levy, Y., Shitrit, D., and Dorfman, E., 1997. Geochemistry of cadmium in the Negev phosphorites. Chemical Geology. 142, 87-107.

Notholt, A.J.G., 1980. Economic phosphatic sediments: mode of occurrence and stratigraphical distribution. Journal of the Geological Society of London. 137, 793-805.

Notholt, A.J.G., 1985. Phosphate resources in the Mediterranean (Tethyan) phosphogenic province: A progress report. Sciences Geologiques. Memoire 77, 9-21.

Notholt, A.J.G., Sheldon, R.P., and Davidson, D.F., 1989, Phosphate deposits of the world, Volume 2, Phosphate Rock Resources. Cambridge University Press, Cambridge. 566p.

Notholt, A.J.G., and Jarvis, I., 1990. Phosphorite Research and Development. The Geological Society of London Special Publication 52, The Geological Society of London, Oxford. 326p.

Pedersen, T.E., and Calvert, S.E., 1990. Anoxia vs. Productivity: What controls the formation of organic carbon-rich sediments and sedimentary rocks? AAPG Bulletin. 74, 456-466.

Pemberton, S.G., and Frey, R.W., 1985. The *Glossifungites* ichnofacies: modern examples from the Georgia coast, U.S.A. In: Curran, H.A. (Eds.), Biogenic structures: Their use in interpreting depositional environments. SEPM, Tulsa, 237-259.

Pemberton, S.G., MacEachern, J.A., and Frey, R.W., 1992. Trace fossil facies models: environmental and allostratigraphic significance. In: Walker, R.G., and James, N.P (Eds.), Facies models response to sea level change. Geological Association of Canada, Stittsville, 47-72.

Pickering, K., Stow, D., Watson, M., and Hiscott, R., 1986. Deep-water facies, processes and models: a review and classification scheme for modern and ancient sediments. Earth -Science Reviews. 23, 75-174.

Potter, P.E., and Pettijohn, F.J., 1963. Paleocurrents and Basin Analysis. Springer-Verlag, Berlin. 296p.

Poulsen, C.J., Barron, E.J., Johnson, C.C., and Fawcett, P., 1999. Links between major climatic factors and regional oceanic circulation in the mid-Cretaceous. In: Barrera, E., and Johnson, C.C. (Eds.), Evolution of the Cretaceous ocean-climate system. Geological Society of America, Boulder, Colorado, pp. 73-89.

Powell, J.H., 1989. Stratigraphy and sedimentation of the Phanerozoic rocks in central and south Jordan. Natural Resources Authority, Geological Mapping Division, Amman. 130p.

Pratt, B.R., 1998. Syneresis cracks: subaqueous shrinkage in argillaceous sediments caused by earthquake-induced dewatering. Sedimentary Geology. 117, 1-10.

Pufahl, P.K., Grimm, K.A., Abed, A.M., and Sadaqah, R.M.Y., 1998. Late Cretaceous (Maastrichtian) phosphorites and associated sediments in Jordan: Implications for south Tethyan paleogeography and economic phosphorites. Carrerfour in Earth sciences, Geological Association of Canada Annual Meeting, Abstract Volume, p. A-150.

Pufahl, P.K., Grimm, K.A., Abed, A.M., Sadaqah, R.M.Y., 2000a. Economic phosphorites in Jordan: Implications for the formation of an Upper Cretaceous (Maastrichtian) phosphorite giant. Geological Society of America, Cordilleran Section Meeting, Abstract Volume 32, p. A-63.

Pufahl, P.K., Grimm, K.A., Abed, A.M., and Sadaqah, R.M.Y., 2000b, Upper Cretaceous (Maastrichtian) phosphorites in Jordan: Implications for the formation of a south Tethyan phosphorite giant. GeoCanada 2000, Millennium Geosciences Summit, Abstract Volume, CD-ROM.

Pufahl, P.K., Grimm, K.A., Abed, A.M., and Sadaqah, R.M.Y., 2001, submitted. Upper Cretaceous (Campanian) phosphorites in Jordan: Implications for the formation of a south Tethyan phosphorite giant. Sedimentary Geology, 90p., 15 figures, 4 tables.

Raiswell, R., 1987. Non-steady state microbiological diagenesis and the origin of concretions and nodular limestones. In: Marshall, J.D. (Ed.), Diagenesis of Sedimentary Sequences. Geological Society of London, 41-54.

Rampino, M.R., and Stothers, R.B., 1988. Flood basalt volcanism during the past 250 million years. Science. 241, 663-668.

Raymont, J.E.G., 1980. Plankton and productivity in the ocean, phytoplankton, Vol. 1. Pergamon, New York. 489p.

Reiss, Z., Almogi-Labin, A., Honigstein, A., Lewy, Z., Lipson-Benitah, S., Moshkovitz, S., and Zaks, Y., 1985. Late Cretaceous multiple stratigraphic framework of Israel. Israel Journal of Earth Sciences. 34, 147-166.

Reiss, Z., 1988. Assemblages from a Senonian high-productivity sea. Revue de Paleobiologie. Special Volume 2, 323-332.

Riggs, S.R., and Sheldon, R.P., 1990. Paleoceanographic and paleoclimatic controls of the temporal and geographic distribution of Upper Cenozoic continental margin phosphorites. In: Burnett, W.C., and Riggs, S.R. (Eds.), Phosphate Deposits of the World, Vol. 3. Cambridge University Press, Cambridge, 207-222.

Rusnak, G.A., 1960. Sediments of Laguna Madre, Texas. In: Shepard, F.P., Phleger, F.B., and van Andel, T.H. (Eds.), Recent sediments, Northwest Gulf of Mexico. American Association of Petroleum Geology, Tulsa, 153-196.

Sadaqah, R.M., 2000. Phosphogenesis, Geochemistry, Stable Isotopes and Depositional Sequences of the Upper Cretaceous Phosphorite Formation in Jordan. PhD thesis, University of Jordan, Amman. 257p.

Savrda, C.E., and Bottjer, D.J., 1991. Oxygen-related biofacies in marine strata: an overview and update. In: Tyson, R.V., and Pearson., T.H. (Eds.), Modern and ancient continental shelf anoxia. Geological Society of London Special Publication 58, Oxford, 201-219.

Schuffert, J.D., Kastner, M., and Jahnke, R.A., 1998. Carbon and P burial associated with modern phosphorite formation. Marine Geology. 146, 21-31.

Sheldon, R.P., 1980. Episodicity of phosphate deposition and deep ocean circulation – a hypothesis. In: Bentor, Y.K. (Eds.), Marine Phosphorites - Geochemistry, Occurrence, Genesis. Society of Economic Paleontologists and Mineralogists, 239-247.

Sheldon, R.P., 1981. Ancient marine phosphorites. Annual Review of Earth Planetary Sciences. 9, 251-284.

Shemesh, A., Kolodny, Y., and Luz, B., 1983. Oxygen isotope variations in phosphate of biogenic apatites, II. Phosphorite rocks. Earth and Planetary Science Letters. 64, 405 -416.

Shemesh, A., and Kolodny, Y., 1988. Oxygen isotopes variations in phosphorites from the southeastern Tethys. Israel Journal of Earth Sciences. 37, 1-15.

Silverman, S.R., Fugat, R., and Weiser, J.D., 1952. Quantitative determination of calcite associated with carbonate-bearing apatite. American Mineralogist. 37, 211-222.

Slaughter, M., and Hill, R.J., 1990. The influence of organic matter in organogenic dolomitization. Journal of Sedimentary Petrology. 61, 296-303.

Snedden, J.W., Nummedal, D., and Amos, A.F., 1988. Storm- and fair-weather combined flow on the central Texas continental shelf. Journal of Sedimentary Petrology. 58, 580-595.

Sohn, Y.K., 1997. On traction-carpet sedimentation. Journal of Sedimentary Research. 67, 502 -509.

Soudry, D., Moshkovitz, S., and Ehrlich, A., 1981. Occurrence of siliceous microfossils (diatoms, silicoflagellates and sponge spicules) in the Campanian Mishash Formation, southern Israel. Eclogae Geologicae Helveticae. 74, 97-107.

Soudry, D., and Champetier, Y., 1983. Microbial processes in the Negev phosphorites (southern Israel). Sedimentology. 30, 411-423.

Southard, J.B., Lambie, J.C., Federico, D.C., Pile, H.T., and Weidman, C.R., 1990. Experiments on bed configurations in fine sands under bidirectional purely oscillatory flow, and the origin of hummocky cross-stratification. Journal of Sedimentary Petrology. 60, 1-17.

Steinitz, G., 1977. Evaporite-chert associations in Senonian bedded cherts, Israel. Israel Journal of Earth-Sciences. 26, 55-63.

Suess, E., 1981. Phosphate regeneration from sediments of the Peru Continental margin by dissolution of fish debris. Geochimica et Cosmochimica Acta. 45, p. 577-588.

Suess, E., et al. (eds.), 1990. Proceedings of the Ocean Drilling Program, Scientific Results, 112, College Station. 604p.

Taylor, K.G., and Macquaker, J.H.S., 2000. Spatial and temporal distribution of authigenic minerals in continental shelf sediments: implications for sequence stratigraphic analysis. In: Glenn, C.R., Prevot-Lucas, L., and Lucas, J. (Eds.), Marine Authigenesis: from Global to Microbial. SEPM Special Publication 66. SEPM, Tulsa, 309-323.

Tsujita, C.J., 1995. Origin of concretion-hosted shell clusters in the Late Cretaceous Bearpaw Formation, southern Alberta, Canada. Palaios. 10, 408-423.

Tucker, M.E., and Wright, V.P., 1990. Carbonate Sedimentology. Blackwell Scientific Publications, London. 482p.

Tyson, R.V., and Pearson, T.H. (Eds.), 1991. Modern and ancient continental shelf anoxia, Geological Society of London Special Publication 58, London. 470p.

Upchurch, J., G.R., Otto-Bliesner, B.L., and Scotese, C.R., 1999. Terrestrial vegetation and its effects on climate during the latest Cretaceous. In: Barrera, E., and Johnson, C.C. (Eds.), Evolution of the Cretaceous ocean-climate system. Geological Society of America, Boulder Colorado, 407-426.

Voigt, S., Hay, W.W., Hofling, R., and DeConto, R.M., 1999. Biogeographic distribution of Early to Late Cretaceous rudist-reefs in the Mediterranean as climate indicators. In: Barrera, E., and Johnson, C.C. (Eds.), Evolution of the Cretaceous ocean-climate system. Geological Society of America, Boulder, 91-103.

Walker, R.G., 1977. Deposition of Upper Mesozoic resedimented conglomerates and associated turbidites in southwestern Oregon. Bulletin of the Geological Society of America. 88, 273-285.

Walker, R.G., 1978. Deep water sandstone facies and ancient submarine fans; models for exploration for stratigraphic traps. AAPG Bulletin. 62, 932-966.

Walker, R.G., and Plint, A.G., 1992. Wave- and storm-dominated shallow marine systems. In: Walker, R.G., and James, N.P. (Eds.), Facies models response to sea level change. Geological Association of Canada, Stittsville, 219-238.

Wefer, G., Berger, W.H., and Richter, C., et al. (eds.), 1998. Proceedings of the Ocean Drilling Program, Scientific Results, 175, College Station. CD-ROM.

Wetzel, A., and Allia, V., 2000. The significance of hiatus beds in shallow-water mudstones: an example from the Middle Jurassic of Switzerland. Journal of Sedimentary Research. 70, 170-180.

Wetzel, R., and Morton, D.M., 1959. Contribution a la geologie de la Transjordanie. In: Dubertret, L. (Eds.), Notes et Memoirs sur le Moyen Orient. , 95-191.

Widmark, J.G.V., and Speijer, R.P., 1997. Benthic foraminiferal faunas and trophic regimes at the terminal Cretaceous Tethyan seafloor. Palaios. 12, 354-371.

Wilson, J.L., 1975. Carbonate Facies in Geologic History. Springer-Verlag, New York. 471p.

Wolfe, J.A., and Upchurch, G.R., 1987. North American nonmarine climates and vegetation during the Late Cretaceous. Palaeogeography, Palaeoclimatology, Palaeoecology. 61, 33-77.

Zijlstra, J.J.P., 1995. The Sedimentology of Chalk, 54. Springer-Verlag, Berlin. 194p.

CHAPTER 3

COATED PHOSPHATE GRAINS: THE GRANULAR EQUIVALENT OF CONDENSED BEDS

3.1 ABSTRACT

This study utilizes back scatter electron microscopy (BSE) and energy dispersive spectroscopic (EDS) analysis to study 35 samples of coated grains from differing ages and provenance. Three types of coated grains occur. Unconformity-bounded grains (UB) contain internal discordances and erosional surfaces, attributable to iterative episodes of phosphogenesis and sedimentary reworking. Redox-aggraded (RA) grains consist of concentric phosphate laminae that are intimately intercalated with circumgranular layers containing either chamosite, barite, or pyrite. RA grains record *in situ* diagenetic mineralization accompanied by changes in the redox potential of pore waters. We attribute these changes to variations in the biological oxygen demand within suboxic pore water environments that result from fluctuations in the sedimentation rate of organic carbon. Hybrid grains (H) contain characteristics of both UB and RA grains, and form when episodes of grain exhumation alternate with changes in pore water redox potential.

The circumgranular record of diverse shallow burial and seafloor processes suggests that coated phosphate grains record low and/or net negative rates of sediment accumulation. UB grains form during periods of relative stratigraphic condensation and may aid, when coupled with other sedimentologic data, in the identification of transgressive and highstand systems tracts within the sedimentary record. RA grains record variations in the export of organic carbon to the sea floor, thus recording variability in productivity and/or ecological dynamics in the surface ocean. In each case coated phosphate grains are interpreted as the granular equivalent to a condensed bed.

3.2 INTRODUCTION

Phosphorites commonly contain a variety of grain types recording a wide spectrum of depositional and diagenetic processes. Consequently, sedimentologists have debated the

microenvironments of grain formation and the times and processes of phosphate deposition (Riggs et al., 1997). Most petrographic studies of phosphate grains have reported on their morphology and micro-structure using standard petrographic techniques coupled with secondary electron imaging to understand the complexity of phosphate grain types (e.g. Soudry and Southgate, 1989; Lamboy et al., 1997). However, none of these investigations has examined the internal structure of phosphorite grains using high-resolution microbeam techniques to elucidate the physical/chemical conditions of formation (e.g. Glenn and Arthur, 1988). In this paper we extend this approach by combining back scattered electron (BSE) imaging and elemental microanalysis of individual laminae with carbon isotopic analysis of coated phosphate grains. This information is used to construct a comprehensive model for the formation of coated phosphate grains.

3.3 METHODS

Samples of coated phosphate grains were selected from collections of phosphorite of differing ages and provenance (Fig 3.1; Table 3.1). All samples come from organic-rich stratigraphies interpreted to have been deposited beneath highly productive surface waters (Swirydczuk et al., 1981; Swett and Crowder, 1982; Sturesson 1986, 1988; 1989, 1992; Glenn et al., 1988; Kidder and Swett, 1989; Garrison and Kastner, 1990; Mulabisana, 1998; Grimm, 2000; Harris, 2000; Pufahl et al., in review). The petrography of samples was studied using backscattered electron imaging (BSE). BSE photomicrographs and qualitative analysis of coated grains were acquired with a Philips XL-30 scanning electron microscope equipped with a Princeton Gamm-Tech thin-window detector. Samples intended for carbon stable isotopic analysis of the carbonate anionic complex in francolite were first disaggregated by leaching specimens for 48 hours in tri-ammonium citrate solution at pH 8.1 (Silverman et al., 1952). Stable isotopic analysis of specimens was performed at the University of Western Ontario in the

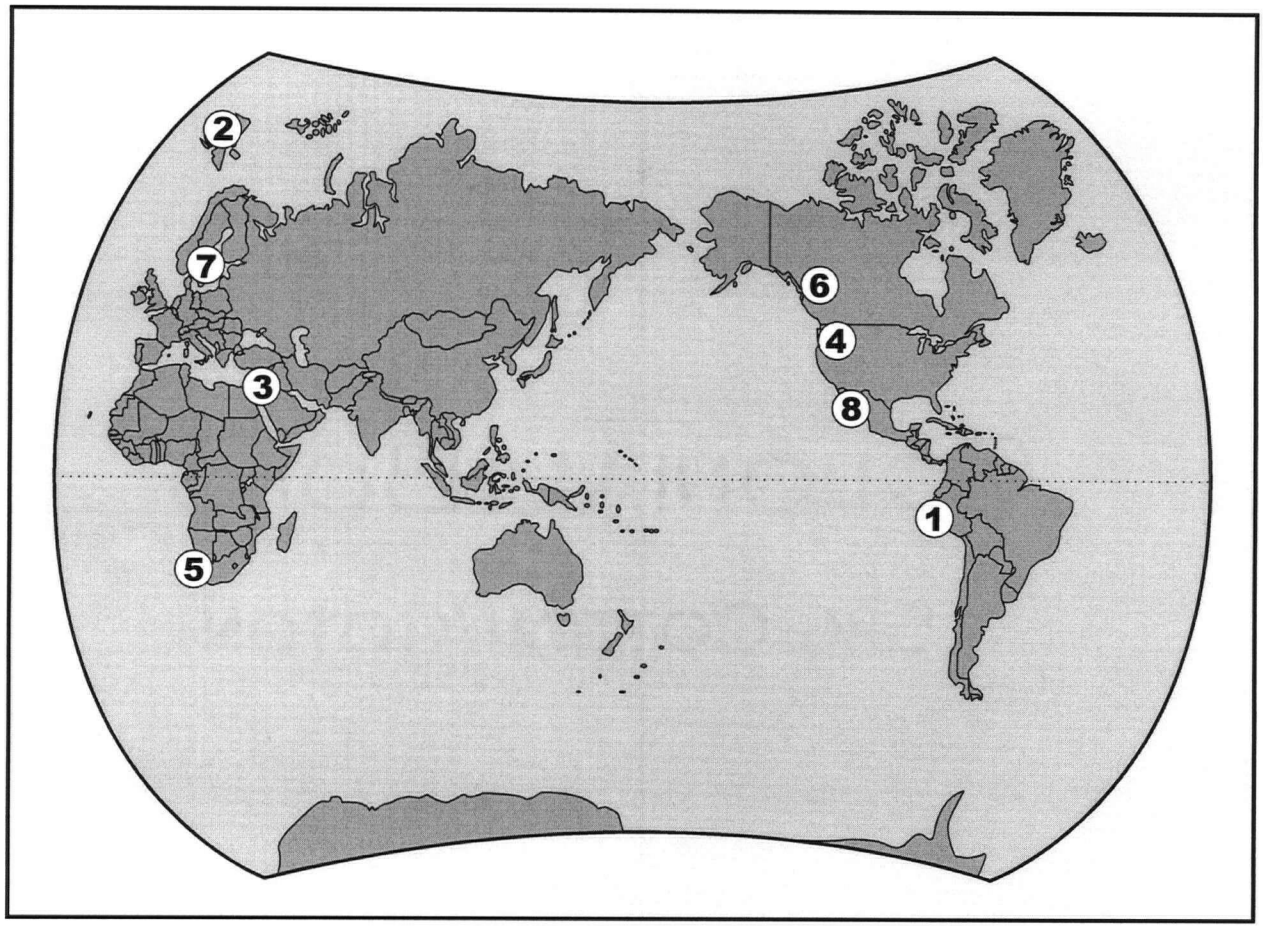

Figure 3.1 Map of the world showing sample locations. Legend: 1 - Peru margin (Quaternary); 2 - Spitsbergen (Cambrian); 3 - Jordan (Campanian); 4 - U.S.A., Idaho (Pliocene); 5 - South Africa (Miocene); 6 - Canada, British Columbia (Triassic); 7 - Sweden (Cambrian, Ordovician); 8 - Mexico, Baja California Sur (Oligo-Miocene).

Table 3.1 Characteristics of samples investigated.

Location	Depositional Environment	Age/Formation	Sample Number	Grain Type	$\delta^{13}C$ (PDB)	Ref.
Peru	Upwelling-related organic-rich sediments on outer shelf/upper slope. Well-developed OMZ.	Quaternary	112-679A-1H-1	UB,H		[1]
			112-679B-6H-1	UB		[1]
			112-687B-3H-5	UB	-8.71	[1]
			BX-2	RA,H	-1.35*	[2]
		Pliocene	112-680B-11H-1	UB	-4.08	[1]
		Pliocene	112-680B-11H-cc	UB		[1]
Spitsbergen	Upwelling-related organic-rich sediments on passive margin.	Cambrian/Tokammane Formation	T-3	RA		[3,4]
Jordan	Upwelling-related organic-rich sediments on storm-dominated epeiric platform.	Campanian/Alhisa Phosphorite Formation	ERM-1	UB		[5]
			ERQ-1	UB		[5]
			M-2	UB		[5]
			M-6	UB		[5]
			OM-1	UB		[5]
			OM-20	UB		[5]
			OM-5	UB	-5.51	[5]
			OM-7	UB		[5]
			OM-8	UB		[5]
			RQ-1	UB	-7.95	[5]
			Q-2	UB		[5]
			Q-4	UB	-8.40	[5]
U.S.A	Nearshore sediments in highly productive lake.	Pliocene/Glenns Ferry Formation	W-1	RA	-2.76	[6]
South Africa	Upwelling-related organic-rich sediments on passive margin.	Miocene	MJM-30b	RA		[7]
			MJM-30d	RA	-15.88	[7]
			MJM-23c	RA		[7]
Canada	Organic-rich sediments on passive margin.	Triassic/Doig Formation	10012	UB,H		[8]
			98090	UB		
Sweden	Organic-rich sediments on carbonate platform.	Ordovician/Gullhögen Formation	H-1	RA,H	-5.55	[9,10]
			G-1	RA	-8.35	[9,10]
		Ordovician/Kunda Formation	O-1	RA, H	-3.16	[11]
	Oragnic-rich sediments on siliciclastic shelf.	Cambrian/Oelendicus Shale Formation	N-1	RA,H	-8.35	[12]
Mexico	Upwelling related organic-rich sediments deposited in an active forearc setting.	Oligo-Miocene/ Timbabichi Formation	RS-5	UB		[13]
			LPB5-B	UB		[13]
			ZEBRA-2	UB		[13]
			CZ-7	UB		[13]
			LV-6	UB		[13]
			ZC-2	UB		[13]

Notes: UB – unconformity bound phosphate grain; RA – redox aggraded phosphate grain; H – hybrid phosphate grain; 1 – Glenn et al. (1988); 2 – Garrison and Kastner (1990); 3 – Swett and Crowder (1982); 4 – Kidder and Swett (1989); 5 – Pufahl et al. (2001); 6 – Swirydczuk et al. (1981); 7 – Mulabisana (1998); 8 – Harris (2000); 9 – Sturesson (1989); 10 – Sturesson (1992); 11 – Sturesson (1986); 12 – Sturesson (1988); 13 – Grimm (2000).
* denotes $\delta^{13}C$ value from Glenn et al. (1988). No sample material was available from the U.S.A. and Mexico for stable isotopic analysis.

Laboratory for Stable Isotope Studies following the methods of McCrae (1950). Carbon and oxygen isotopic results are reported in per mil relative to the PDB standard using the delta notation.

3.4 PHOSPHOGENESIS

Primary phosphogenesis is the process of carbonate fluorapatite (CFA) [$Ca_{10-a-b}Na_aMg_b(PO_4)_{6-x}(CO_3)_{x-y-z}(CO_3{\cdot}F)_{x-y-z}(SO_4)_zF_2$] precipitation at or near the sediment-water interface (Jahnke et al., 1983; Froelich et al., 1988). It is a biogeochemical process governed by the microbial production of phosphate in sediment pore waters at low sedimentation rates. It is the precursor of the hydraulic and biological reworking/winnowing processes that concentrate phosphatic sediment into economic phosphorites (Baturin, 1971; Glenn et al., 1994).

In modern environments phosphogenesis commonly occurs beneath the sites of active upwelling along the coasts western South America, Baja California, south-western Africa, and western India (Sheldon, 1980). Francolite precipitation in these settings is stimulated by the effects of high primary productivities and is primarily driven by the production of pore water phosphate through the suboxic microbial degradation of sedimentary organic matter (Burnett, 1977; Jahnke et al., 1983, Froelich et al., 1988; Ingall and Jahnke, 1997). The diagenesis of organic matter progresses through a sequence of microbially-mediated redox reactions that include oxic respiration, denitrification, metal oxide reduction, sulfate reduction, and methanogenesis (Froelich et al., 1979). These reactions define distinct diagenetic zones that correspond to the profiles of observed pore-water concentrations of O_2, NO_3^-, Mn^{2+}, Fe^{2+}, and SO_4^{2-} (Froelich et al., 1979). Phosphogenesis occurs within 5-20cm of the sediment-water interface in association with the reduction of NO_3^-, Mn-oxides, Fe-oxides, and SO_4^{2-} (Froelich et al., 1988), and is limited at deeper intervals by the lack of seawater-derived fluorine (Jahnke et al., 1983) and the high alkalinities that develop through the cumulative degradation of organic

matter because francolite is unable to accommodate excessive substitution of CO_3^{2-} in its crystal structure (Glenn et al., 1988; Glenn et al., 1994). Francolite precipitated within these zones has very distinctive $\delta^{13}C$ signatures pointing to the derivation of a significant portion of its carbon from microbially degraded organic matter (Irwin et al., 1977; Jarvis et al., 1994). Unlike the other products of organic matter degradation, phosphogenesis is not a redox-controlled reaction, but is regulated only by the concentration of pore water phosphate.

Phosphogenesis in upwelling regions is also commonly associated with *Beggiatoaceae*, a family of sulfur oxidizing bacterial mat formers (Krajewski et al., 1994). These organisms are rich in organic forms of P (C:P ratio of 68 vs. the Redfield value of 106) (Reimers et al., 1990) and bridge the redox boundary between the zones of nitrate and sulfate reduction (Jørgensen and Revsbech, 1983). They extract metabolic energy from the concomitant reduction of nitrate and oxidation of sulfide across this interface (Fossing et al., 1995). *Beggiatoaceae* mats promote phosphogenesis by inhibiting the escape of pore water phosphate through the assimilation of P in their cells, and by supersaturating pore waters with reactive P during postmortem degradation (Reimers et al., 1990). *Beggiatoaceae* also assist in the dissolution of fish debris, an important source of pore water phosphate (Suess, 1981), by lowering the pH of interstitial waters through the production of protons during respiration (Froelich et al., 1988).

In areas not associated with prominent upwelling, such as the eastern margin of Australia (Heggie et al., 1990) and the continental slope off southern Baja California (Schuffert et al., 1998), dissolved pore water phosphate is regulated by iron redox pumping. Iron redox pumping is a cyclic mechanism that enriches phosphate in pore waters by the release of phosphate sorbed onto iron oxyhydroxides. For this mechanism to operate efficiently as a P pump requires either repeated mixing of the sediment to the iron redox boundary or else an iron redox boundary that oscillates vertically with time (Shaffer, 1986; Schuffert et al., 1998).

3.5 RESULTS AND DISCUSSION

Three types of coated grains occur (Table 3.1): unconformity bounded (UB), redox aggraded (RA), and hybrid (H) grains. UB grains are formed of discontinuous and irregular phosphatic laminae, 10-100 μm thick, that are erosionally truncated by successive layers (Fig. 3.2). Laminae vary in thickness around the circumference of the grain and are sometimes endolithically bored. RA grains consist of concentric phosphatic laminae that are intimately intercalated with circumgranular layers composed predominantly of either pyrite, chamosite, or barite (Fig. 3.3). Laminae are thinner and less well defined than those composing UB grains, ranging in thickness from 5-30 μm. RA laminae show little variation in thickness and are sublaminated on an ultrafine scale. Hybrid grains (H) contain characteristics of both UB and RA grains. Grain nuclei consist of phosphatic intraclasts, phosphatized foraminifera tests, carbonate ooids, authigenic glauconite and dolomite grains, and silt-sized detrital quartz and feldspar clasts.

The range of $\delta^{13}C$ (CO_3-carbonate fluorapatite) values shown in Table 3.1 (-1.35 to -15.88‰) in comparison with modern pore water total dissolved $\delta^{13}C$ values from anoxic sediments and from other ancient deposits (Benmore et al., 1983; Shemesh et al., 1983; McArthur et al., 1980, 1986; Glenn et al., 1988; Glenn and Arthur, 1990; McArthur and Herczeg, 1990; Compton et al., 1993; Pufahl et al., 2001) is consistent with phosphogenesis within 5-20cm of the sediment-water interface in association with the suboxic to anoxic degradation of organic matter. Marine organic matter is highly depleted in ^{13}C, typically ranging between -20 and -28‰, and when microbially oxidized produces dissolved inorganic carbon of the same isotopic composition (Jarvis et. al., 1994). In the oxic and suboxic upper layers of the sediment, where oxygen, and then nitrate and metal oxide, reduction are used sequentially as an oxygen source, there is an increase in the dissolved organic carbon with depth, causing decreasing pore water inorganic $\delta^{13}C$ values to a minimum of ~ -6‰ (Jarvis et al., 1994). Below this sulfate reduction leads to an increase in bicarbonate production and a pronounced decrease in $\delta^{13}C$ to

Figure 3.2 BSE photomicrographs of unconformity bounded (UB) coated phosphate grains. Note how the phosphatic layers are erosionally truncated by successive laminae and how the thickness of the phosphatic coatings change around the circumference of the grain. A) BSE photomicrograph of UB grain in sample OM-7. The grain nucleus consists of a rounded phosphatic intraclast. B) BSE photomicrograph of UB phosphate grain in sample M-6. The grain nucleus consists of a phosphatized foraminifera test that is partially occluded with phosphate. C) BSE photomicrograph of UB phosphate grain nucleated around a silt-sized, angular quartz grain in sample 10012. D) BSE photomicrograph of UB grains nucleated around subangular silt-sized quartz grains in sample 112-687B-3H-5. The black regions are intrapeloidal voids. E) BSE photomicrograph of a H grain in sample 112-687B-3H-5. The grain is nucleated around a rounded phosphatic intraclast containing subangular, silt-sized quartz grains. Note the thin RA laminae that coat the nucleus. F) BSE photomicrograph of UB coated grain nucleated around an angular, silt-sized quartz grain in sample BX-2. G) BSE photomicrograph of UB grains in sample LV-6. H) BSE photomicrograph of UB grain in sample LPB5-B. Round black areas within grains in G and H are endolithic borings.

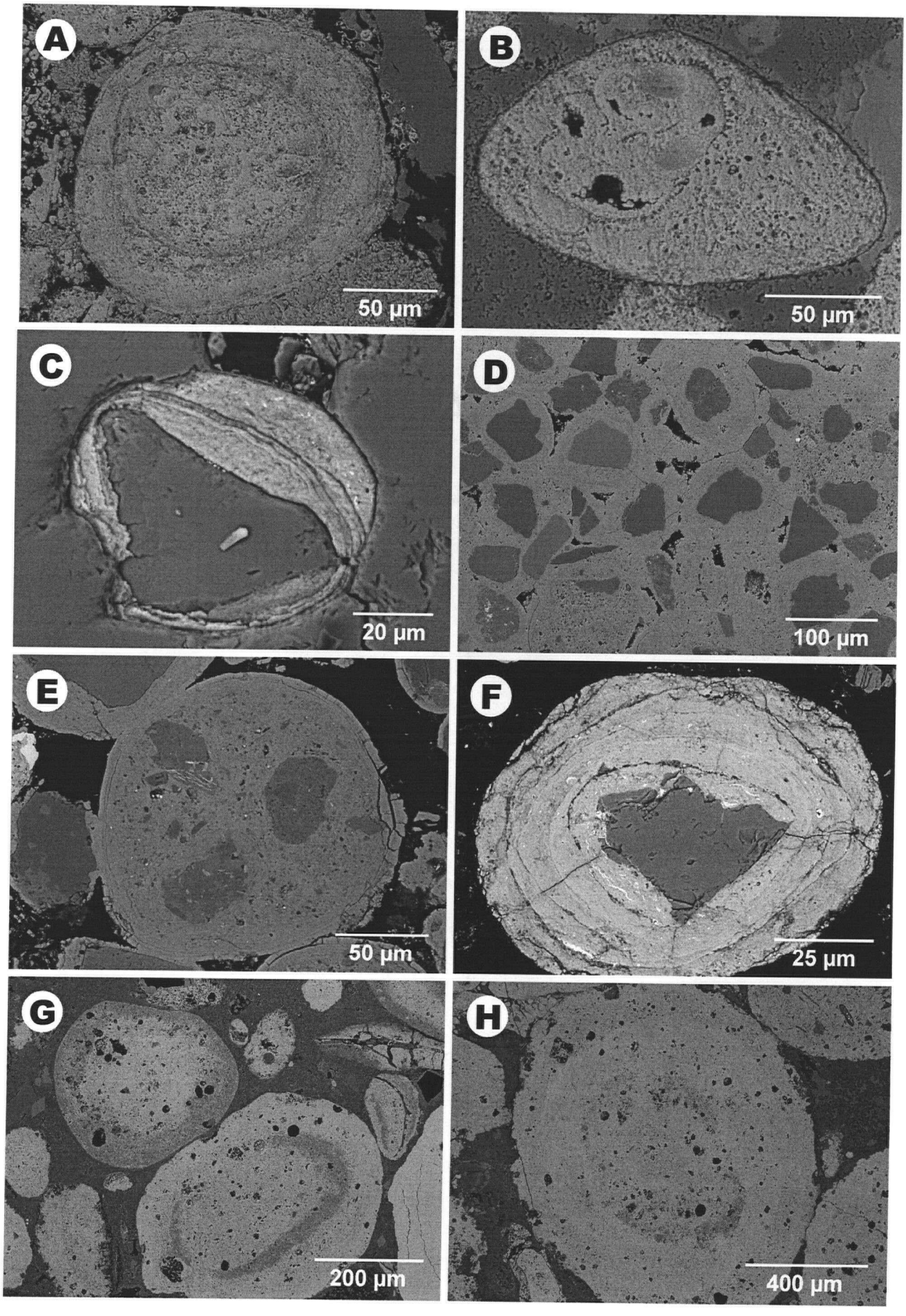
A
50 µm
B
50 µm
C
20 µm
D
100 µm
E
50 µm
F
25 µm
G
200 µm
H
400 µm

Figure 3.3 BSE photomicrographs of redox aggraded (RA) coated phosphate grains. Note how concentric phosphate coatings are of uniform thickness and that laminae composition varies across individual grains. A) BSE photomicrograph of RA grain nucleated around a silt-sized feldspar grain in sample BX-2. The innermost lamina is compositionally distinct from the other layers and contains abundant framboidal pyrite (white specs). The contacts between some phosphatic layers are also demarcated by thin, discontinuous pyrite laminae. B) BSE photomicrograph of RA nodule in sample MJM-30d. Photomicrograph shows the alternation of pyrite-rich (white specs) and pyrite-poor (dark gray) phosphatic laminae within the nodule. Note how layer boundaries are diffuse suggesting gradual shifts in the redox potential of pore waters. C) BSE photomicrograph of RA grain nucleated around a silt-sized glauconite clast in sample N-1. The alternating dark and light bundles of laminae reflect changes in layer composition from phosphate (light gray) to chamosite (dark gray). D) BSE photomicrograph of H grain in sample O-1. The grain is nucleated around a silt-sized grain of glauconite. As in N-1 the alternation of dark and light laminae records the intercalation of phosphatic and chamositic coatings. E) BSE photomicrograph RA grain nucleated around a phosphatic intraclast in sample G-1. The light gray laminae are barite. F) BSE photomicrograph of H grain nucleated around a silt-sized fragment of carbonate in sample 112-687B-3H-5. The innermost lamina is a UB layer that is erosionally truncated and discontinuously coats the nucleus. Successive layers are interpreted as RA laminae that completely coat the grain. G) BSE photomicrograph of RA grains in sample T-3. Grain nuclei consist of rounded, fine sand-sized quartz grains. H) BSE photomicrograph of RA grains in sample W-1. Coatings are thin and are of equal thickness around the circumference of the grain. The coated grain on the left is nucleated around a silt-sized plagioclase grain. The nucleus of the coated grain on the right consists of a partially dissolved ooid.

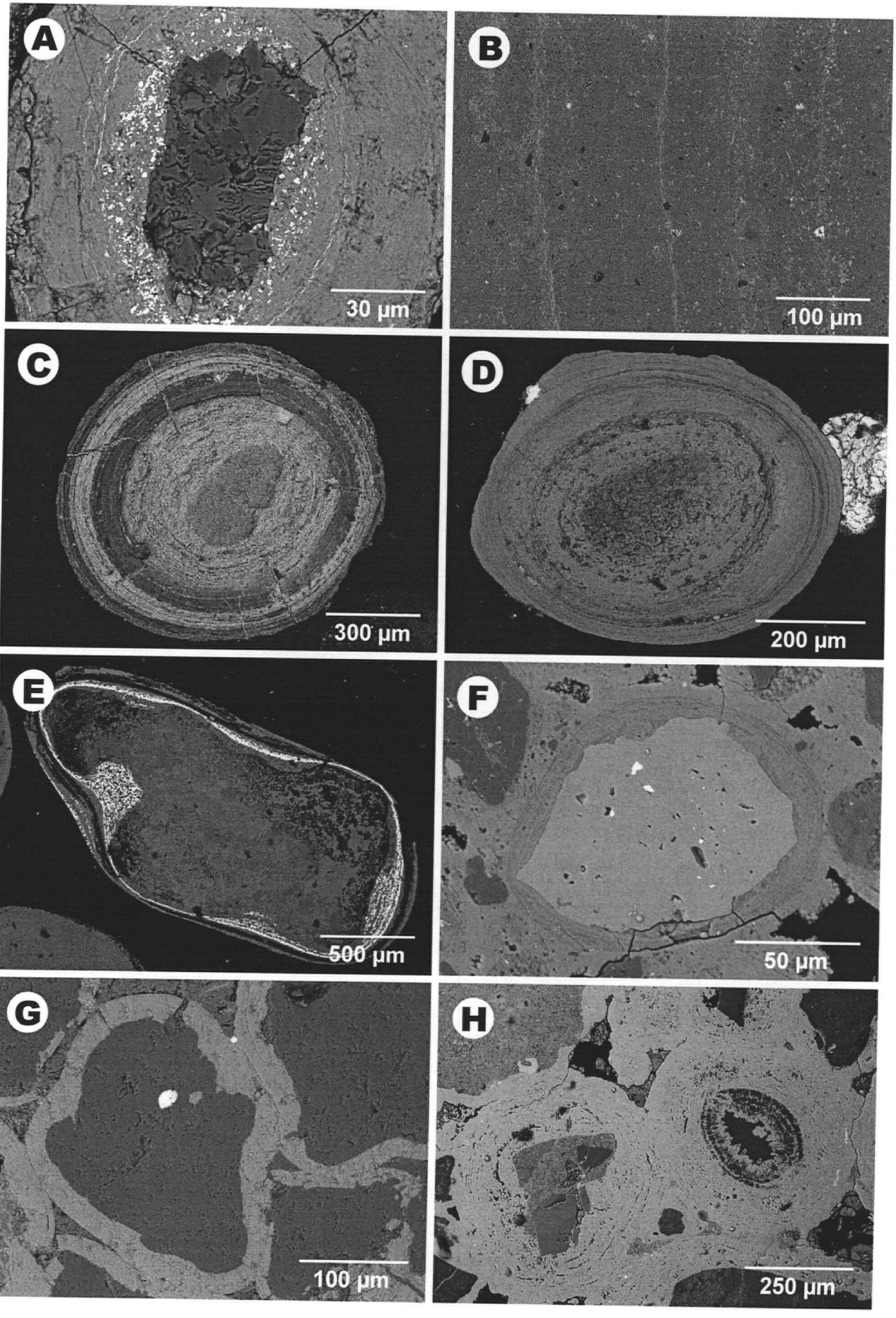
A
30 µm
B
100 µm
C
300 µm
D
200 µm
E
500 µm
F
50 µm
G
100 µm
H
250 µm

~-25‰ (Irwin et al., 1977).

UB grains formed through multiple episodes of phosphatization, exhumation and erosion, and reburial into the zone of phosphogenesis (ZOP) (Fig. 3.4A). Grains that are endolithically bored also record colonization of exhumed grains between repeated episodes of burial and phosphogenesis. Garrison and Kastner (1990) have proposed a similar model for the formation of coated phosphate grains from the Peru continental margin.

Changes in pore water redox chemistry are recorded in RA grains by the intimate intercalation of francolite laminae with circumgranular phosphate layers that contain either chamosite, pyrite, or barite. RA grains were produced by *in situ* francolite precipitation within the zone of phosphogenesis accompanied by changes in the redox potential of pore waters (Fig. 3.4B). Chamosite contains iron in both its reduced and oxidized states (Harder, 1978, 1980), indicating that it forms very early, soon after the partial microbial reduction of Fe^{3+} within Fe-oxides (Harder, 1978, 1980). It precipitates under identical diagenetic conditions as glauconite, which precipitates close to the Fe-redox boundary (Glenn and Arthur, 1988; Glenn, 1990). Glauconite also contains ferric and ferrous iron but forms within sediments with appreciably more silica than sediments that precipitate chamosite (Harder, 1980). Pyrite precipitates within the zone of sulfate reduction through a series of metastable reactions when Fe^{2+}, derived from redox controlled cation exchange reactions of clay minerals and dissolution of Fe-oxides, combines with sulfide produced via the microbial reduction of pore water sulfate (Berner and Raiswell, 1983; Berner, 1984, 1985; Lyons and Berner, 1992). Authigenic barite forms within organic-rich sediments just above the zone of sulfate reduction (van Os et al., 1993; Torres et al., 1996; Bréhéret et al., 2000; Dickens, 2001). Sea water sulfate diffuses downward from the sediment-water interface into the zone of sulfate reduction, where it meets with upward diffusing Ba^{2+} and precipitates barite. The Ba^{2+} is derived from the dissolution of sedimentary barite (Torres et al., 1996) and celestite tests such as *Acanthria* (Bernstein et al., 1992). In barium-rich

Figure 3.4 A) Formation of UB coated phosphate grains. This model is dependent upon erosion-deposition cycles that cause the zone of phosphogenesis (ZOP) to migrate up and down within the sediment column. 1 – The zone of phosphogenesis occurs a few centimeters below the sediment-water interface. Grains within the ZOP become coated with carbonate fluorapatite. 2 – During an erosive episode grains are exhumed through current winnowing and transport of sediment across the seafloor. Phosphatic laminae precipitated in 1 become mechanically abraded producing erosionally truncated layers of unequal thickness. During these periods the ZOP migrates down through the sediment column in response to erosion at the sediment-water interface. 3 – Reburial of phosphatic grains and migration of ZOP upward through the sediment column. During this stage phosphate grains are once again within the ZOP and another coating of CFA precipitates. B) Formation of RA coated phosphate depends upon the episodic flux of organic carbon to the sea floor through time causing redox interfaces associated with microbial respiration of sedimentary organic matter to shift vertically in the sediment column in response to changes in the biological oxygen demand (BOD). 1 – The zone of phosphogenesis occurs a few centimeters below the sediment-water interface. Grains within the ZOP become coated with carbonate fluorapatite. Under low organic carbon fluxes the SO_4^{2-}/H_2S redox interface is below the ZOP. 2 – An episodic increase in the organic carbon flux to the sea floor causes the iron and SO_4^{2-}/H_2S redox boundaries to both telescope and move upwards through the sediment column as oxidants are utilized in the degradation of organic matter. Telescoping facilitates the formation of pyrite-rich laminae by positioning grains within the zones of iron and sulfate reduction. 3 – Once all the organic matter is oxidized and/or the flux of organic carbon to the seafloor decreases the redox interfaces expand and move down through the sediment column facilitating the precipitation of chamosite/glauconite-rich laminae. The formation of barite laminae is not shown but would occur when the when the SO_4^{2-}/H_2S redox interface shallows in response to the arrival of a pulse of organic matter at the sea floor, bringing this boundary near the ZOP. The type of laminae that precipitates is governed by the amount of oxidizable organic matter at the sea floor and the bulk composition of the host sediment. C) Hybrid grains containing characteristics of both UB and RA grains may form when both processes act in concert to produce coated grains.

A
UNCONFORMITY BOUNDED
1
2
3
ZOP
B
REDOX AGGRADED
1
2
3
ZOP
BOD
BOD
Fe^{3+}
Fe^{2+}
SO_4^{2-}
H_2S
Fe^{3+}
Fe^{2+}
SO_4^{2-}
H_2S
Fe^{3+}
Fe^{2+}
C
HYBRIDS

sediments microbial sulfate reduction leads to undersaturation of barite within pore waters, which mobilizes and considerably enriches this zone with Ba^{2+} (Van Os et al., 1993). The origin of barite enrichment in sediments is still under debate, but appears to result from increased flux rates of microcrystalline barite crystals to the sea floor associated with high primary productivities (Schmitz, 1987; McManus et al., 1998). Bishop (1988) proposed an abiotic origin of barite in microenvironments in settling particles containing decaying organic matter and siliceous phytoplankton and direct biological precipitation within highly productive surface waters has been observed in microflagellate algae (Bertram and Cowen, 1997). The co-occurrence of barite nodules and phosphorites in the geological record has also been cited as evidence for a productivity-related origin of authigenic barite (Bréhéret et al., 2000).

We propose that variable input of sedimentary organic matter, perhaps seasonally or over longer timescales, induced the changes in pore water redox chemistry recorded in RA grains (Fig. 3.4B). An increase in the flux of organic carbon would cause an increase in the biological oxygen demand at the sediment-water interface, which in turn would cause the redox zones to telescope and move up through the sediment column. Once the bulk of organic matter has been oxidized, oxygen can diffuse deeper into the sediments, causing the redox zones to expand and move downward. Barite laminae form when the SO_4^{2-}/H_2S redox interface shallows in response to the arrival of a pulse of organic matter at the sea floor, bringing this boundary near the ZOP. The precipitation of pyrite laminae will occur when the SO_4^{2-}/H_2S redox boundary passes completely through the ZOP. We infer that chamosite layers form once the majority of organic matter has been respired and the diffusion of oxygen into the sediment column pushes the Fe^{3+}/Fe^{2+} redox boundary into the ZOP. We postulate that repeated vertical oscillation of these redox interfaces within the sediment column gives rise to multiply coated RA grains. Unlike the formation of UB grains this process does not necessitate complete exhumation and reburial of grains into the ZOP, but instead requires an episodic flux of organic carbon to the sea floor. The

type of laminae that precipitates is thus governed by the delivery rate of oxidizable organic matter to the sea floor and the bulk composition of the host sediment.

Oscillations in pore water redox potential have been directly measured using mircoelectrodes by Rasmussen and Jørgensen (1992) in Aarhus Bay, Denmark. Aarhus Bay is characterized by a strong seasonality in primary production resulting from spring phytoplankton blooms. Rasmussen and Jørgensen (1992) found that after the deposition of the spring bloom the oxic zone decreased in thickness four-fold, and a zone of intense sulfate reduction formed immediately under the oxic layer, just beneath the sediment-water interface. These changes occurred on the order of a few days after the bloom. Thamdrop et al. (1994) measured the concentration of Mn^{2+}, Fe^{2+}, and H_2S within pore waters over a seventeen month period in Aarhus Bay, and confirmed that the zones of manganese, iron, and sulfate reduction expanded and contracted concomitantly with changes in the export of organic carbon to the seafloor. Primary productivity induced redox oscillations in the sediment have also been tracked by the vertical movements of *Beggiatoaceae* and related mat bacteria (Jørgensen, 1977; Bussmann and Reichardt, 1991). The concept of vertically fluctuating redox zones has also been used to explain discrepancies between solid-phase and dissolved Mn in sediments from the East Pacific Rise (Pedersen et al., 1986) and from the continental margins of the Arctic and north-eastern Atlantic oceans (Gobeil et al., 1997). In each case the depth in the sediment where Mn is being precipitated was found to be deeper than the contemporaneous solid phase distribution. They attributed this discrepancy to a decrease in ocean productivity, a corresponding decrease in the organic carbon flux to the sea floor, and a subsequent migration of the Mn^{4+}/Mn^{2n+} redox boundary deeper into the sediment.

In our model the formation of multiply coated phosphate grains necessitates long residence times at the sediment-water interface. This interpretation is supported by sedimentologic evidence that indicates that at least some of the samples examined in this study

are associated with depositional hiatuses and omission surfaces associated with hardgrounds and carbonate concretionary horizons (Swirydczuk et al., 1981; Sturesson, 1986, 1989; Garrison and Kastner, 1990; Grimm, 2000; Pufahl et al., in review). Low net sedimentation rates and/or repeated reworking of the substrate facilitate phosphogenesis by allowing high concentrations of phosphate and fluoride to build up within pore waters (Föllmi et al., 1991). If the sedimentation rate is too high coated grains are progressively buried, within the sediment column, and are moved quickly out of the ZOP.

UB grains record repeated cycles of erosion and reburial into the ZOP. RA grains document episodic fluctuations in the export of organic carbon accompanied by low net sedimentation rates. H grains record episodes of complete exhumation and reburial with changes in the flux of sedimentary organic matter to the sea floor. In each case coated phosphate grains may be considered the granular equivalent of a condensed bed (Grimm et al., 1993; Grimm and Gallway, 1995). UB grains form during periods of relative stratigraphic condensation and may aid, when coupled with other sedimentologic data, in the identification of transgressive and highstands systems tracts within the sedimentary record. RA grains record variations in the rate of export of organic carbon to the sea floor, thus recording changes in productivity and/or ecological dynamics in the overlying water mass (Grimm et al., 1997). Concepts discussed in this paper are directly applicable to the interpretation of other types of coated grains and concretions that contain Eh sensitive minerals, such as iron ooids (e.g. Heikoop et al., 1996; Sturesson, 2000) and polymineralic concretions (e.g. Medrano and Piper, 1997).

3.6 REFERENCES CITED

Baturin, G.N., 1971. Stages of phosphorite formation on the ocean floor. Nature. 232, 61-62.

Benmore, R.A., Coleman, M.L., and McArthur, J.M., 1983. Origin of sedimentary francolite from its sulphur and carbon isotope composition. Nature. 302, 516-518.

Berner, R.A., and Raiswell, R., 1983. Burial and organic carbon and pyrite sulfur in sediments over Phanerozoic time: a new theory. Geochimica et Cosmochimica Acta. 47, 855-862.

Berner, R.A., 1984. Sedimentary pyrite formation. Geochimica et Cosmochimica Acta. 48, 605-615.

Berner, R.A., 1985. Sulphate reduction, organic matter decomposition and pyrite formation. Philosophical Transactions of the Royal Society of London. 315, 5-38.

Bernstein, R.E., Byrne, R.H., Betzer, P.R., Greco, A.M., 1992, Morphologies and transformations of celestite in seawater; the role of acantharians in strontium and barium geochemistry. Geochimica et Cosmochimica Acta. 56, 3273-3279.

Bertram, M.A., and Cowen, J.P., 1997. Morphological and compositional evidence for biotic precipitation of marine barite. Journal of Marine Research. 55, 577-593.

Bishop, J.K.B., 1988. The barite-opal-organic carbon association in oceanic particulate matter. Nature. 331, 341-343.

Bréhéret, J.G., and Brumsack, H.J., 2000. Barite concretions as evidence of pauses in sedimentation in the Marnes Bleues Formation of the Vocontian Basin (SE France). Sedimentary Geology. 130, 205-228.

Burnett, W.C., 1977. Geochemistry and origin of phosphorite deposits from off Peru and Chile. Geological Society of America Bulletin. 88, 813-823.

Bussman, I., and Reichardt, W., 1991. Sulfate-reducing bacteria in temporarily oxic sediments with bivalves. Marine Ecology Progress Series. 78, 97-102.

Compton, J.S., Hodell, D.A., Garrido, J.R., and Mallinson, D.J., 1993. Origin and age of phosphorite from the south-central Florida Platform; relation of phosphogenesis to sea level fluctuations and delta ^{13}C excursions. Geochimica et Cosmochimica Acta. 57, 131 -146.

Dickens, G.R., 2001. Sulfate profiles and barium fronts in sediment on the Blake Ridge: Present and past methane fluxes through a large gas hydrate reservoir. Geochimica et Cosmochimica Acta. 65, 529-543.

Föllmi, K.B., Garrison, R.E., and Grimm, K.A., 1991. Stratification in phosphatic sediments: illustrations from the Neogene of California. In: Einsele, G., Ricken, W., and Seilacher, A. (Eds.), Cycles and Events in Stratigraphy. Springer-Verlag, Berlin, Heidelberg, 492 -507.

Fossing, H., Gallardo, V.A., Jorgensen, B.B., Huttel, M., Nielsen, L.P., Schulz, H., Canfield, D.E., Forster, S., Glud, R.N., Gundersen, J.K., Kuver, J., Ramsing, N.B., Teske, A., Thamdrup, B., and Ulloa, O., 1995. Concentration and transport of nitrate by the mat -forming sulphur bacterium *Thioploca*. Nature. 374, 713-715.

Froelich, P.N., Klinkhammer, G.P., Bender, M.L., Luedtke, N.A., Heath, G.R., Cullen, D., Dauphin, P., Hammond, D., Hartman, B., and Maynard, V., 1979. Early oxidation of organic matter in pelagic sediments of the eastern equatorial Atlantic: suboxic diagenesis. Geochimica et Cosmochimica Acta. 43, 1075-1090.

Froelich, P.N., Arthur, M.A., Burnett, W.C., Deakin, M., Hensley, V., Jahnke, R., Kaul, L., Kim, K.H., Roe, K., Soutar, A., and Vathakanon, C., 1988. Early diagenesis of organic matter in Peru continental margin sediments: phosphorite precipitation. Marine Geology. 80, 308-343.

Garrison, R.E., and Kastner, M., 1990. Phosphatic sediments and rocks recovered from the Peru margin during ODP Leg 112. In: Suess, E., von Heune R., et al. (Eds.), Proceedings of the Ocean Drilling Program, Scientific Results. Ocean Drilling Program, College Station, pp. 111-134.

Glenn, C.R., Arthur, A., Yeh, Hseuh-wen, Burnett, W.C., 1988. Carbon isotopic composition of Peru-Chile margin phosphorites. Marine Geology. 80, 287-307.

Glenn, C.R., and Arthur, M.A., 1988. Petrology and major element geochemistry of Peru margin phosphorites and associated diagenetic minerals: authigenesis in modern organic rich sediments. Marine Geology. 80, 231-268.

Glenn, C.R., 1990. Depositional sequences of the Duwi, Sibaiya and Phosphate Formations, Egypt; phosphogenesis and glauconization in a Late Cretaceous epeiric sea. In: Notholt, A.J.G., and Jarvis, I. (Eds.), Phosphorite Research and Development: Geological Society Special Publications. The Geological Society, Oxford, 205-222.

Glenn, C.R., and Arthur, M.A., 1990. Anatomy and origin of a Cretaceous phosphorite -greensand giant, Egypt. Sedimentology. 37, 123-154.

Glenn, C.R., Follmi, K.B., Riggs, S.R., Baturin, G.N., Grimm, K.A., Trappe, J., Abed, A.M., Galli-Oliver, C., Garrison, R.E., Ilyin, A.V., Jehl, C., Rohrlich, V., Sadaqah, R.M.Y., Schidlowski, M., Sheldon, R.E., and Siegmund, H., 1994. P and phosphorites: sedimentology and environments of formation. Eclogae Geologicae Helveticae. 87, 747 -788.

Gobeil, C., MacDonald, R.W., Sundby, B., 1997. Diagenetic separation of cadmium and manganese in suboxic continental margin sediments. Geochimica et Cosmochimica Acta. 61, 4647-4654.

Grimm, K.A., 2000. Stratigraphic condensation and the redeposition of economic phosphorite: allostratigraphy of Oligo-Miocene shelfal sediments, Baja California Sur, Mexico. In: Glenn, C.R., Prevot-Lucas, L., and Lucas, J. (Eds.), Marine authigenesis: from global to microbial: SEPM Special Publications. Society for Sedimentary Geology, Tulsa, pp. 325 -347.

Grimm, K.A., Garrison, R.E., Compton, J.S., 1993. The Baturin Cycle revisited: Phosphorites and sequence stratigraphy in Oligo-Miocene strata of Baja California Sur, Mexico.

Concepts and Controversies in Phosphogenesis Workshop, ETH, Zurich, Abstract Volume.

Grimm, K.A., and Galway, S., 1995. Phosphorite grain stratigraphies from the Oligo-Miocene sediments, Baja California Sur, Mexico: Clues towards shelf-to-basin correlation. Peninsular Geological Society, Third International Conference on the Geology of Baja California (Mexico), Abstract Volume.

Grimm, K.A., Lange, C.B., and Gill, A.S., 1997. Self-sedimentation of fossil phytoplankton blooms in the geologic record. Sedimentary Geology, 110, 151-161.

Harder, H., 1978. Synthesis of iron layer silicate minerals under natural conditions. Clays and Clay Minerals. 26, 65-72.

Harder, H., 1980. Synthesis of Glauconite at surface temperatures. Clays and Clay Minerals. 28, 217-222.

Harris, R., 2000. Triassic Doig Formation sand bodies in the Peace River Area of western Canada: depositional and structural models, and the impact of diagenesis on reservoir properties. M.Sc. thesis, The University of British Colombia, Vancouver.

Heggie, D.T., Skyring, G.W., O'Brien, G.W., Reimers, C., Herczeg, A., Moriarty, D.J.W., Burnett, W.C., and Milnes, A.R., 1990. Organic carbon cycling and modern phosphorite formation on the East Australia continental margin: an overview. In: Notholt, A.J.G., and Jarvis, I. (Eds.), Phosphorite research and development. The Geological Society, Oxford, 87-117.

Heikoop, J.M., Tsujita, C.J., Risk, M.J., Tomascik, T., and Mah Anmarie, J., 1996. Modern iron ooids from a shallow marine volcanic setting; Mahengetang, Indonesia. Geology. 24, 759-762.

Ingall, E., and Jahnke, R., 1997. Influence of water-column anoxia on the elemental fractionation of carbon and P during sediment diagenesis. Marine Geology. 139, 219-229.

Irwin, H., Curtis, C. and Coleman, M., 1977. Isotopic evidence for source of diagenetic carbonates formed during burial of organic-rich sediments. Nature. 269, 209-213.

Jahnke, R.A., Emerson, S.R., Roe, K.K., and Burnett, W.C., 1983. The present day formation of apatite in Mexican continental margin sediments. Geochimica et Cosmochimica Acta. 47, 259-266.

Jarvis, I., Burnett, W.C., Nathan, Y., Almbaydin, F.S.M., Attia, A.K.M., Castro, L.N., Flicoteaux, R., Hilmy, M.E., Husain, V., Quatawnah, A.A., Serjani, A., and Zanin, Y.N., 1994. Phosphorite geochemistry: State-of-the-art and environmental concerns. Eclogae Geologicae Helveticae. 87, 643-700.

Jørgensen, B.B., 1977. Distribution of colorless sulfur Bacteria (*Beggiatoa* spp.) in a coastal marine sediment. Marine Biology. 41, 19-28.

Jørgensen B.B., and Revsbech, N.P., 1983, Colourless sulfur bacteria, *Beggiatoa* sppp. And *Thiovulum* sppp., in O_2 and H_2S microgradients. Applied and Environmental Biology. 45, 1261-1270.

Kidder, D.L., and Swett, K., 1989. Basal Cambrian reworked phosphates from Spitsbergen (Norway) and their implications. Geological Magazine. 126, 79-88.

Krajewski, K.P., Van Cappellen, P., Trichet, J., Kuhn, O., Lucas, J., Martin-Algarra, A., Prevot, L. Tewari, V.C., Gaspar, L., Knight, R.I., Lamboy, M., 1994. Biological processes and apatite formation in sedimentary environments. Eclogae Geologicae Helveticae. 87, 701 -745.

Lamboy, M., Rao, V.P., Ezzat, A., Ahmed, E., and Azzouzi, N., 1994. Nannostructure and significance of fish coprolites in phosphorites. Marine Geology. 120, 373-383.

Lyons, T.W., and Berner, R.A., 1992. Carbon-sulfur-iron systematics of the uppermost deep -water sediments of the Black Sea. Chemical Geology. 99, 1-27.

McArthur, J.A., and Herczeg, A., 1990. Diagenetic stability of the isotopic composition of phosphate oxygen: paleoenvironmental implications. In: Notholt, A.J.G., and Jarvis, I. (Eds.), Phosphorite Research and Development. The Geological Society Publishing House, Avon, 119-124.

McArthur, J.M., Coleman, M.L., and Bremner, J.M., 1980. Carbon and oxygen isotopic composition of structural carbonate in sedimentary francolite. Journal of the Geological Society of London. 137, 669-673.

McArthur, J.M., Benmore, R.A., Coleman, M.L., Soldi, C., Yeh, H.W., and O'Brien, G.W., 1986. Stable isotopes characterisation of francolite formation. Earth and Planetary Science Letters. 77, 20-34.

McCrea, J.M., 1950. On the isotopic chemistry of carbonates and a plaeotemperature scale. The Journal of Chemical Physics. 18, 849-857.

McManus, J., Berelson, W.M., Klinkhammer, G.P., Johnson, K.S., Coale, K.H., Anderson, R.F., Kumar, N., Burdige, D.J., Hammond, D.E., Brumsack, H.J., McCorkle, D.C., and Rushdi, A., 1998. Geochemistry of barium in marine sediments: implications for its use as a paleoproxy. Geochimica et Cosmochimica Acta. 62, 3453-3473.

Medrano, M.D., and Piper, D.Z., 1997. Fe-Ca-phosphate, Fe-silicate, and Mn-oxide minerals in concretions from the Monterey Formation. Chemical Geology, 138, 9-23.

Mulabisana, M.J., 1998. Petrographic evidence for the origin of phosphorite nodules from the western continental shelf of South Africa. B.Sc. thesis, University of Cape Town, Cape Town.

Pedersen, T.F., Vogel, J.S., and Southon, J.R., 1986. Copper and manganese in hemipelagic sediments at 21°N, East Pacific Rise: diagenetic contrasts. Geochimica et Cosmochimica Acta. 50, 2019-2031.

Pufahl, P.K., Grimm, K.A., Abed, A.M., and Sadaqah, R.M.Y., 2001, submitted. Upper Cretaceous (Campanian) phosphorites in Jordan: Implications for the formation of a south Tethyan phosphorite giant. Sedimentary Geology, 90p., 15 figures, 4 tables.

Rasmussen, H., and Jørgensen, B.B., 1992. Microelectrode studies of seasonal oxygen uptake in a coastal sediment: role of molecular diffusion. Marine Ecology Progress Series. 81, 289 -303.

Reimers, C.E., Kastner, M., and Garrison, R.E., 1990. The role of bacterial mats in phosphate mineralization with particular reference to the Monterey Formation. In: Burnett, W.C., and Riggs, S.R. (Eds.), Phosphate deposits of the world, Neogene to Modern phosphorites, IGCP, Project 156. Cambridge University Press, Cambridge.

Riggs, S., Stille, P., and Ames, D., 1997. Sr isotopic age analysis of co-occurring Miocene phosphate grain types on the north Carolina shelf. Journal of Sedimentary Research. 67, 65-73.

Schmitz, B., 1987. Barium, equatorial high productivity, and the northward wandering of the Indian continent. Paleoceanography. 2, 63-67.

Schuffert, J.D., Kastner, M., and Jahnke, R.A., 1998. Carbon and P burial associated with modern phosphorite formation. Marine Geology. 146, 21-31.

Shaffer, G., 1986. Phosphate pumps in the Black Sea. Nature. 321, 515-517.

Sheldon, R.P., 1980. Episodicity of phosphate deposition and deep ocean circulation – a hypothesis. In: Bentor, Y.K. (Eds.), Marine Phosphorites - Geochemistry, Occurrence, Genesis. Society of Economic Paleontologists and Mineralogists, 239-247.

Shemesh, A., Kolodny, Y., and Luz, B., 1983. Oxygen isotope variations in phosphate of biogenic apatites, II. Phosphorite rocks. Earth and Planetary Science Letters. 64, 405 -416.

Silverman, S.R., Fugat, R., and Weiser, J.D., 1952. Quantitative determination of calcite associated with carbonate-bearing apatite. American Mineralogist. 37, 211-222.

Soudry, D., and Southgate, P.N., 1989. Ultrastructure of a middle Cambrian Primary nonpelletal phosphorite and its early transformation into phosphate vadoids: Georgina Basin, Australia. Journal of Sedimentary Petrology. 59, 53-64.

Sturesson, U., 1986. Lower Ordovician ooids from northern Öland, Sweden. Geologiska Föreningens i Stockholm Förhandlingar. 108, 331-348.

Sturesson, U., 1988. Ooids and oncoids in a Middle Cambrian sandstone from Närke, Sweden. Geologiska Föreningens i Stockholm Förhandlingar. 110, 143-155.

Sturesson, U., 1989. Coated grains in Lower Viruan limestones in Västergöland, central Sweden. Geologiska Föreningens i Stockholm Förhandlingar. 111, 273-284.

Sturesson, U., 1992. The lower-middle Ordovician transition in south central Sweden: phosphorite and iron ooid formation induced by volcanic ash. Geologiska Föreningens i Stockholm Förhandlingar. 114, 431-445.

Struresson, U., Heikoop, J.M., and Risk, M.J., 2000. Modern and Paleozoic iron ooids; a similar volcanic origin. Sedimentary Geology. 136, 137-146.

Suess, E., 1981. Phosphate regeneration from sediments of the Peru continental margin by dissolution of fish debris. Geochimica et Cosmochimica Acta. 45, 577-588.

Swett, K., and Crowder, K., 1982. Primary phosphatic oolites from the lower Cambrian of Spitsbergen. Journal of Sedimentary Petrology. 52, 587-593.

Swirydczuk, K., Wilkinson, B.H., and Smith, G.R., 1981. Synsedimentary lacustrine phosphorites from the Pliocene Glenns Ferry Formation of southwestern Idaho. Journal of Sedimentary Petrology. 51, 1205-1214.

Thamdrup, B., Fossing, H., and Jorgensen, B.B., 1994. Manganese, iron, and sulfur cycling in a coastal marine sediment, Aarhus Bay, Denmark. Geochimica et Cosmochimica Acta. 58, 5115-5129.

Torres, M.E., Brumsack, H.J., Bohrmann, G., Emeis, K.C., 1996. Barite fronts in continental margin sediments: A new look at barium remobilization in the zone of sulfate reduction and formation of heavy barites in diagenetic fronts. Chemical Geology. 127, 125-139.

van Os, B.M., J.J., and de Lange, G.J., 1993. Possible diagenetic mobilization of barium in sapropelic sediments from the eastern Mediterranean. In: van Os, B. (Eds.), Primary and diagenetic signals in Mediterranean sapropels and north Atlantic turbidites. Origin and fate of trace metals and palaeo-proxies. , Utrecht, 13-32.

CHAPTER 4

Mg/Ca AND Sr/Ca RATIOS IN OYSTER CALCITE AS PALEOTEMPERATURE AND SALINITY PROXIES

4.1 ABSTRACT

Trace element (Mg and Sr) concentrations were determined in sclerochronological profiles through several shells of the modern oyster *Crassostrea gigas* from coastal British Colombia, and compared to the trace element chemistry of Cretaceous *Oscillopha figari* from Jordan. Trends in trace element data from *C. gigas* do not clearly correlate with temporal changes in sea water salinity and temperature. The lack of consistent relationships between trace metal and environmental data may reflect the fact that oysters do not form continuous growth laminae, and/or is a result of poor sampling resolution across sclerochronological profiles. Scattergrams comparing Mg and Sr suggest that the partitioning of these trace elements in *C. gigas* is controlled by growth rate. In slow growing oysters vital effects appear to govern the relative abundance of Mg and Sr within the shell, whereas the distribution of these elements in fast growing oysters is kinetically controlled.

Comparison of the trace element chemistry of *C. gigas* and fossil *O. figari* is equivocal, and suffers from the lack of a concrete understanding of how environmental and metabolic processes affect oyster shell chemistry, and uncertainty in the effects of diagenesis on the distribution of trace elements in biogenic carbonates. In spite of these uncertainties, such a comparison suggests that *O. figari* grew at rapid rates at sea water temperatures below 15°C. Sedimentologic data support this interpretation and indicate that Cretaceous oyster buildups in Jordan developed on a highly productive epeiric platform that underwent periods of intense upwelling.

The lack of significant correlations between skeletal Mg and Sr to environmental parameters suggests that the trace element chemistry of oyster shells may not be suitable for paleoenvironmental analysis. The relative abundances of Mg and Sr cannot be related to a single environmental parameter, and are more likely the result of a combination of environmental and physiologic variables. Future sclerochronological studies should include oysters from

Gryphaeidae in order to permit the comparison of trace metal data between families. Such a study may illuminate further the factors that control the concentration of Mg and Sr in oysters, and give more credibility to comparing trace element data from modern and ancient oyster species. The effects of diagenesis on the distribution of Mg and Sr in *O. figari* also require further investigation so that more meaningful interpretations of the trace element chemistry of ancient oysters can be made.

4.2 INTRODUCTION

The trace element compositions of skeletal carbonate of marine and fresh water molluscs have been the subject of numerous paleoenvironmental studies (e.g. Chave, 1954; Dodd, 1965; Lerman, 1965; Rossenberg and Hughes, 1991; Klein et al., 1996a,b, 1997; Stueber, 1998; Leng and Pearce, 1999; Purton et al., 1999). In bivalves, trace element distributions may provide a proxy for changes in salinity, temperature, and productivity. Environmental parameters may also be reconstructed from the $\delta^{18}O$ and $\delta^{13}C$ of fossil bivalves, but such data suffer from vital effects and uncertainties in the isotopic composition of the seawater from which the shell precipitated (Wefer and Berger, 1991; Corfield, 1995). However, trace element chemistry is supposedly more robust for paleoenvironmental analysis because individual trace elements have been shown to be a proxy for a single environmental factor and are thought to be less affected by metabolic processes (Chave, 1954; Dodd, 1967; Klein et al., 1996a,b; 1997).

The primary purpose of this paper is to study the variation in skeletal Mg and Sr in the modern oyster *Crassostrea gigas* from the coastal waters of British Colombia (Fig. 4.1) to investigate the sensitivity of this organism as an environmental indicator. Besides Ca, Mg and Sr are the major trace elements occurring in calcareous organisms (Walls et al., 1977) and their concentrations are known to be influenced by salinity and temperature (Rucker and Valentine, 1961; Eisma et al., 1976; Dodd, 1967; Dodd and Crisp, 1982; Morrison and Brand, 1986; Klein

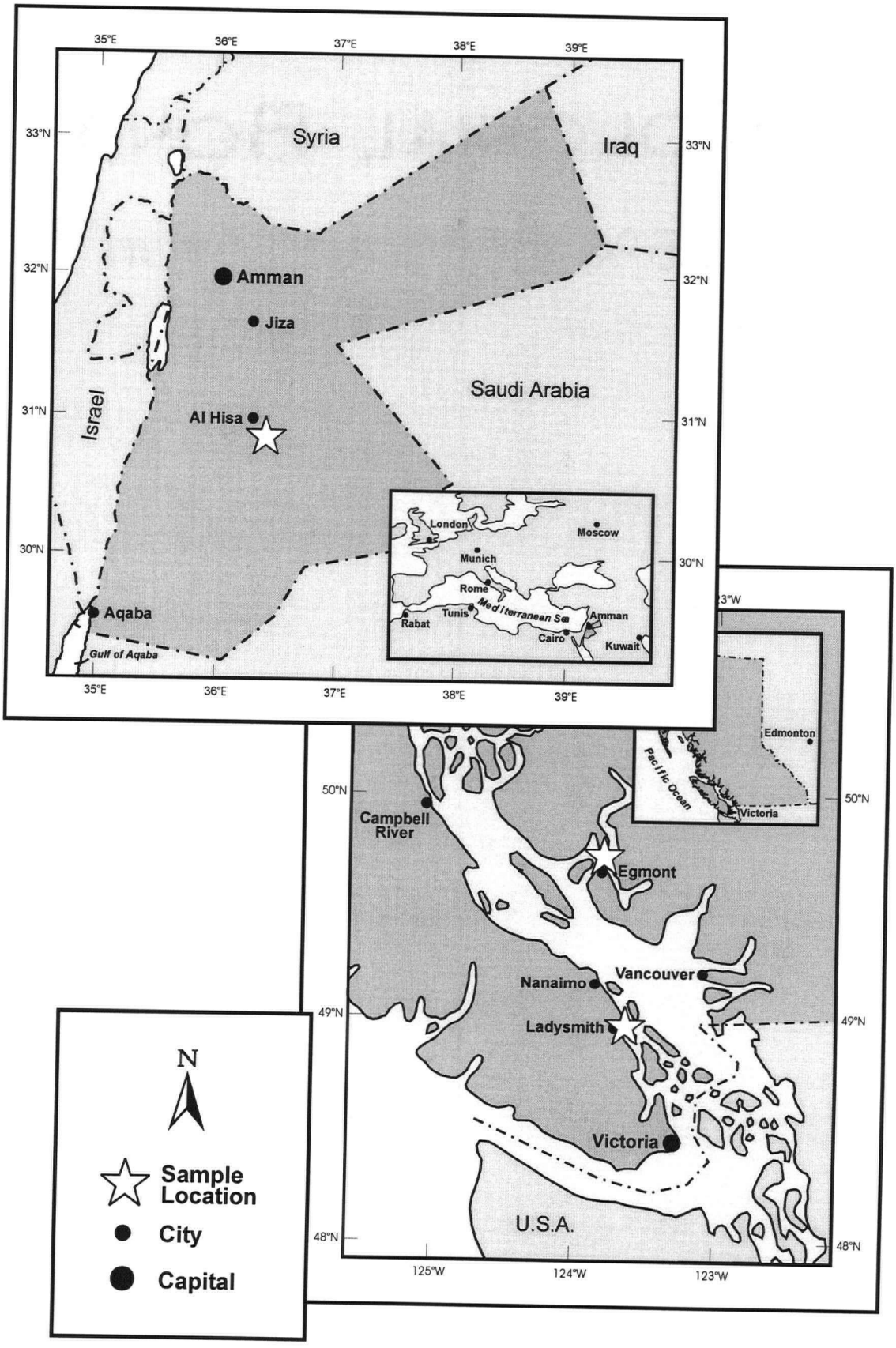

Figure 4.1 Maps of Jordan and southwestern British Columbia showing sample locations.

et al., 1996a,b, 1997). Oysters have great potential as environmental indicators because they are highly adaptable to a range of seawater conditions and thrive in marginal marine settings with widely fluctuating salinities and temperatures (Stenzel, 1971; Britton and Morton, 1989). Only one other study has evaluated the utility of using the trace metal geochemistry of oyster shells to proxy environmental conditions (Lerman, 1965). However, the present investigation is the first high resolution analysis of the trace metal content of modern and ancient oyster calcite in sclerochronological profile.

A secondary focus is to use these data as a baseline on which to interpret the Mg and Sr composition of fossil Cretaceous *Oscillopha figari* from Jordan (Fig. 4.1). *O. figari* together with *Ambigostrea villei* form large (~10 m in height x several kms), laterally extensive oyster banks in southern and central Jordan (Pufahl et al., 2001). The purpose of this work is to elucidate the salinity and temperature regimes that governed bank development and to gain a better understanding of the paleoenvironmental factors that led to the formation of economic phosphorite in Jordan.

4.3 EXPERIMENTAL

4.3.1 Collection of samples and environment

C. gigas samples were provided by Limberis Sea Products of Ladysmith, British Colombia, and Pearl Sea Products of Sechelt, British Colombia (Fig. 4.2A). Specimens supplied by Limberis Sea Products were introduced to Ladysmith Harbour as veliger larvae in June 1998 and allowed to set on artificial reefs composed of oyster shell debris. Some uncertainty surrounds their exact age because a few oysters may have set naturally. Oysters were emergent twice daily at low tide and ranged in length from 10.5 to 13.5 cm at the time of harvesting in October, 2000. Oysters provided by Pearl Sea Products were raised in a FLUPSY nursery system (Floating Upwelling System) (Manders, 2001, written comm.) while in their larval stage

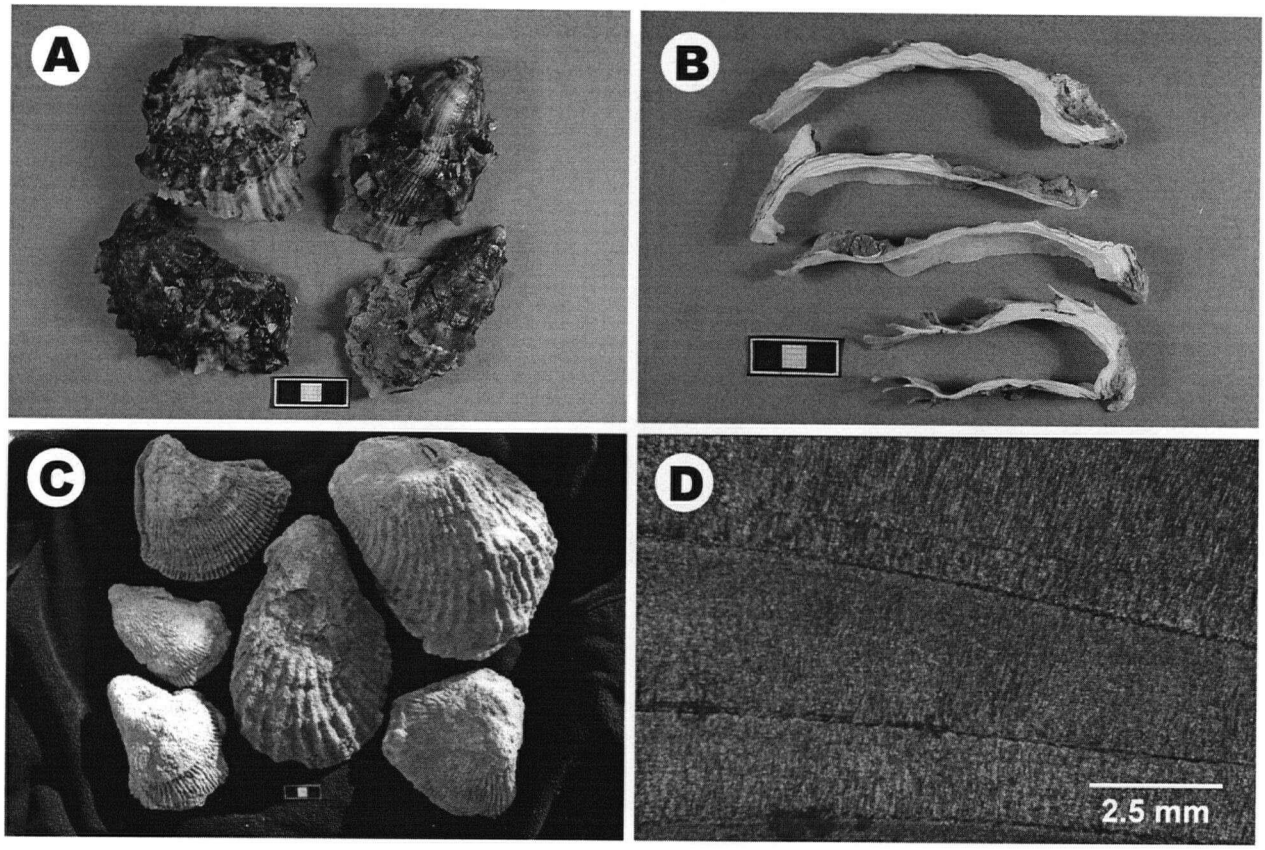

Figure 4.2 A) Recent *Crassostrea gigas* used in this study. B) *C. gigas* shells cut perpendicular to the hinge axis for sampling of calcitic growth laminae. C) Campanian *Oscillopha figari* and *Ambigostrea villei* from Jordan. The large specimens in the centre and upper right of the photo are *O. figari*. D) Transmitted light photomicrograph of unrecrystallized *O. figari* showing simply foliated shell structure.

before they were placed in rafts of floating trays for continued grow-out within Jervis Inlet, British Colombia, in June of 1999. This method of oyster culturing suspends the animal at a water depth of approximately 1m and maintains them in the productive surface waters, producing an animal that grows significantly quicker with a softer, more delicate shell than oysters that are emergent at low tide. Growth rates for *C. gigas* from Ladysmith Harbour averaged 4.4 mm/month while those from Jervis inlet averaged 6.1 mm/month (~39% faster). Maximum shell growth rates occur in the summer months when primary productivity is highest and water temperatures are the warmest (Stenzel, 1971; Manders, 2000, written comm.). At harvest in October of 2000 oysters from Jervis Inlet ranged in length from 8.5 to 10.5cm. *C. gigas* shells used in this study are appreciably thinner than those of *O. figari*. Individual valves range in thickness from 1 to 2 mm at the ventral margin to a maximum of 5 to 10 mm in the hinge area. Five of the thickest-shelled specimens were selected from each locality for trace element analysis.

Water temperature and salinity varied significantly during the life span of the oysters. Temperatures ranged from 6.1°C in the winter to 24.1°C in the summer in Ladysmith Harbour, and from 5.1°C to 21.9°C in Jervis Inlet. Salinities were appreciably lower in the summer as a result of melting snow-pack from the surrounding mountains (Inglet, 2000, pers. comm.; Manders, 2000, pers. comm.). In Ladysmith Harbour salinities ranged from 21‰ to a winter high of 30‰, and from 14.1‰ to 30.8‰ in Jervis Inlet. During the summer months (June, July, and August) when oyster growth is at a maximum, the average water temperatures in Ladysmith Harbour and Jervis Inlet were 18.0°C and 18.4°C, respectively.

Fossil *O. figari* specimens were collected from oyster banks in central Jordan (Fig. 4.1). These buildups form the Bahiya Coquina member of the Alhisa Phosphorite Formation, an upper Campanian succession of interbedded phosphatic marls, granular phosphorites, and oyster coquinas (Pufahl et al., 2001). Stratigraphic and sedimentologic data indicate that oyster banks

developed on a carbonate-dominated epeiric platform along the South Tethyan margin. Oyster banks are composed predominantly of *Abigostrea villei* and consist of a basal bed of *highly fragmental oyster rudstone* overlain by a set of *megacrossbedded oyster rudstone* that is truncated at its top by a bed of *chalk-rich highly fragmental oyster rudstone* (see Chapter 2 for a complete description of these lithofacies). *O. figari* occur in life position along bank bases within the *highly fragmental oyster rudstone*. A total of twenty oyster valves were collected. Individual shells range in length from 16 to 30 cm and are 3 to 6 cm thick. *O. figari* are distinguished from other oyster species by their large, strongly ribbed valves (Fig. 4.2C) and their thick foliated growth laminae (Fig. 4.2D) (Aqrabawi, 1993).

4.3.2 Sample treatment and environmental data

C. gigas were sectioned radially through the hinge along the mid axis of the valves (parallel to the maximum growth direction) (Stenzel, 1971) (Fig 4.2B). The animals were first frozen to increase the rigidity of each specimen before sawing on a fine lapidary saw. The thin and fragile nature of the growth laminae precluded the use of a dental drill to extract samples. Instead, individual growth layers were separated in sectioned valves following the procedure of Nelson (1964). In this method samples are heated to 400°C for three to four hours to remove volatile organic matter. After this treatment 1 to 2 mm thick clusters of 2 to 3 shell laminae could be easily separated by careful use of a scalpel and tweezers, producing sample sizes that ranged between 4 to 35 mg. Sampling of the prismatic layer of *C. gigas* was concentrated in the hinge area where the shell is the thickest.

O. figari valves were also sectioned radially through the hinge along the mid axis. To evaluate diagenetic alteration polished thin sections of shells were studied using transmitted light microscopy and cathodoluminescence (CL). CL is an extremely sensitive to the presence of diagenetic Mn^{2+} (~700ppb) (Habermann et al., 1999). Replacement of Ca^{2+} in carbonates with

Mn^{2+}, a common trace metal in diagenetic fluids, causes the altered carbonate to luminesce (Machel et al., 1991). Following the protocol of Elorza and García-Garmilla (1998) five of the thickest unrecrystallized, non-luminescing shells were selected for trace element analysis. CL work was performed at Lakehead University using a Nuclide ELM-3R Luminiscope coupled to a SPEX 1681 Spectrophotometer operating at 20 mTorr with an excitation voltage of 10kV. Individual growth laminae within the prismatic layer of *O. figari* valves were drilled with a 0.2 mm tungsten dental burr, which permitted very small samples (8 to 15 mg) of calcite powder to be removed. Shell material from the first few revolutions of the drill bit were discarded to avoid contamination from sawing.

Samples were sequentially cleaned according to the methods of Hastings et al. (1998) in order to reduce contaminants that affect the trace metal composition of biogenic carbonates. Shell material was first rinsed with deionized water three times, pipetting out the rinse water and ultrasonicating for 2 minutes each time, to remove ashed organics and detrital clays caught between growth laminae. Samples were then cleaned in 1mL of 0.1N $NaOH/H_2O_2$ at 80 to 90°C for 30 minutes to remove residual organics, rinsed with deionized water three more times, and dried and weighed. For each sample, shell material was dissolved in 6.0 mL 0.3 N ultrapure nitric acid prepared with deionized water for determination of Ca, Mg, and Sr concentrations.

Trace metal concentrations were analyzed at Lakehead University using a Thermo Jarrell Ash ICAP 9000 inductively coupled plasma atomic emission spectrophotometer (ICP-AES) operating at 1300 watts RF (radio frequency). Detection limits for Ca, Mg, and Sr are 0.01, 0.01, and 0.02 ppm respectively. Analytical precision was better than ±2.4% for Ca, ±1.4% for Mg, and ±2.2% for Sr. Samples containing more than 15 mg of shell material were diluted prior to analysis to minimize matrix interferences and viscosity influences. All elemental ratios are reported in the text as molar ratios.

Seawater temperature and salinity were recorded on a daily basis from Ladysmith Harbour by personnel from Limberis Sea Products between June, 1998 and October, 2000 using a Fisher Scientific thermometer and refractometer. Environmental data were recorded on a weekly basis in Jervis Inlet by employees from Pearl Sea Products between June, 1999 and October, 2000 using a Hana HI 9050 thermometer and a Hana A366TC refractometer.

4.4 RESULTS AND DISCUSSION

The time series Mg/Ca and Sr/Ca are plotted against laminae number from the hinge area toward the ventral margin in Figures 4.3, 4.4, and 4.5. The distance of each sample from the hinge is related to time. Laminae 1 in Figures 3 and 4 roughly correlates to the time that the specimens were introduced into their respective environments and the highest laminae number is equivalent to the harvest time of each organism. The time of introduction and harvest of the oysters corresponds to the beginning and end of the time frames depicted on the plots of sea water salinity and temperature from Ladysmith Harbour and Jervis Inlet in Figures 4.3F and 4.4F.

In both *C. gigas* and *O. figari* the sclerochronological profiles of Mg/Ca and Sr/Ca ratios show that changes in the Mg and Sr contents of shells can covary nearly in phase with each other (Figs. 4.3B, 4.4B,D,E, and 4.5A), show no correlation (Fig. 4.3C,E and 4.5B,C,D), or exhibit a combination of the two (Figs. 4.3A,D and 4.4A,C). There appears to be no relationship between the Mg/Ca and Sr/Ca ratios in *C. gigas* and temperature or salinity except in two cases, samples L3 and E2 (Figs. 4.3D and 4.4C). The Mg/Ca curve for each of these samples shows a weak visual correlation with the seasonal fluctuation in sea water temperature of Ladysmith Harbour and Jervis Inlet (Figs 4.3F and 4. 4F). The three prominent peaks and troughs in the Mg/Ca profile of sample L3 appear to positively correlate with high summer and low winter temperatures in Ladysmith Harbour. The correlation in sample E2 is less striking but the same

Figure 4.3 Mg/Ca and Sr/Ca ratios across sclerochronological profiles of the hinge area of *C. gigas* from Ladysmith Harbour. An increase in laminae number corresponds with an increase in the age of the organism. A) Sample L1. B) Sample L2. C) Sample L3. D) Sample L4. E) Sample L5. F) Temperature and salinity data from Ladysmith Harbour for the life of the organism. Error bars are less than or equal to the width of individual data points.

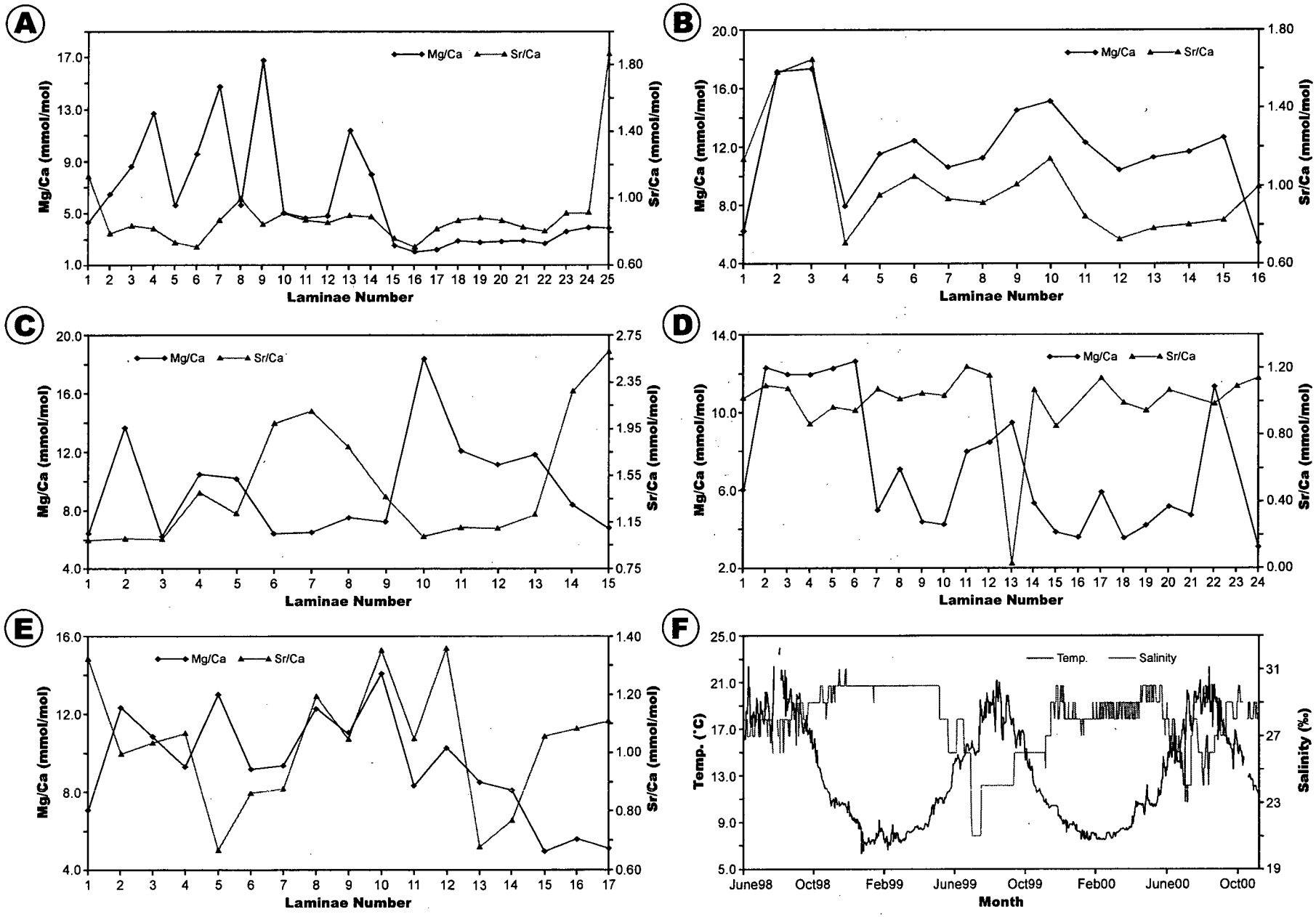
A
Mg/Ca
Sr/Ca
Mg/Ca (mmol/mol)
Sr/Ca (mmol/mol)
Laminae Number
B
Mg/Ca
Sr/Ca
Mg/Ca (mmol/mol)
Sr/Ca (mmol/mol)
Laminae Number
C
Mg/Ca
Sr/Ca
Mg/Ca (mmol/mol)
Sr/Ca (mmol/mol)
Laminae Number
D
Mg/Ca
Sr/Ca
Mg/Ca (mmol/mol)
Sr/Ca (mmol/mol)
Laminae Number
E
Mg/Ca
Sr/Ca
Mg/Ca (mmol/mol)
Sr/Ca (mmol/mol)
Laminae Number
F
Temp.
Salinity
Temp. (°C)
Salinity (‰)
June98
Oct98
Feb99
June99
Oct99
Feb00
June00
Oct00
Month

Figure 4.4 Mg/Ca and Sr/Ca ratios across sclerochronological profiles of the hinge area of *C. gigas* from Jervis Inlet. An increase in laminae number corresponds to an increase in the age of the organism. A) Sample E1. B) Sample E2. C) Sample L3. D) Sample L4. E) Sample L5. F) Temperature and salinity data from Jervis Inlet for the life of the organism. Error bars are less than or equal to the width of individual data points.

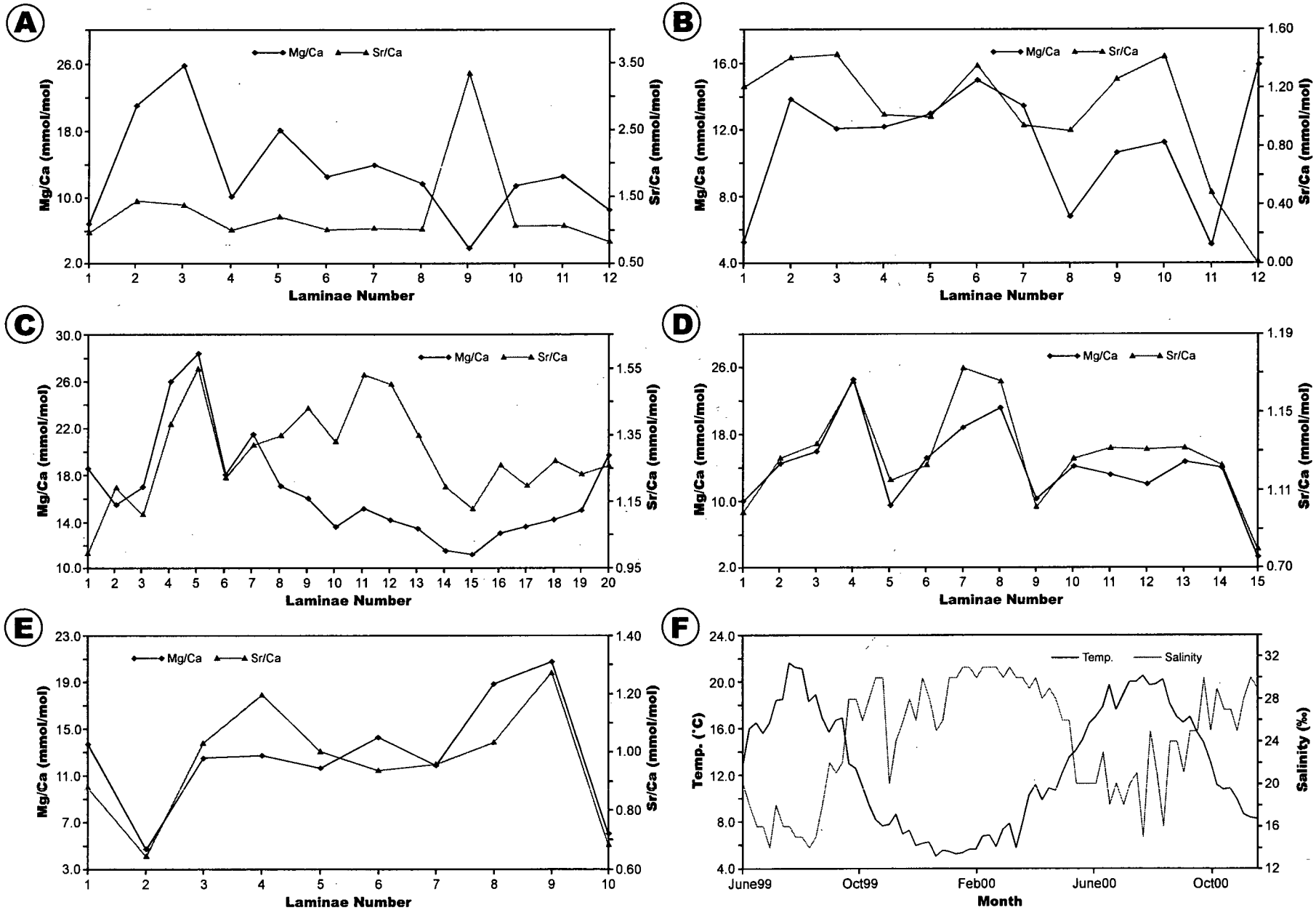
A
Mg/Ca
Sr/Ca
Mg/Ca (mmol/mol)
Sr/Ca (mmol/mol)
Laminae Number
B
Mg/Ca
Sr/Ca
Mg/Ca (mmol/mol)
Sr/Ca (mmol/mol)
Laminae Number
C
Mg/Ca
Sr/Ca
Mg/Ca (mmol/mol)
Sr/Ca (mmol/mol)
Laminae Number
D
Mg/Ca
Sr/Ca
Mg/Ca (mmol/mol)
Sr/Ca (mmol/mol)
Laminae Number
E
Mg/Ca
Sr/Ca
Mg/Ca (mmol/mol)
Sr/Ca (mmol/mol)
Laminae Number
F
Temp.
Salinity
Temp. (°C)
Salinity (‰)
June99
Oct99
Feb00
June00
Oct00
Month

Figure 4.5 Mg/Ca and Sr/Ca ratios across sclerochronological profiles of *O. figari* from the Cretaceous of Jordan. An increase in laminae number corresponds with an increase in the age of the organism. A) Sample J1. B) Sample J2. C) Sample J3. D) Sample J4. Error bars are less than or equal to width of individual data points.

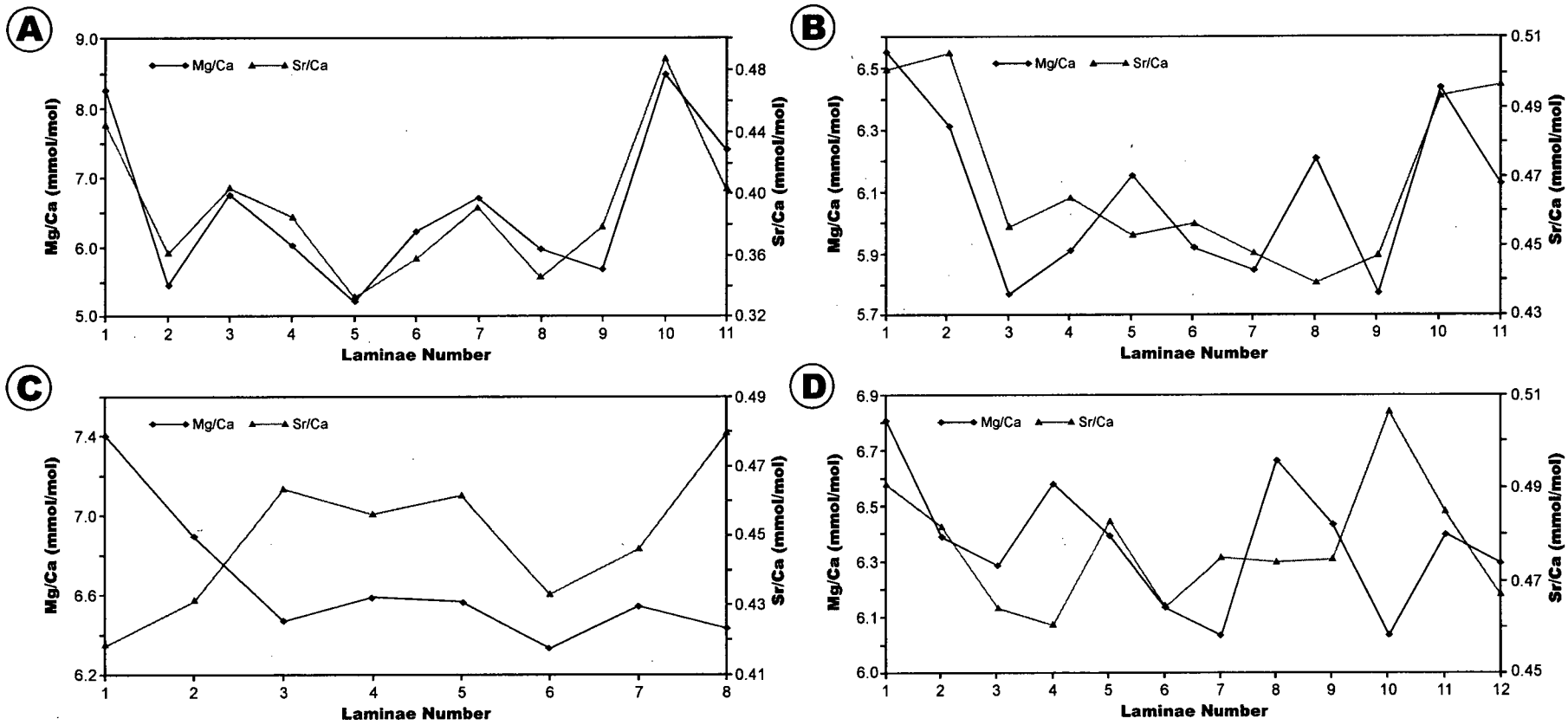
A
Mg/Ca
Sr/Ca
Mg/Ca (mmol/mol)
Sr/Ca (mmol/mol)
Laminae Number
B
Mg/Ca
Sr/Ca
Mg/Ca (mmol/mol)
Sr/Ca (mmol/mol)
Laminae Number
C
Mg/Ca
Sr/Ca
Mg/Ca (mmol/mol)
Sr/Ca (mmol/mol)
Laminae Number
D
Mg/Ca
Sr/Ca
Mg/Ca (mmol/mol)
Sr/Ca (mmol/mol)
Laminae Number

relationship seems to exist. The peak in the Mg/Ca curve may correspond to summer seawater temperatures and the trough might record seasonal lows in temperature during the winter of 1999. Sr/Ca ratios show no relationship to either sea water temperature or salinity in each of these samples.

The apparent absence of meaningful correlations between the Mg and Sr content and seawater salinity/temperature may reflect the fact that oysters, unlike other bivalves, do not form easily discernable continuous growth laminae within their shells (Kirby et al., 1998). Oysters precipitate calcite irregularly from the extrapallial fluid between the mantle and shell, producing growth laminae that pinch and swell throughout the thickness of the valve (Stenzel, 1971). The lack of correlation between the trace metal and environmental data may also be an artefact of poor sampling resolution within the shell. Although the utmost care was taken to ensure that the sclerochronological record produced was of the highest possible temporal resolution, the sampling technique did not permit the extraction of individual growth laminae under 1mm in thickness. Samples consisting of more than one lamina may have produced Mg/Ca and Sr/Ca ratios that are homogenized, and record a range of temperatures and salinities, thus obscuring prominent trends in the data.

Insight into the constraints on the Mg and Sr contents in *C. gigas* are provided when these two trace metals are compared (Fig. 4.6). Figure 4.6A is a plot of Sr/Ca vs. Mg/Ca for *C. gigas* from Ladysmith Harbour. Mg/Ca ratios of these shells vary between 2.0 and 18.0 mmol/mol and average 8.4 mmol/mol. Sr/Ca ratios range from 0.7 to 2.6 mmol/mol and average 1.05 mmol/mol. As the plot shows there is no correlation between Mg and Sr ($r^2 = 0.002$) suggesting that the incorporation of these two trace metals into the oyster shells from Ladysmith Harbour is governed by different processes. The position of the six data points above, and one below the cluster in the central region of the scattergram, are not readily explained. The laminae from which these outliers are derived are macroscopically identical in every respect to the other

Figure 4.6 A) Sr/Ca vs. Mg/Ca for *C. gigas* from Ladysmith Harbour. B) Sr/Ca vs. Mg/Ca for *A. villei* from Jervis Inlet. C) Sr/Ca vs. Mg/Ca for *O. figari* from Jordan. Numbers next to data points correspond to sample numbers of growth laminae from individual shells. Error bars are less than or equal to the width of individual data points.

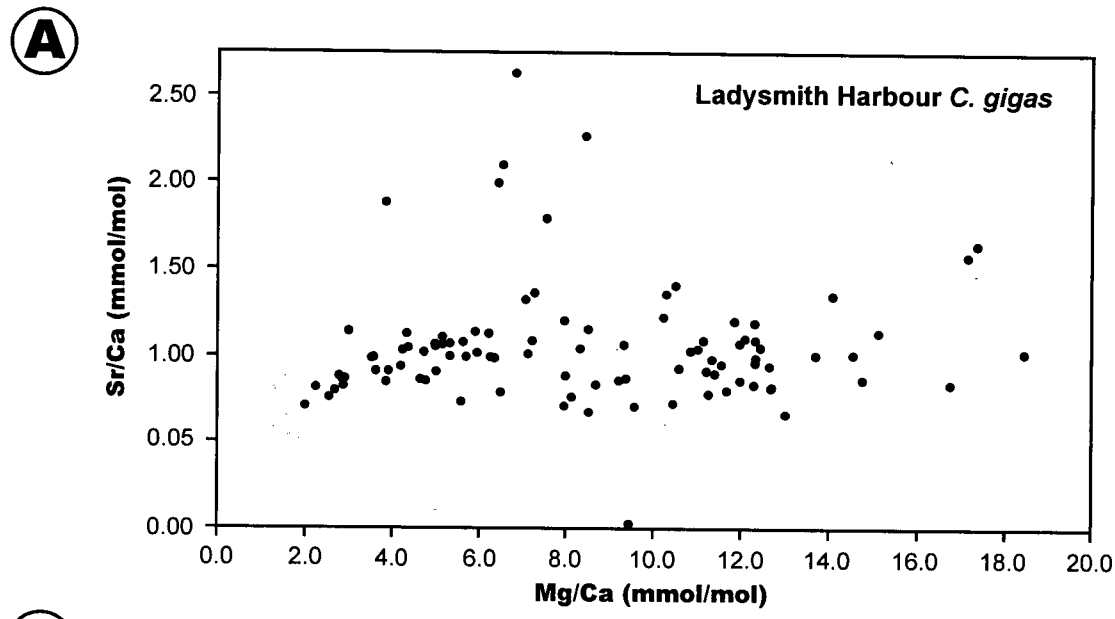
A
Ladysmith Harbour C. gigas
Sr/Ca (mmol/mol)
Mg/Ca (mmol/mol)
0.00
0.05
1.00
1.50
2.00
2.50
0.0
2.0
4.0
6.0
8.0
10.0
12.0
14.0
16.0
18.0
20.0

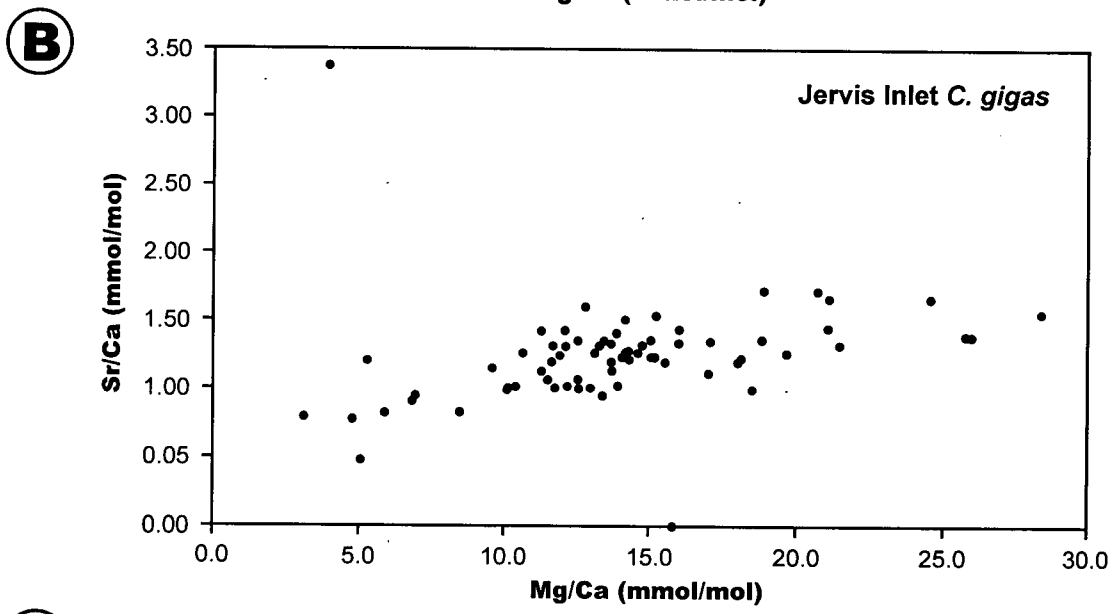
B
Jervis Inlet C. gigas
Sr/Ca (mmol/mol)
Mg/Ca (mmol/mol)
0.00
0.05
1.00
1.50
2.00
2.50
3.00
3.50
0.0
5.0
10.0
15.0
20.0
25.0
30.0

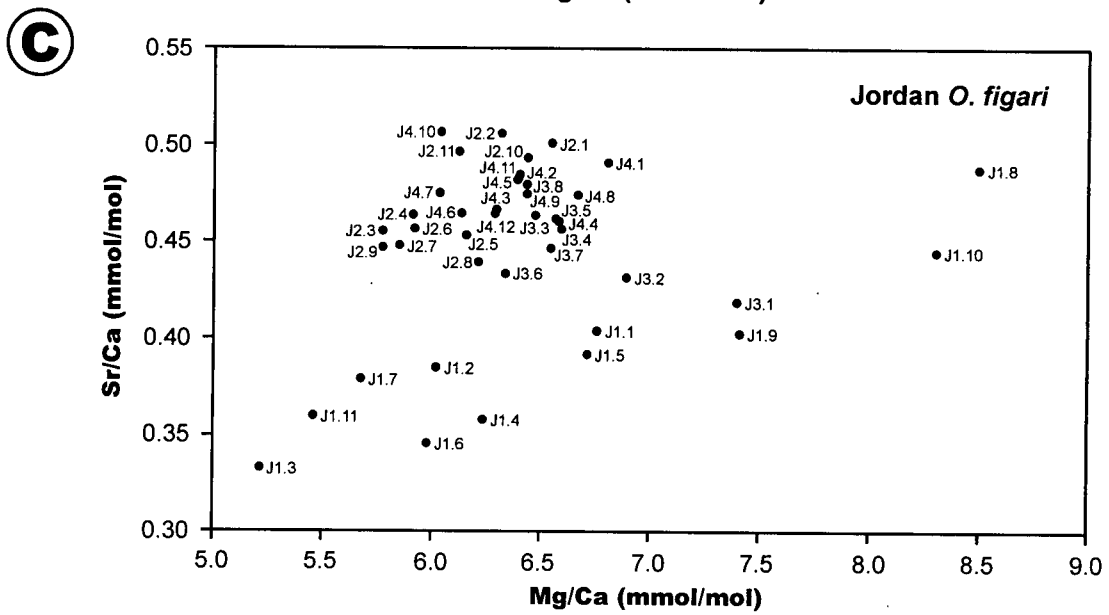
C
Jordan O. figari
Sr/Ca (mmol/mol)
Mg/Ca (mmol/mol)
0.30
0.35
0.40
0.45
0.50
0.55
5.0
5.5
6.0
6.5
7.0
7.5
8.0
8.5
9.0
J4.10
J2.2
J2.1
J2.11
J2.10
J4.1
J4.11
J4.2
J4.5
J3.8
J1.8
J4.7
J4.3
J4.9
J4.8
J2.4
J4.6
J3.5
J2.3
J2.6
J4.12
J3.3
J4.4
J3.4
J2.9
J2.7
J2.5
J3.7
J1.10
J2.8
J3.6
J3.2
J3.1
J1.1
J1.9
J1.5
J1.2
J1.7
J1.11
J1.4
J1.6
J1.3

laminae extracted from specimens of *C. gigas* from Ladysmith Harbour for trace element analysis. As the data set was collected from modern oysters the observed distribution of these seven points cannot be a result of diagenesis. It is more likely that the position of these data points is a result of experimental error and/or vital effects.

Figure 4.6B is the same type of plot for oysters from Jervis Inlet. Mg/Ca and Sr/Ca ratios for these shells range from 4.0 up to 28.0 mmol/mol, and 0.00 to 3.40 mmol/mol, and average 13.9 mmol/mol and 1.2 mmol/mol, respectively. However, unlike Figure 4.6A, this plot shows a very weak positive correlation between Mg and Sr ($r^2 = 0.051$) suggesting that the distribution of these elements within the shell may be controlled by a common process or set of processes. Like the outliers in Fig. 4.6B, the two data points that do not plot within this trend cannot be readily explained, but given their extreme position it is possible that these values are a result of errors introduced during data collection, and when removed from the data set an r^2 value of 0.461 is obtained.

I hypothesize that this apparently conflicting result between oysters from Ladysmith Harbour and Jervis Inlet may record the disparity in growth rate between these two populations. This interpretation is consistent with the findings of earlier studies that demonstrate high growth rates produce skeletal Mg/Ca and Sr/Ca ratios that co-vary and are higher than Mg/Ca and Sr/Ca ratios from slowly growing bivalves (Lorens, 1981; Carpenter and Lohmann, 1992; Klein et al., 1996a; Lorens, 1981). Klein et al. (1996a) have demonstrated that the variations in the Sr/Ca ratio within the mussel *Mytilus edulis* is a function of changes in the metabolic activity of the mantle. The mantle is the organ responsible for shell formation, which precipitates in the extrapallial fluids in the region between the mantle and the forming valve (Stenzel, 1971). They attribute lower Sr/Ca ratios observed in slow growing *M. edulis* to record more efficient pumping of Ca from the mantle into the extrapallial fluids where shell secretion occurs, whereas the valves of fast growing mussels are thought to have higher Sr concentrations because mantle pumping of

Ca is less efficient at high growth rates. Rosenberg and Hughes (1991) have documented a similar inverse relationship between skeletal Mg content and metabolic activity in *M. edulis*. With increasing growth rate, less time is available for the metabolic partitioning of shell-forming components (Mg, Sr, and Ca) (Dodd, 1967), and Mg and Sr concentrations increase linearly with precipitation rate as more of these trace elements are trapped in the crystal lattice of the developing shell (Lorens, 1981; Carpenter and Lohmann, 1992). These data suggest that the positive linear co-variation of Mg and Sr observed in rapidly growing *C. gigas* is kinetically controlled, and that Ca-pumping is not important in governing the skeletal trace element chemistry of oysters at high growth rates.

Figure 4.6C is a plot of Mg/Ca and Sr/Ca for *O. figari*. The numbers next to data points refer to sample numbers in Appendix 1. Mg/Ca and Sr/Ca ratios of these shells are appreciably lower than those from *C. gigas*. Mg/Ca ratios vary from 5.2 to 8.4 mmol/mol, and Sr/Ca ratios range between 0.33 to 0.50 mmol/mol. Average values for Mg/Ca and Sr/Ca ratios are 6.4 mmol/mol and 0.45 mmol/mol respectively. As the scattergram illustrates the data fall into two groups. The first group defines a linear trend showing a positive correlation between Mg and Sr and consists of all samples from oyster J1 and two samples from J3 ($r^2 = 0.547$). The second group contains a cluster of data points that lie above the linear trend of the first group. The positive correlation between Mg and Sr in the first group may record a primary trace element signature and the cluster of data points above this group may reflect diagenetic remobilization of trace elements. The degree of variance in the data from *C. gigas* shows that oysters incorporate Mg and Sr over a range of concentrations that in some cases is positively correlated (Figure 4.6B). I thus speculate that the linear trend defined by data points from samples J1 and J3 may record a primary trace metal signature, and the cluster of data points might record diagenetic equilibration with pore waters during sub-sea diagenesis. Krinsley and Bieri (1959) have shown that early diagenesis in the marine realm leads to an increase in the skeletal trace element content

as the shell equilibrates with seawater trapped within the pore spaces. This is contrary to the effects of meteoric diagenesis which tends to deplete Mg and Sr from biogenic carbonates through the diffusive flux of these trace elements into pore waters (Walls et al., 1977).

This interpretation is highly speculative and warrants further investigation. A logical next step would be to analyse the trace element content of visibly recrystallized shell material and plot these data on the scattergram in Figure 4.6C to see if these data do in fact record diagenesis. If the trace element data from *O. figari* do in fact indicate sub-sea diagenesis then these findings are consistent with other trace metal and stable isotope investigations of fossil molluscs that demonstrate the preservation of the original shell microstructure does not preclude diagenetic alteration of its isotopic and trace metal composition (e.g. Land, 1967; Stueber, 1998).

Figure 4.7 is a composite plot incorporating all trace metal data and includes Lerman's (1965) Mg and Sr data from *Crassostrea virginica* and *Crassostrea rhyzophorae*. Lerman investigated the temperature dependent incorporation of Mg and Sr using bulk samples of *Crassostrea virginica* from a number of localities along the eastern seaboard of the United States and Puerto Rico. Lerman demonstrated that the incorporation of Sr and Mg in *C. virginica* and *C. rhyzophorae* is to some degree temperature dependent. The numbers next to his data points correspond to average summer sea water temperatures during one summer of growth of his specimens. Lerman's data have been contoured to provide crude temperature fields in order to make comparisons between data sets easier. Like the Mg/Ca and Sr/Ca ratios from *C. gigas* from Ladysmith Harbour, there is no visible correlation between Mg and Sr in Lerman's data, which suggests that a factor other than temperature influences the trace element chemistry in *Crassostrea*. Nevertheless, Lerman's data do provide a useful benchmark for comparison. The samples of *C. gigas* from Ladysmith Harbour all plot within the same region as Lerman's specimens suggesting that non-equilibrium precipitation of oyster calcite is the norm. There is

Figure 4.7 Composite Sr/Ca vs. Mg/Ca for populations of both *C. gigas* and *O. figari*. Contours of sea water temperature are based on published Mg/Ca, Sr/Ca ratios from bulk *C. virginica* and *C. rhyzophorae* and corresponding temperature data (Lerman, 1965). The numbers next to individual data points correspond to average summer sea water temperatures during one summer of growth.

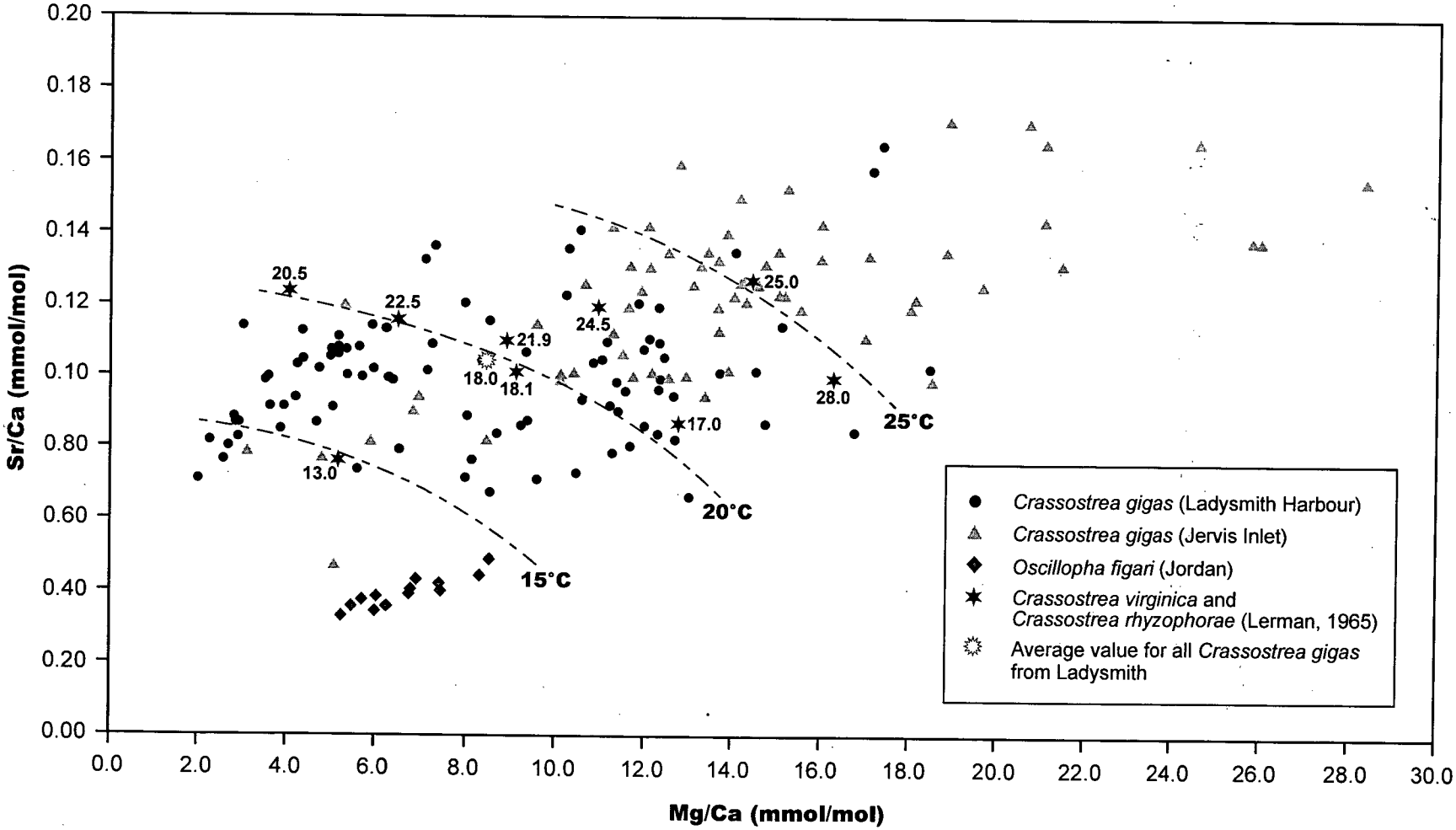
Sr/Ca (mmol/mol)
Mg/Ca (mmol/mol)
0.20
0.18
0.16
0.14
0.12
0.10
0.80
0.60
0.40
0.20
0.00
0.0
2.0
4.0
6.0
8.0
10.0
12.0
14.0
16.0
18.0
20.0
22.0
24.0
26.0
28.0
30.0
20.5
22.5
21.9
18.0
18.1
24.5
25.0
28.0
17.0
13.0
25°C
20°C
15°C
Crassostrea gigas (Ladysmith Harbour)
Crassostrea gigas (Jervis Inlet)
Oscillopha figari (Jordan)
Crassostrea virginica and Crassostrea rhyzophorae (Lerman, 1965)
Average value for all Crassostrea gigas from Ladysmith

also good agreement between Lerman's data and the average Mg/Ca and Sr/Ca ratios for all oyster samples from Ladysmith Harbour and the mean summer temperature of the sea water in which they grew. The Mg/Ca and Sr/Ca ratios average 8.4 mmol/mol and 1.05 mmol/mol, respectively, and the average summer temperature in Ladysmith Harbour was 18.0ºC. These data plot very close to Lerman's data point with a corresponding sea water temperature of 18.1ºC suggesting that temperature may play a minor role in partitioning Mg and Sr in *C. gigas* at slow growth rates.

The Mg/Ca and Sr/Ca ratios from *O. figari* samples J1 and J3 fall well below the data field defined by *C. gigas*, *C. virginica*, and *C. rhyzophorae*. If the trace element signature in sample J1 is a primary signature then the positive correlation between Mg and Sr may record rapid growth in sea water temperatures below 15ºC. Sedimentologic data support this interpretation and indicates that the development of oyster banks occurred on a productive epeiric platform that underwent periods of intense upwelling (Pufahl et al., 2001). An abundant food supply would promote rapid oyster growth that may result in a positive linear correlation between skeletal Mg and Sr, providing the relationship between growth rate and trace element content in *C. gigas* is also true for *O. figari*. Although this temperature range is quite low in relation to paleotemperatures (22 to 29ºC) derived from the analysis of oxygen isotope ratios in economic phosphorites from Israel (Kolodny and Garrison, 1994), sea water temperatures of 15ºC and less are not uncommon in upwelling areas (Matul, 1998; Prasada and Nelson, 1992; Prasada and Jayawardane, 1994).

The lack of significant correlations between Mg and Sr in *C. gigas* to environmental parameters precludes a more detailed discussion of their use as paleoenvironmental proxies here. Nevertheless, data presented in this paper do suggest that the trace element chemistry of oyster shells may not be suitable for paleoenvironmental analysis because the concentration of trace

metals cannot be related to a single environmental parameter, but are more likely a combination of environmental and physiological variables.

4.5 SUMMARY AND CONCLUSIONS

The trace element (Mg and Sr) concentrations were determined in sclerochronological profiles through several shells of the modern oyster *C. gigas* from coastal British Colombia, and compared to the trace element chemistry of Cretaceous *O. figari* from Jordan. These results were in turn compared to published trace metal data from modern *C. virginica* and *C. rhyzophorae*. The major findings are summarized below:

(1) Trends in Mg/Ca and Sr/Ca ratios in *C. gigas* do not correlate with seasonal changes in sea water salinity and temperature. The lack of any consistent relationship between Mg/Ca and Sr/Ca ratios and environmental data may reflect the fact that oysters do not form continuous growth laminae, and/or a result of poor sampling resolution across sclerochronological profiles. Nevertheless, the lack of correlation does suggest that the trace element chemistry of oyster shells may not be suitable for paleoenvironmental analysis.

(2) Scattergrams comparing Mg/Ca and Sr/Ca ratios suggest that the partitioning of trace elements in *C. gigas* may be controlled by growth rate. The lack of correlation between Mg and Sr in slow growing oysters is interpreted to record the effects of metabolic processes, such as mantle pumping of Ca, on the partitioning of these trace elements within the shell. A weak positive linear correlation between Mg and Sr in fast growing oysters is postulated to reflect a kinetic control on the skeletal abundances of these trace elements, and suggests that vital effects are not important in governing the trace element chemistry of oysters at high growth rates.

(3) Comparison of Mg/Ca and Sr/Ca ratios in macroscopically pristine *O. figari* suggest that at least some of the specimens record diagenetic alteration. If this interpretation is correct, then these findings are consistent with other trace metal and stable isotope investigations that

demonstrate the preservation of the original shell microstructure does not preclude diagenetic alteration of its isotopic and trace metal composition. The possibility of diagenetic alteration of "pristine looking" fossil invertebrate skeletons must therefore be taken into consideration and addressed when interpreting their chemistry.

(4) Comparison of Mg/Ca and Sr/Ca ratios of *C. gigas* from this study with published trace element data from *C. virginica* and *C. rhyzophorae* suggests that non-equilibrium precipitation in oyster calcite is the norm rather than the exception. A similar comparison between *C. gigas* and *O. figari* suggests that the trace element signature in unaltered *O. figari* valves records rapid growth in sea water temperatures below 15°C. Sedimentologic data support this interpretation and indicate that the development of oyster banks occurred on a highly productive epeiric platform that underwent periods of intense upwelling.

Although data presented in this paper suggest that the trace element chemistry of oyster shells may not be suitable for paleoenvironmental analysis, a number of interesting trends and relationships were discovered that warrant further investigation. Future work should implement the use of a microdrill (Dettman and Lohmann, 1995) to ensure that sclerochronological profiles are produced with the highest possible temporal resolution for correlation to environmental data. These investigations should also include oysters from *Gryphaeidae* in order to permit the comparison of trace elements data between families. Such a study may further illuminate the environmental factors controlling the trace element distribution in oysters and may give more credibility to comparing Mg and Sr concentrations between modern and ancient oyster species. The effects of diagenesis on trace elements in *O. figari* also require further investigation so that more meaningful interpretations of the trace element chemistry of ancient oysters can be made. These questions are the focus of my postdoctoral research that will be undertaken at Queen's University in the fall of 2001, under the direction of N.P. James.

4.6 REFERENCES CITED

Aqrabawi, M., 1993. Oysters (Bivalvia-Pteromorphia) of the Upper Cretaceous rocks of Jordan; paleontology, stratigraphy and comparison with upper Cretaceous oysters of Northwest Europe. Mitteillungen aus Geologisch-Palaeontologischen Institute der Universitat Hamburg. 75, 1-135.

Britton, J.C., and Morton, B., 1989. Shore ecology of the Gulf of Mexico, University of Texas Press, Austin, 381p.

Carpenter, S.J., and Lohmann, K.C., 1992. Sr/Mg ratios of modern marine calcite: Emperical indicators of ocean chemistry and precipitation rate. Geochimica et Cosmochimica Acta. 56, 1837-1849.

Chave, K.E., 1954. Aspects of the biochemistry of Magnesium 1.Calcareous Marine organisms. Journal of Geology. 62, 266-283.

Corfield, R.M., 1995. An introduction to the techniques, limitations and landmarks of carbonate oxygen isotope palaeothermometry. In: Bosence, D.W., and Allison, P.A. (Eds.), Marine paleoenvironmental Analysis from fossils. Geological Society Special Publication No.83, 27-42.

Dettman, D.L., and Lohmann, K.C., 1995. Microsampling carbonates for stable isotope and minor element analysis: Physical separation of samples on a 20 micrometer scale. Journal of Sedimentary Research. 65, 566-569.

Dodd, J.R., 1965. Environmental control of Strontium and magnesium in *Mytilus**. Geochimica et Cosmochimica Acta. 29, 385-398.

Dodd, J.R., and Crisp, E.L., 1982. Non-linear variation with salinity of Sr/Ca and Mg/Ca ratios in water and aragonitic bivalve shells and implications for paleosalinity studies. Palaeogeography, Palaeoclimatology, Palaeoecology. 38, 45-56.

Dodd, R.J., 1967. Magnesium and strontium in calcareous skeletons: A review. Journal of Paleontology. 41, 1313-1329.

Eisma, D., Mook, W.G., and Das, H.A., 1976. Shell characteristics, isotopic composition and trace-element contents of some euryhaline molluscs as indicators of salinity. Palaeogeography, Palaeoclimatology, Palaeoecology. 19, 39-62.

Elorza, J., and Garcia-Garmilla, F., 1998. Palaeoenvironmental implications and diagenesis of inoceramid shells (Bivalvia) in the mid-Maastrichtian beds of the Sopelana, Zumaya and Bidart sections (coast of the Bay of Biscay, Basque Country). Palaeogeography, Palaeoclimatology, Palaeoecology. 141, 303-328.

Habermann, D., Neuser, R.D>, and Richter, D.K., 1998. Low limit of Mn^{2+} activated cathodoluminescence of calcite: state of the art. Sedimentary Geology. 116, 13-24.

Hastings, D.W., Russell, A.D., and Emerson, S.R., 1998. Foraminferal magnesium in Globeriginoides sacculifer as a paleotemperature proxy. Paleoceanography. 13, 161-169.

Kirby, M.X., Soniat, T.M., and Spero, H.J., 1998. Stable isotope sclerochronology of Pleistocene and Recent oyster shells (*Crassostrea virginica*). Palaios. 13, 560-569.

Klein, R.T., Lohmann, K.C., and Thayer, C.W., 1996a. Sr/Ca and $^{13}C/^{12}C$ ratios in skeletal calcite of *Mytilus trossulus:* Covariation with metabolic rate, salinity, and carbon isotopic composition of seawater. Geochimica et Cosmochimica Acta. 60, 4207-4221.

Klein, R.T., Lohmann, K.C., and Thayer, C.W., 1996b. Bivalve skeletons record sea-surface temperature and ^{18}O via Mg/Ca and $^{18}O/^{16}O$ ratios. Geology. 24, 415-418.

Klein, R.T., Lohmann, K.C., and Kennedy, G.L., 1997. Elemental isotopic proxies of paleotemperature and paleosalinity: Climate reconstruction of the marginal northeast Pacific ca. 80Ka. Geology. 25, 363-366.

Kolodny, Y., and Garrison, R.E., 1994. Sedimentation and diagenesis in paleoupwelling zones of epeiric sea and basinal settings: A comparison of the Cretaceous Mishash Formation of Israel and the Miocene Monterey Formation of California: 29th International Geological Congress. VSP, Utrecht, 133-158.

Krinsley, D.A.B., 1959. Changes in the chemical composition of pteropod shells after the deposition on the sea floor. Journal of Paleontology. 33, 682-684.

Land, L.S., 1967. Diagenesis of skeletal carbonates. Journal of Sedimentary Petrology. 37, 914 -930.

Leng, M.J., and Pearce, N.J.G., 1999. Seasonal variation of trace element and isotopic composition in the shell of a costal mollusk, *Mactra isabelleana*. Journal of Shellfish Research. 18, 569-574.

Lerman, A., 1965. Strontium and magnesium in water and in Crassostrea calcite. Science. 150, 745-751.

Machel, H.G., Mason, R.A., Mariano, A.N., Mucci, A., 1991. Causes and emission of luminescence in calcite and dolomite. In: Barker, C.E., and Kopp, C. (Eds.), Luminescence microscopy and spectroscopy: Qualitative and quantitative applications. Society for Sedimentary Geology, Tulsa, 9-26.

Matul, A.G., 1998. On the radiolaria from the surface layer of the bottom sediments of the northeastern sector of the Benguela upwelling. Oceanology. 38, 687-692.

Prasada, R.C., and Nelson, C.S., 1992. Oxygen and carbon isotope fields for temperate shelf carbonates from Tasmania and New Zealand. Marine Geology. 103, 253-268.

Prasada, R.C., and Jayawardane, M.P.J., 1994. Major minerals, elemental and isotopic composition in modern temperate shelf carbonates, eastern Tasmania, Australia;

implications for the occurrence of extensive ancient non-tropical carbonates. Palaeogeography, Palaeoclimatology, Palaeoecology. 107, 49-63.

Pufahl, P.K., Grimm, K.A., Abed, A.M., and Sadaqah, R.M.Y., submitted. Upper Cretaceous (Campanian) phosphorites in Jordan: Implications for the formation of a south Tethyan phosphorite giant.

Purton, L.M.A., Shields, G.A., Brasier, M.D., and Grime, G.W., 1999. Metabolism controls Sr/Ca in fossil aragonitic mollusks. Geology. 27, 1083-1086.

Rosenburg, G.D., and Hughes, W., 1991. A metabolic model for the determination of shell composition in the bivalve mollusc, *Mytilus edulis*. Lethaia. 24, 83-96.

Rucker, J.B., and Valentine, J.W., 1961. Salinity response of trace element concentration in *Crassostrea virginica*. Nature. 190, 1099-1101.

Stenzel, H.B., 1971, Oysters, Treatise on invertebrate paleotology, Part N, Bivalvia, *in* Moore, R.C., and Teichert, C., ed., Treatise on invertebrate paleontology. Lawrence, Kansas, Geological Society of America, N953-N1224.

Stueber, T., 1999. Isotopic and chemical intra-shell variations in low-Mg calcite of rudist bivalves (Mollusca-Hippuritacea): disequilibrium fractionations and late Cretaceous seasonality. International Journal of Earth Sciences. 88, 551-570.

Walls, R.A., Ragland, P.C., and Crisp, E.L., 1977. Experimental and natural early diagenetic mobility of Sr and Mg in biogenic carbonates. Geochimica et Cosmochimica Acta. 41, 1731-1737.

Wefer, G., and Berger, W.H., 1991. Isotope Paleontology: growth and composition of extant calcareous species. Marine Geology. 100, 207-248.

CHAPTER 5

CONCLUSIONS

5.1 SUMMARY AND CONCLUSIONS

Economic phosphorites in Jordan are part of the South Tethyan Phosphogenic Province (STPP), and were deposited on a storm-dominated, mixed carbonate-phosphorite epeiric platform along the south Tethyan margin during the Late Cretaceous. Phosphatic and associated strata examined in this dissertation belong to the Belqa Group, a 1000m thick fining upward succession of Late Coniacian to Eocene cherts, micritic limestones, phosphorite, and hemipelagic chalks (Bender, 1974; Powell, 1989). The Belqa Group is divisible into five conformable formations: the Ghudran (G), Amman Silicified Limestone (ASL), Alhisa Phosphorite (AP), Muwaqqar (M), and the Umm Rijam Formations (UM) (Powell, 1989). The G consists of detrital chalks and disconformably overlies peritidal carbonates of the Ajlun Group. The ASL is chert-rich and contains chert, chalk and minor phosphorite. The AP is a condensed stratigraphy that consists predominantly of interbedded phosphatic marls and granular phosphorite with subordinate oyster coquina. In central Jordan the AP is divisible into three stratigraphic members: the Sultani Phosphorite, Bahiya Oyster Coquina, and Qatrana Phosphorite members. The AP is conformably overlain by hemipelagic chalks of the M that are in turn overlain by cherts and chalks of the UM. The characteristics of individual lithofacies and their associations indicate that the Belqa Group forms the upper portion of a transgressive systems tract (TST) that culminated with the widespread deposition of chalk.

The major results and interpretations are summarized below. These findings provide a stratigraphic and genetic foundation for other studies in the STPP, and have further expanded our knowledge of the sedimentologic and oceanographic controls that governed the formation of "phosphorite giants".

5.1.1 Phosphogenesis

The south Tethyan margin was characterized by phosphogenesis in sedimentary environments spanning near-shore, mid-shelf, and distal shelf settings; pristine phosphates, a range of phosphatic event strata, and thick amalgamated phosphorites form a mosaic of facies that were deposited in a range of depositional environments (Abed, 1988; Abed and Amireh, 1999; Pufahl et al., 2001). This "phosphorite nursery" is a non-uniformitarian phenomenon and may reflect the upwelling of nutrient-rich seawater and its transport away from the upwelling centre through lagoonal circulation (Chapter 2). The combined effect of upwelling and lagoonal circulation is to support primary production and phosphogenesis in an array of sedimentary environments by cyclically pumping and sequestering P across the platform.

The absence of Fe-bearing authigenic minerals within Belqa Group strata suggests that Fe-pumping of pore water phosphate (Heggie et al., 1990) likely played a minimal role in the precipitation of carbonate fluorapatite (Chapter 2). On the Jordanian shelf, siliciclastics were trapped in nearshore environments, thereby starving the platform of a source of Fe. Phosphogenesis over the platform is thus inferred to have been stimulated by a highly productive surface ocean, and propelled by the production of pore water phosphate through the microbial respiration of sedimentary organic matter (Jahnke et al., 1983) and the dissolution of fish debris (Suess, 1981). Stable carbon isotopic data from phosphatic peloids support this interpretation and indicate that the precipitation of carbonate fluorapatite occurred within the zone of sulfate reduction (Chapter 2). The trace metal (Mg and Sr) geochemistry of skeletal calcite from the Cretaceous oyster *O. figari* is also consistent with this interpretation and indicates that phosphogenesis occurred within cool ambient ocean water associated with coastal upwelling (Chapter 4).

Comparison of the petrographic characteristics of coated phosphate grains from the AP with other coated grains of differing age and provenance suggests that phosphogenesis is

accompanied by changes in the redox potential of pore waters (Chapter 3). These changes are interpreted to reflect fluctuations in the biological oxygen demand within suboxic pore water environments resulting from variations in the surface productivity and/or ecological dynamics in the overlying water column (Grimm et al., 1997). The circumgranular record of diverse shallow burial and seafloor processes also suggests that coated phosphate grains record low and/or net negative rates of sediment accumulation, and are the granular equivalents to condensed beds (Grimm et al., 1993; Grimm and Galway, 1995).

5.1.2 Phosphorite depositional processes

The preponderance of redeposited bored concretions, the presence of offshore directed paleocurrents from oriented baculitid ammonites, coquinas containing shallow water faunas in hemipelagic environments, and hummocky cross-stratification indicate that the Jordanian shelf was a storm-dominated depositional system (Aigner, 1985). Sharply-based tabular beds of massive, normally graded, and indistinctly stratified layers of intraclastic phosphorite in the AP are interpreted as storm-generated event deposits.

Amalgamation of phosphatic grainstones derived from pristine phosphate facies produced the economic phosphorites. Event beds formed by the successive winnowing, transport and redeposition of phosphatic grains from pristine facies via storm-generated single-surge high density turbidity currents, and sustained, highly competent, shore parallel geostrophic currents. The sedimentologic data are consistent with an interpretation that an increase in storm frequency and intensity with time may have been a prerequisite for the formation of economic phosphorite.

Syndepositional phosphogenesis and amalgamation to form economic phosphorites contrasts sharply with the principles of "Baturin Cycling" for the origin of phosphorites (Baturin, 1971), and does not necessitate major rises and falls in relative sea level to produce economic phosphorite. A TST coupled with high surface productivity, creates detritally starved settings for

establishment of a "phosphorite nursery"; storm reworking of pristine facies produces granular phosphorite; and amalgamation of storm-generated granular event beds forms economic phosphorite in a single systems tract.

5.2 FUTURE RESEARCH DIRECTION

Further information is required from modern and ancient phosphogenic systems before the array of enigmatic processes governing the formation of economic phosphorites can be assessed and predicted. Future research should include:

(1) Continued development of the "phosphorite nursery" concept and the storm depositional model for the formation of economic phosphorites presented in this dissertation to explain the genesis of other ancient "phosphorite giants" (i.e. the Phosphoria Formation). The Late Permian Phosphoria Formation in the western United States contains approximately $1.5x10^{12}$ tonnes of phosphate, and is attributed to upwelling along the western margin of a broad, shallow, evaporitic epeiric platform (Stephens and Carroll, 1999). The Phosphoria Formation thus provides an ideal testing ground to further assess the function of large storms in forming economic phosphorite, and to evaluate the role lagoonal circulation may play in transporting and sequestering nutrients across the platform. This research should utilize a multidisciplinary approach (using concepts from sedimentology, paleontology, ichnology, taphonomy, and geochemistry) to yield insight into the array of sedimentologic and oceanographic processes that governed the accumulation of Phosphoria strata.

(2) Further evaluation of the role changes in relative sea level, tectonism, and climate play in P supply and accumulation (e.g. Föllmi et al., 1994). This research should integrate sequence stratigraphic investigations of phosphogenic systems with high-resolution geochemical studies aimed at quantifying the history of P burial rates (e.g. Filippelli and Delaney, 1996) in time-bound sedimentary successions. This research will provide important insight into whether

or not "phosphorite giants" record an accelerated P cycle, and clarify the importance of fluctuations in P burial to temporal changes in the global C cycle and thus climate.

(3) Further refinement to the coated grain model presented in this dissertation, and the extension of this model to other types of coated grains and concretions containing Eh sensitive minerals (Heikoop et al., 1996; Medrano and Piper, 1997; Sturesson, 2000). Future investigations of coated grains should incorporate laser ablation inductively coupled plasma mass spectrometry (Laser Ablation ICP-MS) of individual circumgranular layers to generate stable isotope ($\delta^{13}C$, $\delta^{34}S$) microstratigraphies through grains. This will provide a high-resolution record of pore water redox chemistry, and will test the hypothesis that vertically fluctuating redox zones within the sediment column are important in forming some types of coated grains and concretions.

(4) Future research focusing on the applicability of using the trace metal chemistry of oyster calcite to proxy sea water conditions should implement the use of a microdrill (Dettman and Lohmann, 1995) to ensure that sclerochronological profiles are produced with the highest possible temporal resolution for correlation to environmental data. These investigations should also include oysters from *Gryphaeidae* in order to permit the comparison of trace elements data between families. Such a study may further illuminate the environmental factors controlling the trace element distribution in oysters and give more credibility to comparing Mg and Sr concentrations between modern and ancient oyster species. The effects of diagenesis on trace element in *O. figari* also requires further investigation so that more meaningful interpretations of the trace element chemistry of ancient oysters can be made.

5.3 REFERENCES CITED

Abed, A.M., 1988. Eleventh International Field Workshop and Symposium - Guidebook: Third Jordanian Geological Conference International Geological Correlation Program Project 156 - Phosphorites. 124p.

Abed, A.M., and Amireh, B.S., 1999. Sedimentology , geochemistry, economic potential and palaeogeography of an Upper Cretaceous phosphorite belt in the southeastern desert of Jordan. Cretaceous Research. 20, 119-133.

Aigner, T., 1985. Storm Depositional Systems. Springer-Verlag, Berlin. 124p.

Baturin, G.N., 1971. Stages of phosphorite formation on the ocean floor. Nature. 232, 61-62.

Bender, F., 1974. Geology of Jordan. Gebrueder Borntraeger, Berlin. 196p.

Dettman, D.L., and Lohmann, K.C., 1995. Microsampling carbonates for stable isotope and minor element analysis: Physical separation of samples on a 20 micrometer scale. Journal of Sedimentary Research. 65, 566-569.

Filippelli, G.M., and Delaney, M.L., 1996. Phosphorus geochemistry of equatorial Pacific sediments. Geochimica et Cosmochimica Acta. 60, 1479-1495.

Föllmi, K.B., Weissert, H., Bisping, M., and Funk, H., 1994. Phosphogenesis, carbon-isotope stratigraphy, and carbonate-platform evolution along the Lower Cretaceous northern Tethyan margin. Geological Society of America Bulletin. 106, 729-746.

Grimm, K.A., and Galway, S., 1995. Phosphorite grain stratigraphies from the Oligo-Miocene sediments, Baja California Sur, Mexico: Clues towards shelf-to-basin correlation. Peninsular Geological Society, Third International Conference on the Geology of Baja California (Mexico), Abstract Volume.

Grimm, K.A., Lange, C.B., and Gill, A.S., 1997. Self-sedimentation of fossil phytoplankton blooms in the geologic record. Sedimentary Geology, 110, 151-161.

Heggie, D.T., Skyring, G.W., O'Brien, G.W., Reimers, C., Herczeg, A., Moriarty, D.J.W., Burnett, W.C., and Milnes, A.R., 1990. Organic carbon cycling and modern phosphorite formation on the East Australia continental margin: an overview. In: Notholt, A.J.G., and Jarvis, I. (Eds.), Phosphorite research and development. The Geological Society of London, Oxford, 87-117.

Heikoop, J.M., Tsujita, C.J., Risk, M.J., Tomascik, T., and Mah Anmarie, J., 1996. Modern iron ooids from a shallow marine volcanic setting; Mahengetang, Indonesia. Geology. 24, 759-762.

Imbrie, J., and Imbrie, K.P., 1979. Ice ages: solving the mystery. Enslow, Hillside. 224p.

Jahnke, R.A., Emerson, S.R., Roe, K.K., and Burnett, W.C., 1983. The present day formation of apatite in Mexican continental margin sediments. Geochimica et Cosmochimica Acta. 47, 259-266.

Jarvis, I., Burnett, W.C., Nathan, Y., Almbaydin, F.S.M., Attia, A.K.M., Castro, L.N., Flicoteaux, R., Hilmy, M.E., Husain, V., Quatawnah, A.A., Serjani, A., and Zanin, Y.N., 1994. Phosphorite geochemistry: Stateof-the-art and environmental concerns. Eclogae Geologicae Helveticae. 87, 643-700.

Medrano, M.D., and Piper, D.Z., 1997. Fe-Ca-phosphate, Fe-silicate, and Mn-oxide minerals in concretions from the Monterey Formation. Chemical Geology, 138, 9-23.

Powell, J.H., 1989. Stratigraphy and sedimentation of the Phanerozoic rocks in central and south Jordan. Natural Resources Authority, Geological Mapping Division, Amman. 130p.

Pufahl, P.K., Grimm, K.A., Abed, A.M., and Sadaqah, R.M.Y., submitted. Upper Cretaceous (Campanian) phosphorites in Jordan: Implications for the formation of a south Tethyan phosphorite giant.

Stephens, N.P., and Carroll, A.R., 1999. Salinity stratification in the Permian Phosphoria sea; a proposed paleoceaonographic model. Geology. 27, 899-902.

Struresson, U., Heikoop, J.M., and Risk, M.J., 2000. Modern and Paleozoic iron ooids; a similar volcanic origin. Sedimentary Geology. 136, 137-146.

Suess, E., 1981. Phosphate regeneration from sediments of the Peru Continental margin by dissolution of fish debris. Geochimica et Cosmochimica Acta. 45, p. 577-588.

APPENDICES

Appendix 1

Oyster Trace Metal Data

Sample	Ca (ppm)	Mg (ppm)	Sr (ppm)	Ca (mol/L)	Mg (mmol/L)	Sr (mmol/L)	Mg/Ca (mmol/mol)	Sr/Ca (mmol/mol)
J1.1	737	3.020	0.650	0.018	0.124	0.0074	6.757	0.403
J1.2	759	2.770	0.638	0.019	0.114	0.0073	6.018	0.384
J1.3	828	2.620	0.603	0.021	0.108	0.0069	5.218	0.333
J1.4	878	3.320	0.687	0.022	0.137	0.0078	6.235	0.358
J1.5	845	3.440	0.723	0.021	0.142	0.0083	6.713	0.391
J1.6	753	2.730	0.569	0.019	0.112	0.0065	5.978	0.346
J1.7	709	2.440	0.587	0.018	0.100	0.0067	5.675	0.379
J1.8	625	3.220	0.666	0.016	0.132	0.0076	8.495	0.487
J1.9	710	3.190	0.624	0.018	0.131	0.0071	7.409	0.402
J1.10	582	2.930	0.565	0.015	0.121	0.0064	8.301	0.444
J1.11	876	2.900	0.689	0.022	0.119	0.0079	5.459	0.360
J2.1	738	2.930	0.808	0.018	0.121	0.0092	6.547	0.501
J2.2	786	3.010	0.869	0.020	0.124	0.0099	6.315	0.506
J2.3	843	2.950	0.839	0.021	0.121	0.0096	5.770	0.455
J2.4	745	2.670	0.755	0.019	0.110	0.0086	5.910	0.464
J2.5	919	3.430	0.910	0.023	0.141	0.0104	6.154	0.453
J2.6	889	3.190	0.887	0.022	0.131	0.0101	5.917	0.456
J2.7	939	3.330	0.919	0.023	0.137	0.0105	5.848	0.448
J2.8	794	2.990	0.762	0.020	0.123	0.0087	6.210	0.439
J2.9	1280	4.480	1.250	0.032	0.184	0.0143	5.771	0.447
J2.10	907	3.540	0.978	0.023	0.146	0.0112	6.436	0.493
J2.11	916	3.400	0.994	0.023	0.140	0.0113	6.121	0.496
J3.1	350	1.570	0.320	0.009	0.065	0.0037	7.397	0.418
J3.2	694	2.900	0.654	0.017	0.119	0.0075	6.890	0.431
J3.3	935	3.670	0.947	0.023	0.151	0.0108	6.472	0.463
J3.4	743	2.970	0.741	0.019	0.122	0.0085	6.591	0.456
J3.5	771	3.070	0.778	0.019	0.126	0.0089	6.566	0.462
J3.6	898	3.450	0.850	0.022	0.142	0.0097	6.335	0.433
J3.7	814	3.230	0.794	0.020	0.133	0.0091	6.543	0.446
J3.8	769	3.000	0.806	0.019	0.123	0.0092	6.433	0.479
J4.1	865	3.570	0.928	0.022	0.147	0.0106	6.806	0.491
J4.2	733	2.840	0.772	0.018	0.117	0.0088	6.389	0.482
J4.3	808	3.080	0.820	0.020	0.127	0.0094	6.286	0.464
J4.4	792	3.160	0.797	0.020	0.130	0.0091	6.579	0.460
J4.5	797	3.090	0.841	0.020	0.127	0.0096	6.393	0.483
J4.6	718	2.670	0.729	0.018	0.110	0.0083	6.132	0.464
J4.7	812	2.970	0.843	0.020	0.122	0.0096	6.031	0.475
J4.8	690	2.790	0.715	0.017	0.115	0.0082	6.668	0.474
J4.9	646	2.520	0.670	0.016	0.104	0.0076	6.432	0.474
J4.10	672	2.460	0.744	0.017	0.101	0.0085	6.036	0.506
J4.11	639	2.480	0.677	0.016	0.102	0.0077	6.400	0.485
J4.12	760	2.900	0.775	0.019	0.119	0.0088	6.292	0.466
L1.1	754	1.977	1.862	0.019	0.081	0.0213	4.323	1.130
L1.2	324	1.273	0.562	0.008	0.052	0.0064	6.484	0.794
L1.3	510	2.684	0.934	0.013	0.110	0.0107	8.680	0.838
L1.4	405	3.116	0.727	0.010	0.128	0.0083	12.681	0.821
L1.5	478	1.616	0.770	0.012	0.066	0.0088	5.574	0.737
L1.6	833	4.835	1.294	0.021	0.199	0.0148	9.568	0.710

L1.7	934	8.357	1.774	0.023	0.344	0.0203	14.756	0.869
L1.8	587	2.024	1.278	0.015	0.083	0.0146	5.688	0.996
L1.9	206	2.092	0.380	0.005	0.086	0.0043	16.760	0.843
L1.10	646	1.960	1.289	0.016	0.081	0.0147	5.001	0.912
L1.11	1109	3.119	2.102	0.028	0.128	0.0240	4.636	0.867
L1.12	982	2.835	1.842	0.024	0.117	0.0210	4.764	0.859
L1.13	582	4.023	1.150	0.015	0.166	0.0131	11.397	0.904
L1.14	428	2.074	0.833	0.011	0.085	0.0095	7.984	0.889
L1.15	556	0.860	0.928	0.014	0.035	0.0106	2.552	0.763
L1.16	426	0.519	0.663	0.011	0.021	0.0076	2.009	0.712
L1.17	475	0.648	0.853	0.012	0.027	0.0097	2.249	0.821
L1.18	294	0.518	0.560	0.007	0.021	0.0064	2.904	0.871
L1.19	410	0.691	0.793	0.010	0.028	0.0091	2.782	0.886
L1.20	111	0.190	0.211	0.003	0.008	0.0024	2.837	0.870
L1.21	112	0.196	0.204	0.003	0.008	0.0023	2.876	0.829
L1.22	108	0.176	0.190	0.003	0.007	0.0022	2.683	0.803
L1.23	732	1.606	1.464	0.018	0.066	0.0167	3.618	0.915
L1.24	310	0.735	0.620	0.008	0.030	0.0071	3.909	0.915
L2.1	640	2.408	1.581	0.016	0.099	0.0180	6.207	1.130
L2.2	624	6.494	2.153	0.016	0.267	0.0246	17.150	1.577
L2.3	694	7.312	2.498	0.017	0.301	0.0285	17.369	1.646
L2.4	954	4.601	1.488	0.024	0.189	0.0170	7.950	0.713
L2.5	646	4.526	1.350	0.016	0.186	0.0154	11.555	0.956
L2.6	991	7.475	2.281	0.025	0.308	0.0260	12.439	1.053
L2.7	663	4.256	1.352	0.017	0.175	0.0154	10.584	0.933
L2.8	637	4.328	1.279	0.016	0.178	0.0146	11.208	0.919
L2.9	686	6.055	1.520	0.017	0.249	0.0174	14.544	1.013
L2.10	653	5.984	1.627	0.016	0.246	0.0186	15.116	1.140
L2.11	769	5.736	1.413	0.019	0.236	0.0161	12.293	0.840
L2.12	1052	6.663	1.673	0.026	0.274	0.0191	10.447	0.728
L2.13	828	5.658	1.423	0.021	0.233	0.0162	11.262	0.786
L2.14	572	4.046	1.007	0.014	0.166	0.0115	11.672	0.806
L2.15	108	0.828	0.194	0.003	0.034	0.0022	12.698	0.825
L2.16	805	2.597	1.759	0.020	0.107	0.0201	5.321	1.000
L3.1	857	3.298	1.854	0.021	0.136	0.0212	6.346	0.989
L3.2	518	4.299	1.142	0.013	0.177	0.0130	13.695	1.009
L3.3	579	2.194	1.260	0.014	0.090	0.0144	6.248	0.995
L3.4	632	4.028	1.947	0.016	0.166	0.0222	10.504	1.409
L3.5	605	3.753	1.622	0.015	0.154	0.0185	10.229	1.226
L3.6	808	3.144	3.522	0.020	0.129	0.0402	6.419	1.995
L3.7	732	2.895	3.361	0.018	0.119	0.0384	6.522	2.100
L3.8	980	4.475	3.838	0.024	0.184	0.0438	7.532	1.792
L3.9	675	2.973	2.013	0.017	0.122	0.0230	7.260	1.364
L3.10	960	10.738	2.147	0.024	0.442	0.0245	18.451	1.023
L3.11	691	5.064	1.669	0.017	0.208	0.0190	12.090	1.105
L3.12	794	5.363	1.899	0.020	0.221	0.0217	11.141	1.094
L3.13	627	4.507	1.652	0.016	0.185	0.0189	11.848	1.205
L3.14	994	5.083	4.932	0.025	0.209	0.0563	8.428	2.268
L3.15	643	2.656	3.696	0.016	0.109	0.0422	6.809	2.629
L4.1	697	2.512	1.554	0.017	0.103	0.0177	5.943	1.020
L4.2	894	6.684	2.140	0.022	0.275	0.0244	12.323	1.095
L4.3	763	5.536	1.794	0.019	0.228	0.0205	11.967	1.076
L4.4	1068	7.759	2.016	0.027	0.319	0.0230	11.982	0.863
L4.5	908	6.785	1.916	0.023	0.279	0.0219	12.318	0.965
L4.6	885	6.785	1.830	0.022	0.279	0.0209	12.648	0.946
L4.7	667	2.012	1.560	0.017	0.083	0.0178	4.975	1.070
L4.8	71	0.305	0.157	0.002	0.013	0.0018	7.115	1.014

L4.9	543	1.436	1.246	0.014	0.059	0.0142	4.357	1.049
L4.10	557	1.429	1.261	0.014	0.059	0.0144	4.230	1.035
L4.11	738	3.558	1.944	0.018	0.146	0.0222	7.952	1.205
L4.12	577	2.976	1.459	0.014	0.122	0.0167	8.500	1.156
L4.13	572	3.277	0.037	0.014	0.135	0.0004	9.450	0.029
L4.14	536	1.727	1.256	0.013	0.071	0.0143	5.316	1.072
L4.15	793	1.852	1.477	0.020	0.076	0.0169	3.852	0.852
L4.16	587	1.270	1.275	0.015	0.052	0.0146	3.566	0.994
L4.17	721	2.578	1.796	0.018	0.106	0.0205	5.897	1.140
L4.18	864	1.847	1.869	0.022	0.076	0.0213	3.524	0.989
L4.19	857	2.177	1.763	0.021	0.090	0.0201	4.187	0.941
L4.20	640	1.996	1.492	0.016	0.082	0.0170	5.146	1.067
L4.21	655	1.875	1.465	0.016	0.077	0.0167	4.721	1.023
L4.22	887	6.098	1.909	0.022	0.251	0.0218	11.339	0.985
L4.23	663	2.898	1.579	0.017	0.119	0.0180	7.213	1.090
L4.24	639	1.160	1.597	0.016	0.048	0.0182	2.994	1.143
L5.1	803	3.433	2.325	0.020	0.141	0.0265	7.054	1.325
L5.2	313	2.339	0.680	0.008	0.096	0.0078	12.331	0.994
L5.3	491	3.230	1.110	0.012	0.133	0.0127	10.848	1.034
L5.4	870	4.918	2.030	0.022	0.202	0.0232	9.322	1.067
L5.5	630	4.976	0.916	0.016	0.205	0.0105	13.015	0.664
L5.6	940	5.246	1.772	0.023	0.216	0.0202	9.203	0.862
L5.7	541	3.072	1.034	0.013	0.126	0.0118	9.362	0.874
L5.8	709	5.292	1.852	0.018	0.218	0.0211	12.309	1.195
L5.9	878	5.870	2.007	0.022	0.242	0.0229	11.020	1.045
L5.10	294	2.507	0.868	0.007	0.103	0.0099	14.077	1.352
L5.11	829	4.181	1.892	0.021	0.172	0.0216	8.320	1.045
L5.12	577	3.603	1.716	0.014	0.148	0.0196	10.290	1.359
L5.13	207	1.069	0.306	0.005	0.044	0.0035	8.519	0.676
L5.14	569	2.799	0.952	0.014	0.115	0.0109	8.118	0.766
L5.15	767	2.314	1.772	0.019	0.095	0.0202	4.978	1.057
L5.16	889	3.028	2.102	0.022	0.125	0.0240	5.617	1.082
L5.17	571	1.781	1.385	0.014	0.073	0.0158	5.146	1.110
E1.1	645	2.707	1.333	0.016	0.111	0.0152	6.923	0.946
E1.2	127	1.625	0.401	0.003	0.067	0.0046	21.073	1.444
E1.3	297	4.635	0.899	0.007	0.191	0.0103	25.767	1.386
E1.4	138	0.846	0.302	0.003	0.035	0.0034	10.118	1.003
E1.5	46	0.501	0.120	0.001	0.021	0.0014	18.002	1.192
E1.6	50	0.384	0.110	0.001	0.016	0.0013	12.554	0.998
E1.7	198	1.665	0.440	0.005	0.069	0.0050	13.900	1.018
E1.8	479	3.406	1.050	0.012	0.140	0.0120	11.730	1.003
E1.9	128	0.305	0.944	0.003	0.013	0.0108	3.924	3.371
E1.10	45	0.315	0.105	0.001	0.013	0.0012	11.485	1.063
E1.11	258	1.959	0.601	0.006	0.081	0.0069	12.523	1.065
E1.12	633	3.247	1.142	0.016	0.134	0.0130	8.453	0.825
E2.1	1083	3.462	2.848	0.027	0.142	0.0325	5.269	1.203
E2.2	84	0.709	0.259	0.002	0.029	0.0030	13.854	1.404
E2.3	196	1.437	0.611	0.005	0.059	0.0070	12.074	1.423
E2.4	322	2.373	0.714	0.008	0.098	0.0081	12.166	1.015
E2.5	378	2.969	0.828	0.009	0.122	0.0095	12.956	1.003
E2.6	254	2.312	0.752	0.006	0.095	0.0086	15.029	1.355
E2.7	753	6.107	1.556	0.019	0.251	0.0178	13.379	0.946
E2.8	404	1.669	0.799	0.010	0.069	0.0091	6.812	0.904
E2.9	5	0.029	0.012	0.000	0.001	0.0001	10.625	1.259
E2.10	268	1.832	0.833	0.007	0.075	0.0095	11.258	1.419
E2.11	341	1.045	0.354	0.009	0.043	0.0040	5.056	0.476
E2.12	139	1.328	0.000	0.003	0.055	0.0000	15.802	0.001

E3.1	531	5.959	1.152	0.013	0.245	0.0131	18.498	0.992
E3.2	644	6.059	1.679	0.016	0.249	0.0192	15.523	1.193
E3.3	159	1.643	0.387	0.004	0.068	0.0044	17.004	1.111
E3.4	118	1.856	0.356	0.003	0.076	0.0041	25.976	1.382
E3.5	445	7.659	1.511	0.011	0.315	0.0172	28.356	1.552
E3.6	213	2.341	0.568	0.005	0.096	0.0065	18.123	1.220
E3.7	150	1.953	0.433	0.004	0.080	0.0049	21.472	1.320
E3.8	280	2.899	0.824	0.007	0.119	0.0094	17.071	1.346
E3.9	54	0.526	0.170	0.001	0.022	0.0019	16.008	1.431
E3.10	144	1.193	0.418	0.004	0.049	0.0048	13.664	1.328
E3.11	200	1.849	0.672	0.005	0.076	0.0077	15.212	1.533
E3.12	144	1.237	0.474	0.004	0.051	0.0054	14.150	1.503
E3.13	47	0.386	0.140	0.001	0.016	0.0016	13.428	1.350
E3.14	97	0.681	0.252	0.002	0.028	0.0029	11.621	1.195
E3.15	278	1.898	0.683	0.007	0.078	0.0078	11.270	1.126
E3.16	116	0.921	0.319	0.003	0.038	0.0036	13.105	1.260
E3.17	338	2.801	0.882	0.008	0.115	0.0101	13.675	1.195
E3.18	52	0.454	0.146	0.001	0.019	0.0017	14.271	1.274
E3.19	97	0.885	0.261	0.002	0.036	0.0030	15.045	1.231
E3.20	132	1.569	0.362	0.003	0.065	0.0041	19.667	1.258
E4.1	948	5.801	2.050	0.024	0.239	0.0234	10.088	0.989
E4.2	382	3.381	1.055	0.010	0.139	0.0120	14.581	1.262
E4.3	133	1.290	0.388	0.003	0.053	0.0044	15.987	1.333
E4.4	63	0.941	0.229	0.002	0.039	0.0026	24.568	1.658
E4.5	416	2.412	1.043	0.010	0.099	0.0119	9.569	1.148
E4.6	202	1.861	0.544	0.005	0.077	0.0062	15.175	1.230
E4.7	158	1.810	0.594	0.004	0.074	0.0068	18.888	1.718
E4.8	156	1.995	0.565	0.004	0.082	0.0064	21.112	1.658
E4.9	359	2.262	0.796	0.009	0.093	0.0091	10.377	1.013
E4.10	201	1.727	0.556	0.005	0.071	0.0063	14.162	1.264
E4.11	347	2.787	0.995	0.009	0.115	0.0114	13.261	1.313
E4.12	167	1.227	0.479	0.004	0.050	0.0055	12.099	1.309
E4.13	235	2.103	0.678	0.006	0.087	0.0077	14.739	1.318
E4.14	125	1.067	0.337	0.003	0.044	0.0038	14.042	1.229
E4.15	796	1.501	1.377	0.020	0.062	0.0157	3.110	0.791
E5.1	145	1.207	0.359	0.004	0.050	0.0041	13.700	1.130
E5.2	1017	2.940	1.720	0.025	0.121	0.0196	4.767	0.773
E5.3	202	1.533	0.596	0.005	0.063	0.0068	12.523	1.350
E5.4	136	1.058	0.477	0.003	0.044	0.0054	12.781	1.597
E5.5	45	0.317	0.129	0.001	0.013	0.0015	11.660	1.313
E5.6	608	5.272	1.613	0.015	0.217	0.0184	14.289	1.213
E5.7	432	3.118	1.175	0.011	0.128	0.0134	11.898	1.243
E5.8	138	1.580	0.411	0.003	0.065	0.0047	18.827	1.357
E5.9	98	1.232	0.367	0.002	0.051	0.0042	20.715	1.713
E5.10	667	2.374	1.195	0.017	0.098	0.0136	5.870	0.820